Spring 2019

Characterization and Optimization of a Propeller Test Stand

Colin Bruce Leighton Benjamin
Old Dominion University, colin_benjamin2000@yahoo.com

CHARACTERIZATION AND OPTIMIZATION OF A PROPELLER TEST STAND

by

Colin Bruce Leighton Benjamin
B.S.M.E. August 2018, Old Dominion University

A Thesis Submitted to the Faculty of
Old Dominion University in Partial Fulfillment of the
Requirements for the Degree of

MASTER OF SCIENCE

AEROSPACE ENGINEERING

OLD DOMINION UNIVERSITY
May 2019

Approved By:

Drew Landman (Director)

Thomas Alberts (Member)

Colin Britcher (Member)

ABSTRACT

CHARACTERIZATION AND OPTIMIZATION OF A PROPELLER TEST STAND

Colin Bruce Leighton Benjamin
Old Dominion University, 2019
Director: Dr. Drew Landman

In recent history, there has been a rapid rise in the use of drones, and they are expanding in popularity each year. The widespread use and future capabilities of these unmanned aerial vehicles (UAVs) will call for increased study and classification of propellers to maximize their performance. As a result, it is necessary to have continuity in the development, maximization, and optimization of propeller test stand's capability to collect accurate and precise measurements. It is of significant advantage to have the capability of accurately characterizing a propeller based on its thrust and torque. In this study, a propeller test stand was improved with specifically designed features in order to obtain a system with high repeatability and defined prediction bounds.

The improvements to the propeller test stand were confirmed at Old Dominion University (ODU) Low-Speed Wind Tunnel using a Design of Experiments (DOE) approach in order to observe the accuracy, repeatability of measurements, and required a mathematical model for aerodynamic characterization. 12x8, 14x12, and 17x12 APC Thin Electric propellers were chosen for comparisons to published data. In addition to these propellers, further experimentation was done on two aluminum fabricated propellers created at ODU, one of a conventional design and the other of a new design with swept blades. The performance data of these propellers were obtained with an emphasis being taken on detailed performance comparisons. Results obtained revealed information that warrants further experimentation with swept designed propellers versus straight blade propellers for application to UAVs. The results of this research showed significant improvement in the propeller test stand and its ability to repeat data with high accuracy and precision in order to predict a propeller's efficiency.

I dedicate this thesis to my son Alexander Franklin Benjamin who gives me the drive and motivation to always continue to strive for excellence. I would also like to give thanks to my two sisters and the love of my life Yuechen Tao who always believed in me and supported me along my journey. Last but not least I thank my mom for raising me the way she did, and for all her care, love, and continuous support.

ACKNOWLEDGMENTS

Many people have contributed and aided in the successful completion of this thesis. First I would like to extend special thanks to my advisor Dr. Drew Landman for his continuous guidance, support, and countless efforts to make this thesis a possibility. I would also like to thank my committee members Dr. Colin Britcher and Dr. Thomas Alberts for their patience and time invested in my research. Finally, I would like to thank Brian Duvall, Arthur Wiedemann, and Engin Baris for sharing their knowledge and their assistance provided throughout this research.

NOMENCLATURE

ANOVA	Analysis of Variance
β	Regression Coefficient
CI	Confidence Interval
C	Cross-Sectional Area of the Wind Tunnel, ft^2
C_T	Coefficient of Thrust
C_Q	Coefficient of Torque
C_P	Coefficient of Power
CAD	Computer Aided Design
CCD	Central Composite Design
DOE	Design-of-Experiments
FEA	Finite Element Analysis
J	Advance ratio
η	Efficiency
T	Thrust, lbf
Q	Torque, in-lbf
ρ	Density, $slug/ft^3$
n	Revolution per second, rev/sec
LSWT	Low-Speed Wind Tunnel
P	Power, Watts
D	Propeller diameter, ft
V	Velocity, ft/sec
t	Time, sec
UAV	Unmanned Aerial Vehicle
N	Number of Samples
Re	Reynolds Number
RPS	Revolutions Per Second
RPM	Revolutions Per Minute
ε	Random Error Term

TABLE OF CONTENTS

Page

LIST OF TABLES

LIST OF FIGURES

Figure Page

CHAPTER 1- INTRODUCTION

With the rapid rate at which drone technology is continually increasing and the need for more efficient propeller designs, it is imperative to have a consistent performance test capability as characteristics of propellers change to meet unique challenges for today's UAVs. This thesis focuses on characterizing and optimizing the accuracy and precision of a propeller test stand.

1.1 THE ORIGINAL ODU PROPELLER TEST STAND

The test stand shown in Figure 1 was designed and built by an undergraduate senior design team and was then used as a part of an M.S. thesis for Brian Duvall. His test stand consisted of a 3D printed nacelle that was manufactured at ODU. Due to the length of this nacelle, it was printed in six sections [1]. The nacelle was created in two halves, with three sections glued together in order to create each half. This design allowed for easy access to the components inside. The cutaway of the propeller test stand below (Figure 1) shows half of the printed nacelle and also the internal components that were integrated into his final developed design. This test stand incorporated an ATI six-axis load cell which was subsequently replaced by the ODU 15 x 15 propeller balance. While the test stand itself performed well, several necessary refinements were identified for the test stand integration. These new features and the quantification of uncertainty associated with the improved test capability are the subjects of this study. The original test stand is shown in Figure 1.

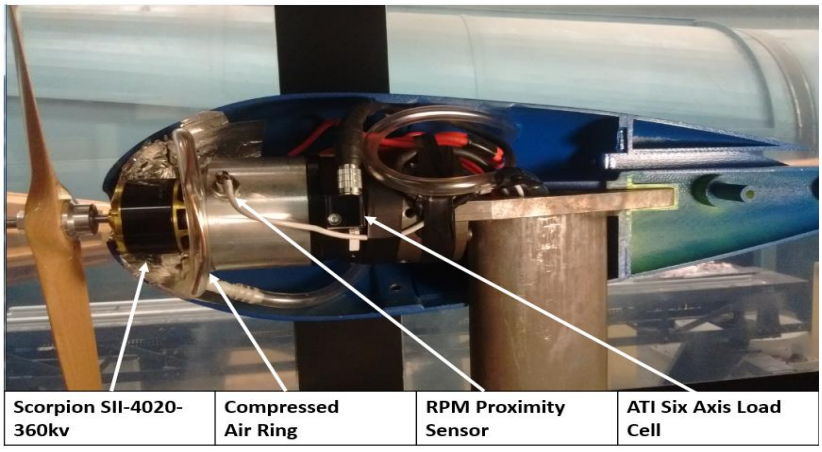

Figure 1- Original propeller test stand [1]

1.2 THE ODU 15 x 15 BALANCE

The ODU 15 x 15 propeller balance was designed and built as an M.S. thesis for Nicholas Sadowski [2]. The balance was calibrated and integrated into an existing propeller test stand that previously used a commercial six-axis load cell. The ODU 15 x 15 balance (load cell) measures loads generated by the propeller which is driven by a brushless motor. These loads generate strains which are in turn read by strain gauges arranged in Wheatstone bridges [2]. This load cell is designed to read 15 lb thrust and 15 in-lb torque. The load cell separates the thrust and torque measurement sections as shown in Figure 2. The original load cell used two of its six available axes in the collection of data.

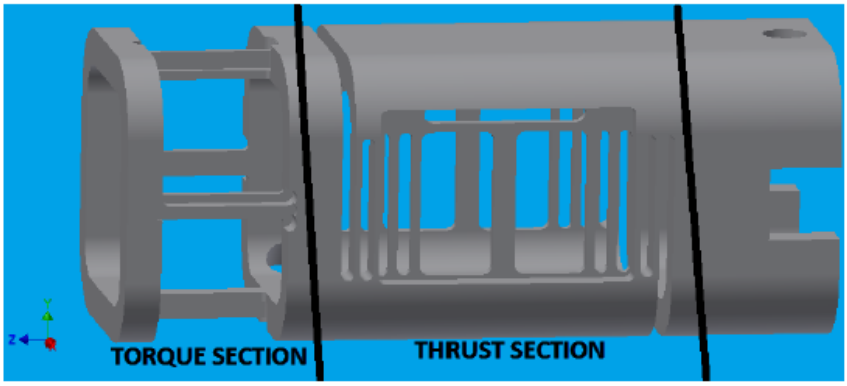

Figure 2- ODU 15 X 15 Balance [2]

1.3 INTEGRATION OF THE ODU 15 x 15

The ODU 15 x 15 balance was integrated into the updated test stand and installed in such a way to work with the other existing components. Such components include a brushless motor, proximity sensor, cooling plenum, and an internal nacelle thermocouple. The motor and proximity sensor was mounted to the forward section of the balance while the cooling plenum and thermocouple were mounted to one half of the nacelle. Direct wiring of electrical connections to the motor and proximity sensor bridged the metric gap of the balance as they had previously with the ATI load cell. The balance was mounted to a rigid strut that was then bolted to the base of the wind tunnel.

In order to capture the RPM of the motor, an inductive proximity sensor was chosen. This sensor produces a pulse when a metallic object comes within a close distance of the sensor. During the operation of the wind tunnel it was necessary to collect tunnel conditions to include; barometric pressure, test section temperature, and dynamic pressure.

The ODU wind tunnel is a closed return design. The test stand is mounted within the high-speed test section of the tunnel. All these devices were integrated into a data acquisition board and monitored using LabVIEW software. This enables the user to have full manual control of the motor speed, tunnel velocity control, and a way to monitor these inputs while capturing thrust and torque data from the load cell.

1.4 SHORTCOMINGS OF THE EXISTING DESIGN

The previous test stand had several features that could be improved upon in order to collect more accurate and consistent data. The previous nacelle was 3D printed in six parts, and due to its required large cross-section, there was a concern with aerodynamic blockage. During experimentation, it was also noticed that the RPM sensor would sometimes miscount the revolutions at higher RPM. This caused inconsistent RPM settings which reduces the accuracy and repeatability of the performance coefficient data. Another concern was the mechanical hysteresis caused by connecting the RPM sensor and motor across the metric gap of the load cell. The motor would also generate excessive heat that would then flow across the load cell which in turn affected the accuracy of the measured data. Lastly, it lacked a way to monitor the operating temperature within the nacelle and a way to maintain a constant wind tunnel velocity during testing.

1.5 OBJECTIVES

Advances were made in designing an improved test stand to address previous issues that led to improved accuracy and precision of measurements. The major issues include:

- the need for a nacelle with lower aerodynamic blockage
- reduction of excessive heat produced by the motor during operation
- reliable temperature monitoring
- more consistent RPM measurements obtained from the proximity sensor

- a way to set and maintain the wind tunnel's velocity at a specific value to obtain the required advance ratios.
- reduction of mechanical hysteresis due to wires connecting the RPM sensor and motor to a power source across the metric gap

Finally, a general test methodology will be developed using statistical engineering principles. There is a need for a test design which provides regression models with confidence and prediction intervals for the performance coefficients. Using the test protocol, three different size props will be evaluated and compared to published results in the literature. The data obtained should be analyzed, modeled, and plotted with C_P vs. J, C_T vs. J, C_Q vs. J and Efficiency vs. J. The new test stand and protocol are necessary for a comparison study with a new swept blade, low-noise propeller design. The 12 x 8, 14 x 12, and 17 x 12 APC Thin Electric propellers to be tested are shown in Figure 3. Also shown in Figures 4 and 5 are the 16 in straight and 16 in swept-blade propellers which will be used for the comparison study.

Figure 3 – 12 x 8, 14 x 12, and 17 x 12 APC Thin Electric propellers respectively

Figure 4 – 16 in straight blade propeller inside ODU LSWT

Figure 5 – 16 in swept-blade propeller inside ODU LSWT

CHAPTER 2 – BACKGROUND: PROPELLER PERFORMANCE CHARACTERIZATION

2.1 AERODYNAMIC PERFORMANCE CHARACTERIZATION

In defining a propeller's aerodynamic performance characteristics, a set of non-dimensional coefficients are used for characterization. Having these non-dimensional parameters simplifies plotting experimental results and making direct comparisons. The most common non-dimensional performance characteristics are efficiency, thrust, torque, and power which are obtained over a specified range of advance ratios. These non-dimensional parameters are calculated according to the following equations.

The coefficient of torque is given by;

$$C_Q = \frac{Q}{\rho n^2 D^5} \tag{1}$$

The coefficient of thrust is given by;

$$C_T = \frac{T}{\rho n^2 D^4} \tag{2}$$

The power is given by;

$$P = 2\pi n Q \tag{3}$$

The coefficient of power is given by;

$$C_P = \frac{P}{\rho n^3 D^5} \tag{4}$$

The advance ratio is given by;

$$J = \frac{V}{nD} \tag{5}$$

Finally, the efficiency is given by;

$$\eta = J\frac{C_T}{C_P} \tag{6}$$

Normally the three performance coefficients and the propeller efficiency are plotted against the advance ratio for a range of RPM values [3]. Some typical performance plots for small propellers can be seen in Figure 6 through 8. These results were obtained from a M.S. thesis by John Brandt under the supervision of Dr. Michael Selig. The results shown are from an APC 12 x 8, 14 x 12, and 17 x 12 propeller [4]. These are the propellers that were tested within this thesis for the comparison to literature.

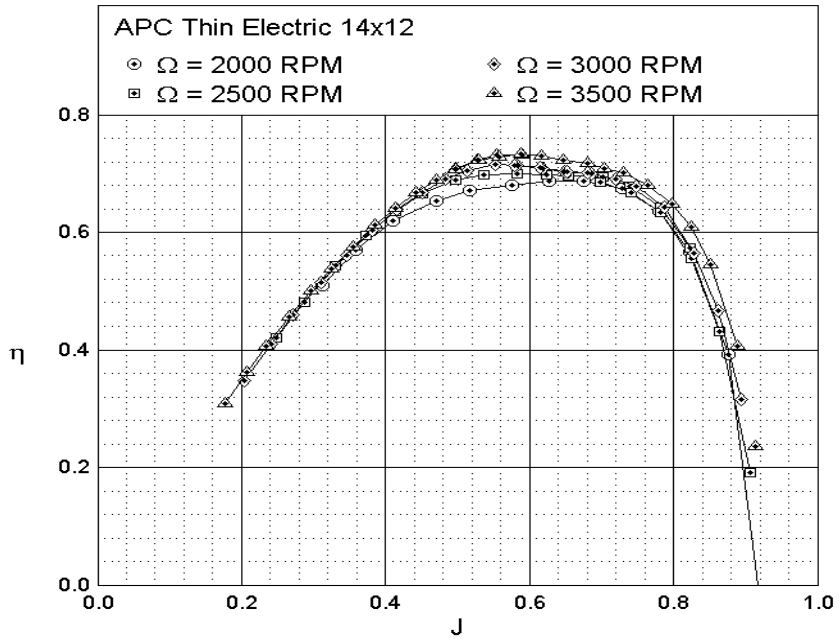

Figure 6- Typical plot of efficiency vs. advance ratio [4]

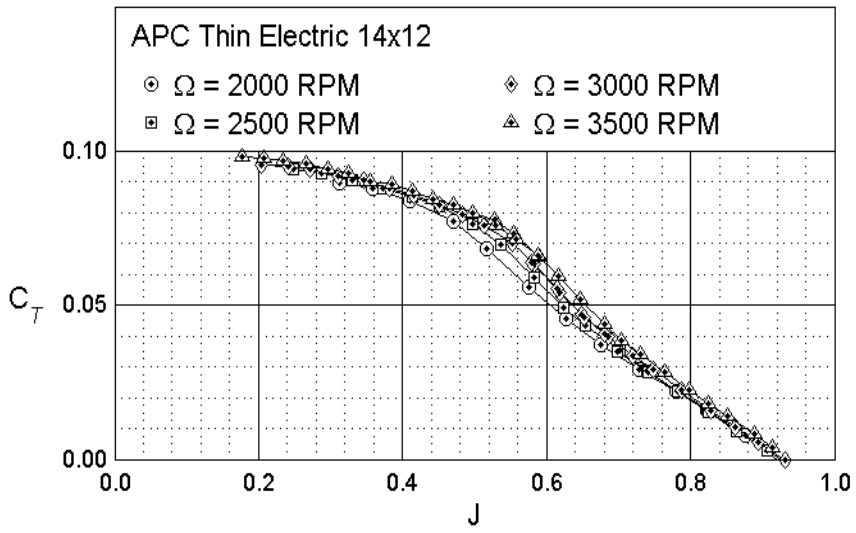

Figure 7- Typical plot of the coefficient of thrust vs. advance ratio [4]

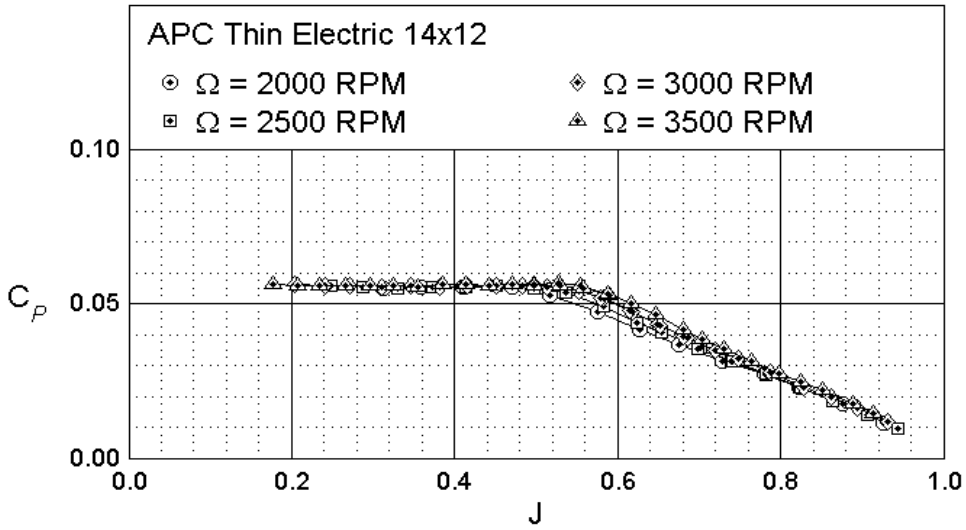

Figure 8- Typical plot of the coefficient of power vs. advance ratio [4]

2.2 REYNOLDS NUMBER CONSIDERATIONS

The application of small propellers is typically for small UAVs, and these vehicles typically operate with propellers at low Reynolds numbers. The range is anywhere from 50,000 to 100,000 based on the propeller chord at the 75% propeller-blade station [4]. To quantify test data at these conditions, tests were performed in the ODU low-speed wind tunnel. In order to examine the Reynolds number effects, the range of RPM tested was between 2,500 to 5,000 RPM depending on the diameter and thrust the propeller was capable of producing. Typically, a propeller's performance increases with higher Reynolds number. Based on the data collected in Selig's experiments this observation becomes apparent as seen in Figure 6. The results from the APC Thin Electric 14 x 12 propeller showed that as the RPM of the propeller increases so does the efficiency. The observations made in this thesis correlate with this trend.

CHAPTER 3 – LITERATURE REVIEW

3.1 SMALL PROPELLER TEST STAND AND BALANCE DESIGNS.

The use of small propeller test stands has become more popular over the past few years [3]. There are many different configurations for the devices; however, choosing one that is easily removed from the ODU low-speed wind tunnel is most attractive since it is used for many other testing apparatuses as well. Compact internal strain-gage balances are used extensively to measure the aerodynamic loads on a test article during an aircraft model wind tunnel test [5]. Figure 9 shows a typical six-component aircraft model internal balance design from NASA Langley Research Center. The axial section design concept with t-strap and measurement beam, visible in the photograph, was used in the ODU 15 x 15 thrust component design. The torque measurement cage design follows the NASA LaRC concept as well. The ODU 15 x 15 is capable of measuring loads of 15 lbs. thrust, and 15 in-lbs. of torque [2]. This balance (load cell) was explicitly designed for a range of expected loads from small propellers.

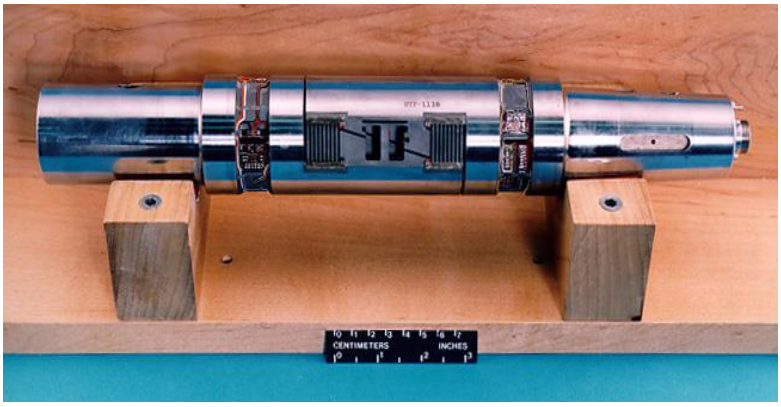

Figure 9- A Representative Six-Component NASA LaRC Wind Tunnel Balance

It is common to see test stands that are designed with a rigid strut and linkage to a sensitive thrust force measurement load cell [6]. The motor is mounted directly to a torque measurement load cell. This setup is popular because of its simplicity, and it has been shown reliable and sensitive. The design minimizes vibrations which negatively influence data, and they are more straightforward compared to other options available. Figure 10 shows Selig's setup used to measure thrust and torque [6]. The test rig is mounted to the top of the ceiling in the wind tunnel. The thrust measurement mechanism is a simple T-shaped structure that pivots about two flexural pivots and

is constrained by a load cell that sits outside of the tunnel [4]. There is a fairing to ensure that the freestream flow does not produce drag force on the beam located within the tunnel.

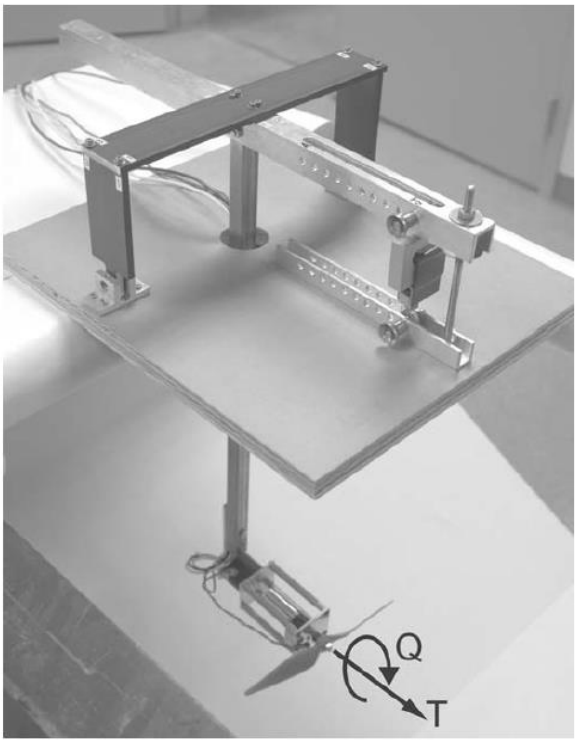

Figure 10- Selig's test apparatus without an aerodynamic fairing

One significant advantage of this test rig is its mechanical advantage, its capability to adjust the linkages allowing the load cell to be loaded at the best level. This design becomes very attractive when measuring uncertainties of thrust measurements. The setup is; however, time-consuming to adjust, and it is not inherently portable which makes it unsuitable to be used in the ODU wind tunnel.

3.2 CALIBRATION

The internal balance is a measurement device. Calibrating any measurement device involves applying known values of the inputs to the device while recording the resulting sensor output(s) [5]. The calibration of the ODU 15 x 15 load cell was done using the calibration set-up shown in Figure 8. The set-up includes a power supply, junction box, weight platens, test stand, arms and a voltage data acquisition system [2]. This rig allows for a known static force to be applied to the balance while recording the voltage outputs of the balance [2].

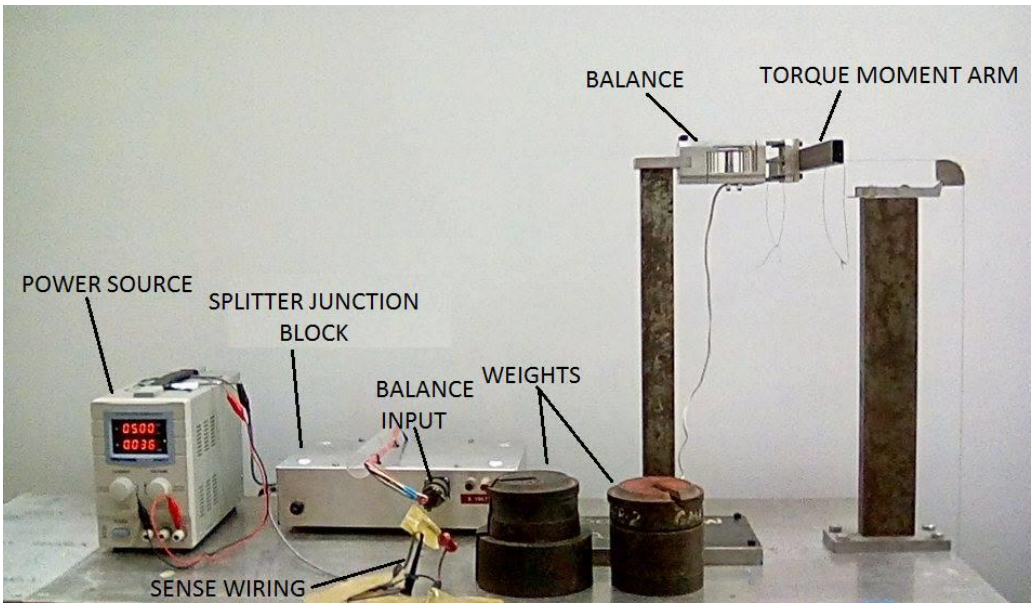

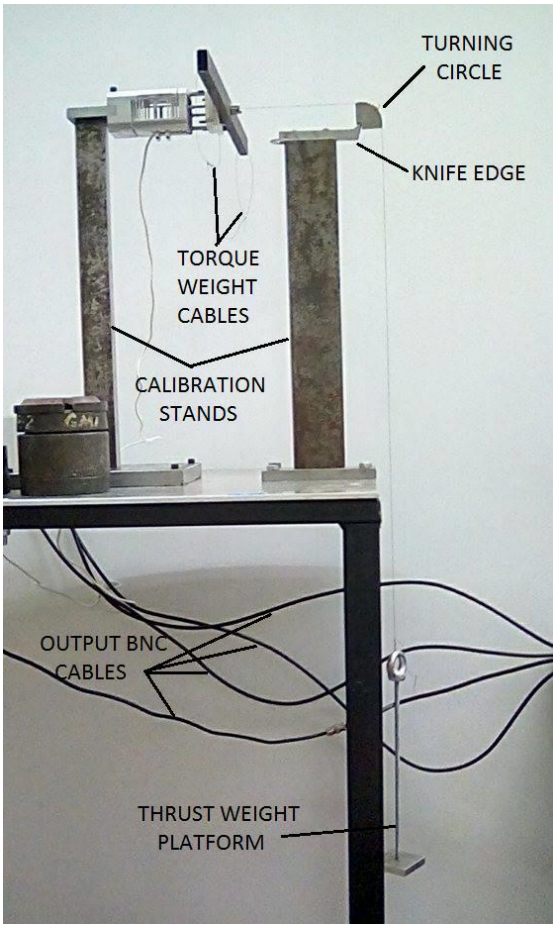

Figure 11- Calibration Set-up [2]

3.3 TEMPERATURE EFFECTS

Most internal balances are temperature compensated [5]. However, some balance designs show sensitivity to temperature gradients. With this in mind, an effort should always be made to minimize temperature gradients across the internal balance during testing within a wind tunnel. Due to the complication of both use and calibration, a temperature difference between the metric and non-metric part is typically not characterized during a balance calibration [5]. In this thesis, all efforts were made to minimize temperature effects during wind tunnel testing, and a thermocouple was integrated within the test stand to monitor the internal temperature of the nacelle constantly. Cooling air is supplied to the nacelle to combat the heat generated by the electric motor.

CHAPTER 4 – PROBLEM STATEMENT

In this study, improvements were made to a previous propeller test stand. Various issues drove the development of the new design and the new features that were integrated. When operating in the proximity of a nacelle, the performance of a propeller could significantly be affected. A need for a low-blockage nacelle was necessary in order to preserve the efficiency of the propellers being tested for comparison studies. A blockage ratio is created between the propeller diameter and the diameter of the nacelle. This affects the efficiency of the propeller and causes a shift in the advance ratio at which peak efficiency occurs [7]. From the previous test stand, zero-shifts were identified from the mechanical hysteresis due to the wires bridging the metric gap. Due to the effects of temperature on the load cell, it is necessary to put forth the best effort to keep a constant temperature over the surface of the load cell. With this in mind, an effort was made to create a chamber that isolated the motor from the load cell using bulkheads. In addition to the bulkheads, an air-cooling manifold was attached to one half of the nacelle which had a vinyl tube connected to it in order to continually supply compressed air across the motor during operation. Integrated with this was an internal thermocouple which monitors the nacelle temperature where the motor is mounted. Since repeatability of data is one of the main concerns, a need to address setting constant motor RPM was necessary. From the previous test stand the RPM was observed to fluctuate during the collection of data, so it was necessary to improve upon setting more stable RPM values. This called for a new method to read the RPM. A metallic head was machined from a single piece of steel and was then attached to the motor shaft using set screws. Since vibration is always of concern, care was taken to make the part symmetrical and balanced. Also, a rubber mount was placed between the bottom plate of the test stand and the base of the wind tunnel to minimize the vibration within the test stand during operation.

Additional improvements were made to an existing LabVIEW code for data acquisition during testing. During operation, it was challenging to maintain a steady tunnel velocity to achieve a set value for the advance ratio, so the code was upgraded in order to maintain closed loop velocity control which allows the user to set the desired velocity to be maintained by the tunnel. This improvement dramatically improved the ability to repeat a specific advance ratio. Sometimes residual forces would remain on the load cell after a test was performed and these forces had to be tarred before initializing another test. In the previous code, the user would have to go within the block diagram portion of LabVIEW to zero out the values of thrust and torque before the next test run. This was a tedious

task and the need for a more convenient way to achieve this was necessary. The code was therefore improved to allow the user to quickly add tare values by the simple adjustment of a knob on the front panel of the LabVIEW software.

CHAPTER 5 – TEST STAND DESIGN AND DEVELOPMENT

5.1 DESIGN AND MANUFACTURE OF THE NACELLE BY A VACUUM BAGGING PROCESS

The nacelle used in the development of this test stand was modeled initially in Autodesk Inventor. A close-fitting pseudo-elliptical geometry was obtained using the spline control vertex tool in the software. A drawing shown in Appendix C.4 gives the x and y coordinates of the nacelle's geometry. Figure 12 shows a CAD model of the test stand and its interior components. The new nacelle is shown in green. The technique employed to manufacture the final product was a process called vacuum bagging. Vacuum bagging is a technique employed to create mechanical pressure on composite laminates during the cure cycle [8]. The completed nacelle was manufactured at ODU in two halves to provide ease of access to the internal components of the test stand when necessary. The two halves of the nacelle were created using a CNC machined tooling-foam plug (Figure 13) created at ODU's machine shop which served as the mold for the fiberglass nacelle in the design process. West System 105 Epoxy Resin and West System 206 slow hardener was used with 24 oz. fiberglass cloth in order to mold the final nacelle.

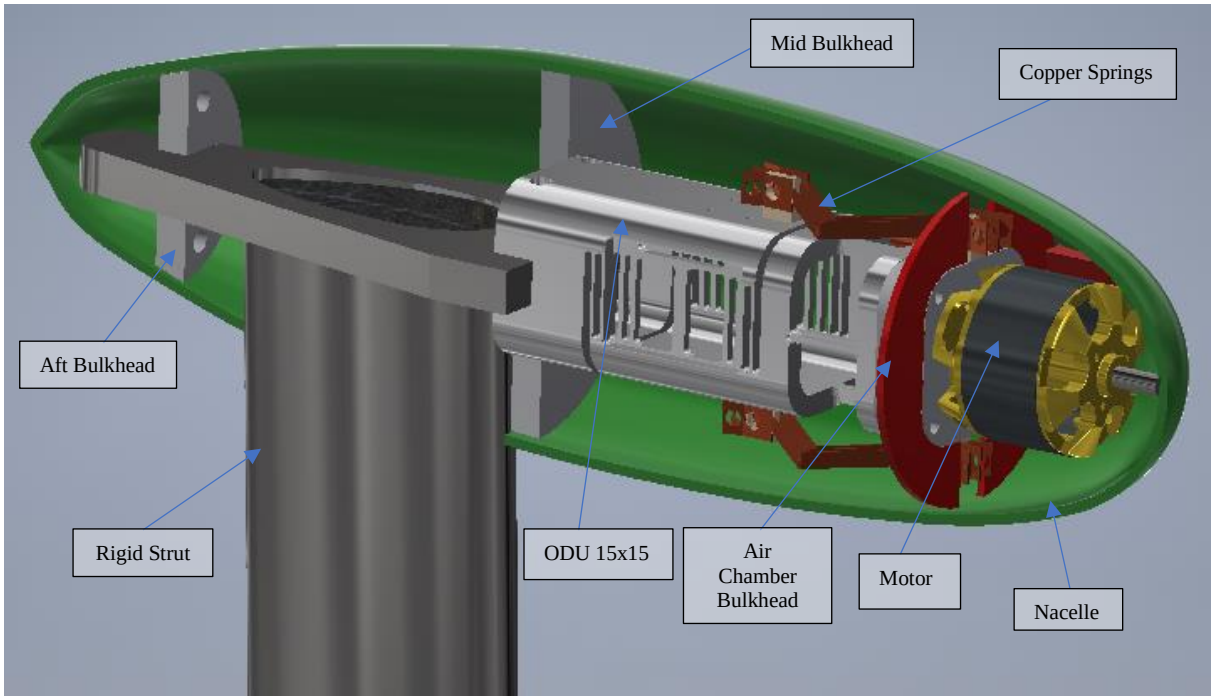

Figure 12- Propeller test stand CAD model

Figure 13 – Machined plug used for vacuum bagging of the nacelle

A vacuum bagging system was created using a Zeny 1 stage vacuum pump. A bleed valve was installed to the vent of the pump which was used to adjust the amount of vacuum pressure that was applied to the system. A hose ran from the suction side of the pump to a catch tank which is used to protect the pump in case excess resin gets pulled from the bagging system during operation. A vacuum gauge installed on the catch tank provided a means to measure the vacuum which is placed on the system and also helped to determine if a leak was present during operation. A second hose which had a vacuum shut off valve was also installed to the catch tank, and this suction line was placed in the plastic bag which housed the part. The machined plug was covered with a breather cloth, peel ply, fiberglass cloth with epoxy resin mixed with a hardener before it was placed in the bag. Figure 14 shows the complete vacuum bagging system during operation. The part remained under a vacuum pressure of approximately 25 -27in Hg for 12 hours. The part then remained in the bag for an additional 12 hours to cure completely. Upon completion, the cured part was then removed from the bag and cleaned and trimmed. This process was then repeated for the other half of the nacelle. Final finishing involved fixing all minor defects by sanding and adding additional layers of fiberglass to the interior where necessary. The nacelle was then painted with several layers of sanding primer followed by sanding and then finally painted and coated with a transparent layer to preserve the final finish.

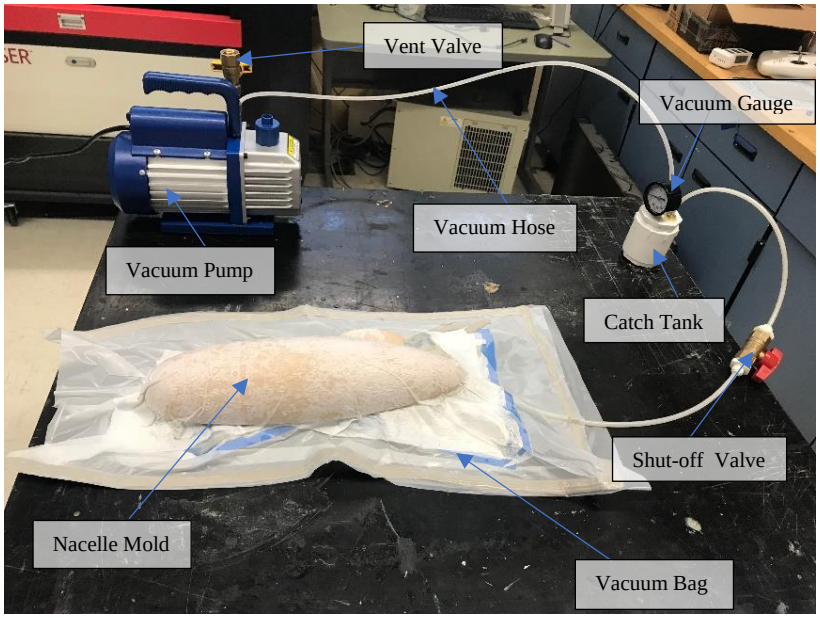

Figure 14 – Vacuum bagging equipment set-up

The completed product can be seen in Figure 15, with the nacelle installed and mounted to the test stand in ODU's low-speed wind tunnel. The nacelle is mounted to an existing rigid strut with a symmetrical airfoil shape which is welded to a base steel plate. The base plate was placed on top of a rubber base in order to reduce vibration effects to the test stand during operation. The test stand was securely bolted to the base of the wind tunnel test section. Figure 16 shows a cross-sectional view of the nacelle mounted in the test section with the interior components assembled. In order to mount the nacelle to the test stand two aluminum bulkheads were machined and mounted to the aft and midsection of the nacelle.

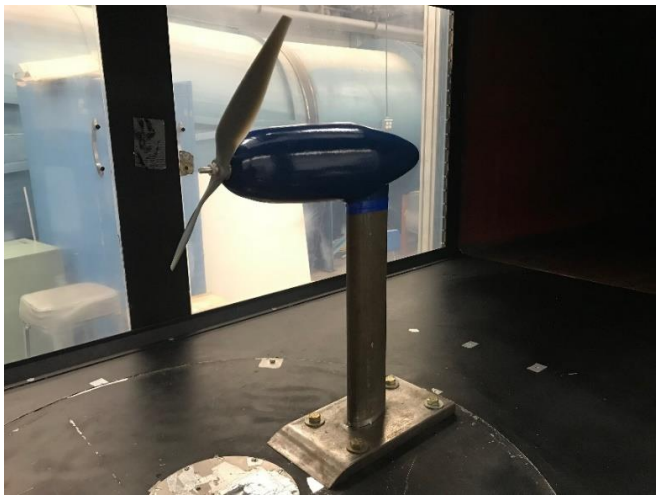

Figure 15 – Nacelle mounted to Test Stand in the wind tunnel

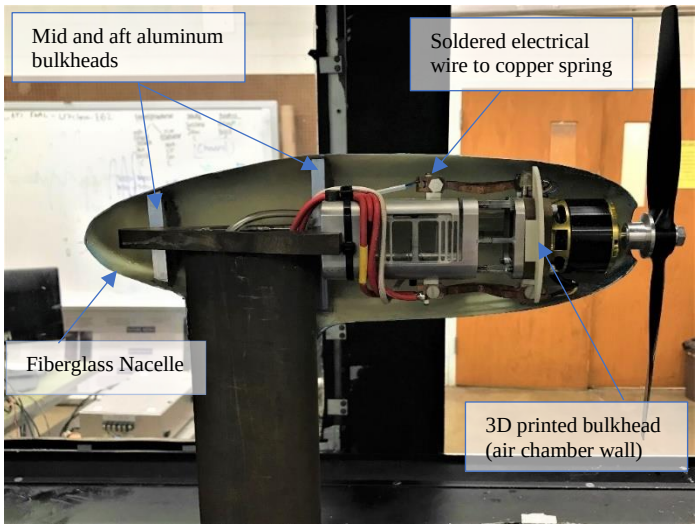

Figure 16 – Cross-sectional view of the propeller test stand

5.2 COPPER BRIDGE DESIGN FOR MOTOR AND RPM SENSOR POWER INPUT OVER METRIC GAP

There was a previous issue which affected the accuracy of data when connecting the electrical wires from the motor and proximity sensor across the load cell. The load cell has the capability of detecting relatively small forces and the tension across the wires would influence the torsional and thrust forces which are being measured by the load cell. To solve this problem a copper spring was designed to serve as a bridge for the connections of all electrical wires across the load cell. Figure 17 shows a CAD model of the copper spring design.

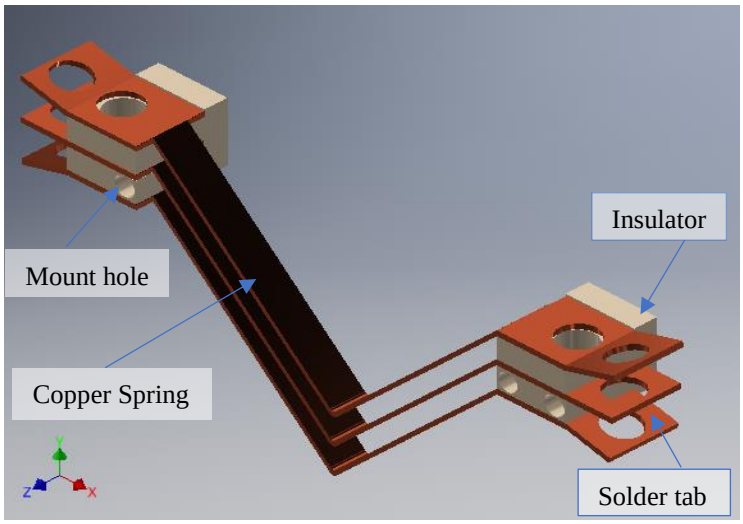

Figure 17 - Inventor model for copper spring design

In order to safely design the copper spring, the current carrying capacity of copper had to be determined, and calculations were done to ensure the cross-sectional area of each copper spring was sufficient enough to carry 50 Amps of current safely [9]. Knowing the cross-sectional area of each spring and using the current load rating a safe area was determined and used in the design of each copper spring [10]

AWG	Diameter *(mm)*	Diameter *(in)*	Square *(mm^2)*	Resistance Copper *(ohm/1000m)* (ohm/1000ft)	Typical Max. Current Load Ratings - Copper *(amps)*[1]					
					Single Core	Multicore				
						up to 3 cores	4 - 6 cores	7 - 24 cores	25 - 42 cores	43 and above
40	0.08	.	0.0050	3420						
39	0.09	.	0.0064	2700						
38	0.10	0.0040	0.0078	2190						
37	0.11	0.0045	0.0095	1810						
36	0.13	0.0050	0.013	1300						
35	0.14	0.0056	0.015	1120						
34	0.16	0.0063	0.020	844						
33	0.18	0.0071	0.026	676						
32	0.20	0.0080	0.031	547						
30	0.25	0.010	0.049	351						
28	0.33	0.013	0.080	232						
27	0.36	0.014	0.096	178						
26	0.41	0.016	0.13	137						
25	0.45	0.018	0.16	108						
24	0.51	0.020	0.20	88	3.5	2	1.6	1.4	1.2	1.0
22	0.64	0.025	0.33	52	5.0	3	2.4	2.1	1.8	1.5
20	0.81	0.032	0.50	34	6.0	5	4.0	3.5	3.0	2.5
18	1.0	0.040	0.82	22	9.5	7	5.6	4.9	4.2	3.5
16	1.3	0.051	1.3	13	15	10	8.0	7.0	6.0	5.0
14	1.6	0.064	2.1	8.5	24	15	12	10	9.0	7.5
13	1.8	0.072	2.6	6.8						
12	2.1	0.081	3.3	5.4	34	20	16	14	12	10
10	2.6	0.10	5.3	3.4	52	30	24	21	18	15
8	3.3	0.13	8.3	2.2	75	40	32	28	24	20
6	4.1	0.17	13.3	1.5	95	55	44	38	33	27
4	5.2	0.20	21.2	0.80	120	70	56	49	42	35
3			26.7		154	80	64	56	48	40
2	6.5	0.26	33.6	0.50	170	95	76	66	57	57
1	7.4	0.29	42.4	0.40	180	110	88	77	66	55
0 (1/0)	8.3	0.33	53.5	0.31	200					
00 (2/0)	9.3	0.37	67.4	0.25	225					
000 (3/0)	10.4	0.41	85.0	0.20	275					
0000 (4/0)	11.7	0.46	107	0.16	325					
250			127		345					
300			152		390					
400			178		415					

Figure 18- Current ratings of PVC-insulated copper single and multicore wiring cables [9].

Figure 18 was used in order to determine the safe cross-sectional area required for the copper springs. From the table provided a safe cross-sectional area of 0.0082 in^2 was required to pass 52 amps safely. To maintain symmetry, two identical sets of three springs were used on opposite sides of the balance.

As seen in Figure 17, 3D printed parts were used to assemble the copper springs, and they also served as insulation between each spring to prevent an electrical short. A Finite Element Model was employed to define the geometry of the copper springs in order to minimize forces imparted by the springs. Previous results from the design of the ODU 15 x 15 balance gave the maximum displacement in the X, Y, Z component. With this displacement, the appropriate

size of the copper springs was chosen to minimize the force of resistance. Figure 19 shows the Autodesk Inventor FEA results for balance displacement [2].

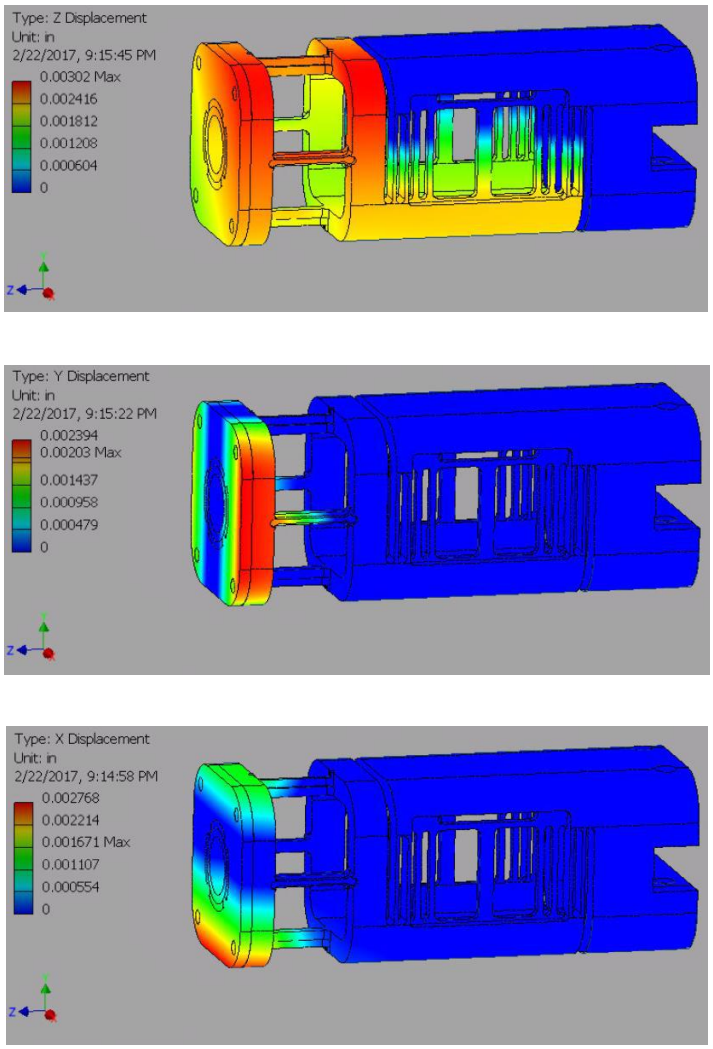

Figure 19- FEA on ODU 15 x 15 balance showing maximum displacement measured in X, Y, Z-component [2]

Figures 20 through 22 show the results obtained when applying forces to the copper spring in order to match the maximum displacement obtained from the FEA on the loadcell. A force of 0.003 lbf, 0.007 lbf, and 0.009 lbf was applied in the F_z, F_y, and F_x plane respectively. These forces were applied to one end of the copper spring while keeping the other end of the spring constrained. The results obtained verified that the thickness of the copper springs would result in negligible, repeatable additional forces.

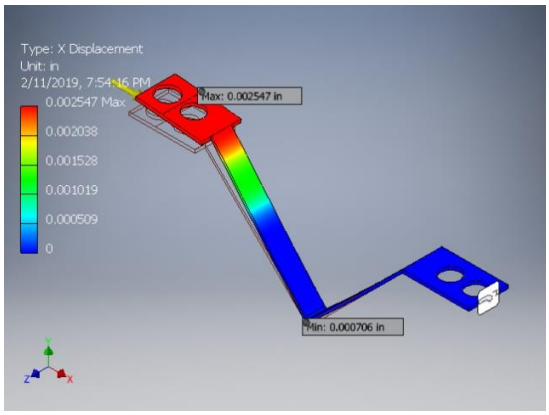

Figure 20- FEA on copper spring in the X-Displacement

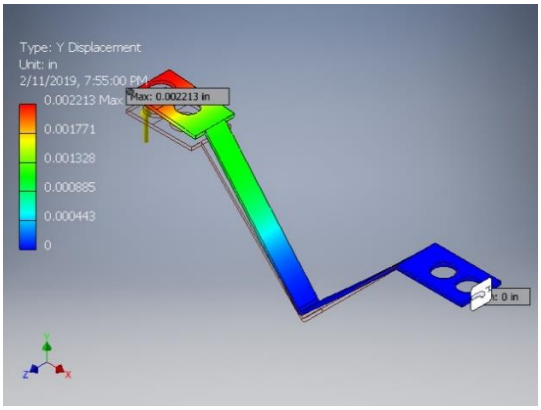

Figure 21- FEA on copper spring in the Y-Displacement

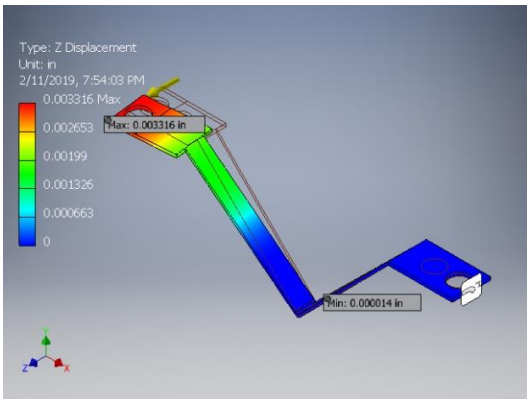

Figure 22- FEA on copper spring in the Z-Displacement

5.3 3D PRINTED AIR COOLING MANIFOLD

Cooling of the motor is necessary during testing in order to protect the motor and prevent it from shutting off during operation due to excessive heat. In order to solve this problem, a cooling plenum was designed and 3D printed and mounted to one half of the nacelle. Compressed air was piped to the cooling plenum through a vinyl

tubing as shown in Figure 23. A chamber was created in the nacelle to house the motor in order to minimize the heat flowing over the load cell. The excessive heat could affect measurements due to the expansion of the metal during data collection. The air flowing over the motor provided a means to cool the motor through convection. The other half of the nacelle had an exit hole where the hot air would escape the nacelle. A thermocouple was placed inside the nacelle in order to monitor the temperature during operation.

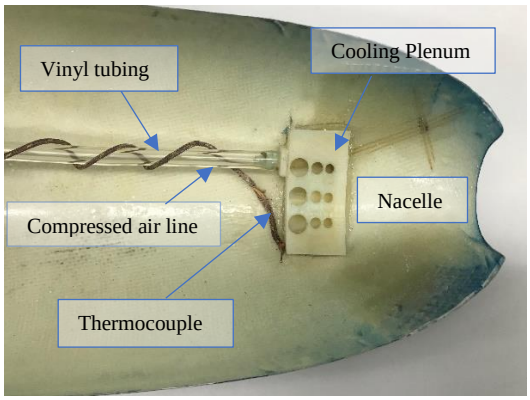

Figure 23- Cooling plenum attached to one half of the nacelle

5.4 RPM COUNTER DESIGN

In the previous test stand, the RPM counter used gave unstable values during operation. It was challenging to set the same RPM for different tests because of fluctuating values. The original design had two screw heads that were designed to be opposite from each other in order to minimize the vibration during operation. The steel hub was attached to the shaft of the motor using two set screws. Since the proximity sensor recorded two pulses per revolution due to the design of the metallic head, the RPM obtained had to be divided by two in order to obtain the actual RPM value. Figure 24 shows the previous design of the rotating screw head used with the proximity sensor.

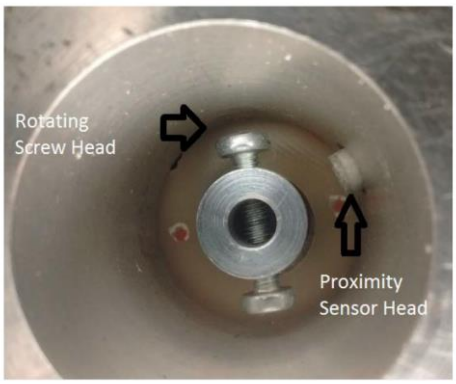

Figure 24 – Proximity Sensor installation [1]

A new counter was machined from a single steel block as shown in Figure 25. This new design showed more stable values of RPM during operations which led to improved repeatability of results. The reason the original design gave inconsistent RPM could be that the geometry was such that at a higher RPM the time the screw head spent near the sensor was too short in duration due to a slot in the screw head. It is remotely possible that there may have been screws backing out during operation causing asymmetry, leading to excessive vibrations during operation. Also since an inductive proximity sensor was used, there could be a possibility that the material composition of the screw head affected the pulse generation. Whatever the reason, pulses were not being reliably generated for each revolution of the rotating screw head.

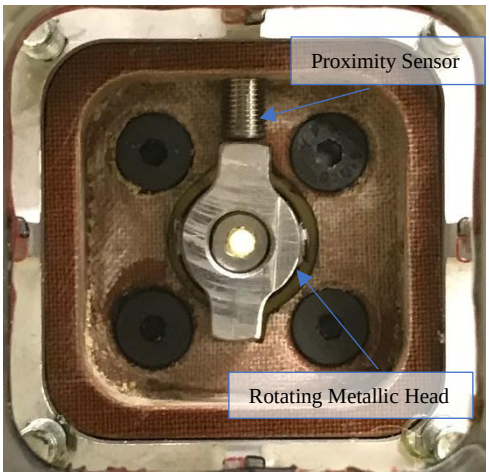

Figure 25 – New RPM counter head with the inductive proximity sensor

5.5 LabVIEW SOFTWARE INTEGRATION

LabVIEW (Laboratory Virtual Instrument Engineering Workbench), is a graphical programming language that utilizes icons instead of lines of text to create specific applications ideal for instrumentation input/output tasks and control. The codes used by LabVIEW are called Virtual Instruments (VIs) which are either created by the user or obtained from credible sources such as National Instruments. In this project, LabVIEW was used for data acquisition, signal processing, and hardware control while operating the low-speed wind tunnel. Figure 26 shows the LabVIEW front panel used for propeller data collection, test stand controls, and the wind tunnel controls. The front panel allowed for setting tunnel speed and motor RPM, hence advance ratio, while enabling real-time visuals for thrust, torque, input current, and input voltage. While operating the wind tunnel, there are constant fluctuations of the motor's RPM and the advance ratio. However, the front panel allows for the monitoring of these fluctuations to

start data collection after the system stabilizes. Also employed is a VI for monitoring the test section and motor section temperature. The LabVIEW software also allowed for the input of the propeller's diameter which is being tested and used in calculations for the performance coefficients.

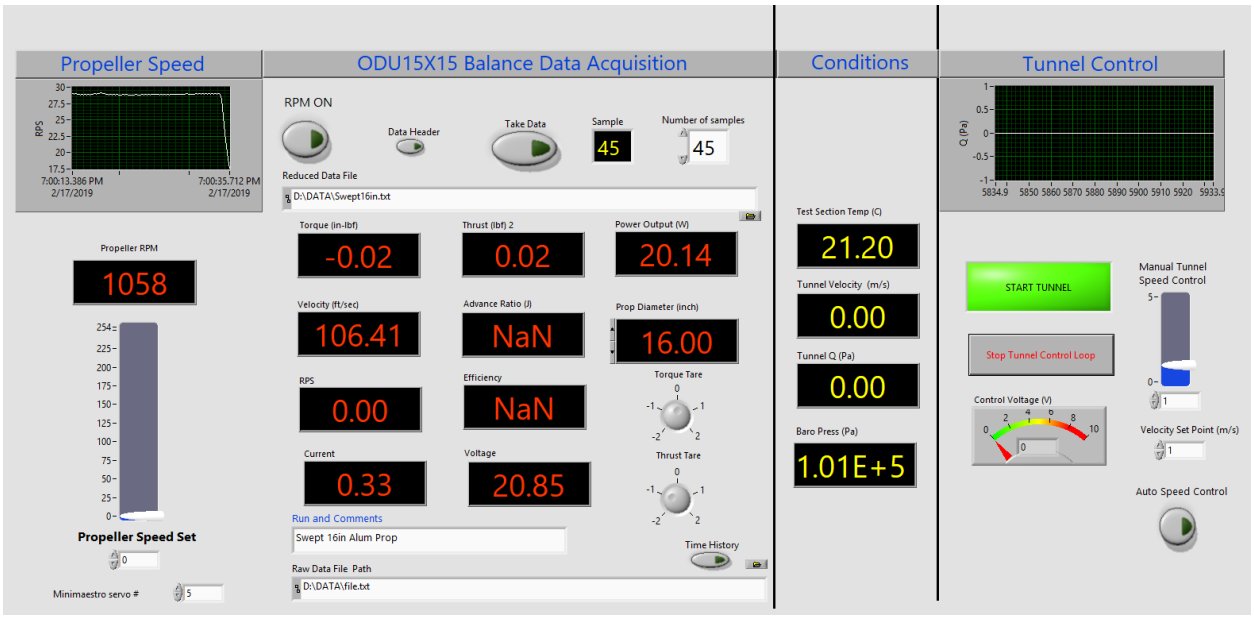

Figure 26 – LabVIEW front panel

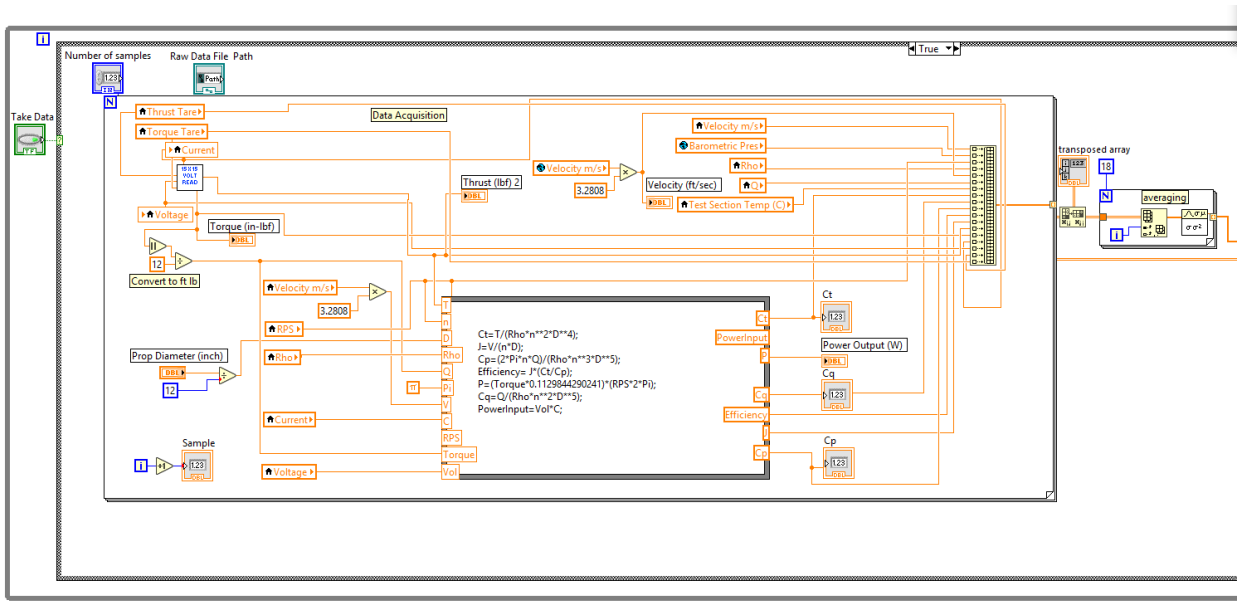

Figure 27 – LabVIEW rear panel of load cell input and formula node showing calculations of coefficients

The rear panel is the section where the code is developed using block diagrams. Figure 27 shows improvements made to a current block diagram which held the formula nodes to calculate the coefficients used in characterizing the tested propellers. Additionally, modifications done in the rear panel allowed for the ability to quickly adjust the tare values for thrust and torque which sometimes have residual values throughout the experimentation, this improvement allowed for the more accurate and consistent collection of data. The propeller test code calls on a NI- data acquisition (DAQ) board (PCI-6221) which is connected to the computer through a PCI card slot. Integrating the DAQ device with the PCI-6221 allowed the user to sample analog voltages from the balance and for motor voltage and current measurement, and also used the counter for the RPM signal. The electronic speed controller is integrated with the Mini Maestro which allows the user to control the motor controller ESC and hence speed via LabVIEW. Coefficient calculations are performed, samples averaged then conveniently written to a text file location selected by the user. Improvements were made to a previous LabVIEW code in order to obtain a closed loop velocity control of the wind tunnel. Velocity is computed using the dynamic pressure, and test section temperature and atmospheric pressure. The tunnel speed is adjusted through an analog voltage out using a PID controller, a built-in function in LabView. The wind tunnel fan speed is set through the variable frequency drive, proportional to the commanded analog voltage. This allows the user to set a precise velocity of the tunnel through the LabVIEW front panel while automatically maintaining that speed through the duration of the data collection. The previous code was modified in order to achieve this. The LabView code is shown in Appendix A and A.1.

5.6 TESTING PROCEDURE

Before the beginning of testing, the compressed air to the nacelle was turned on to ensure sufficient cooling of the motor. The propeller to be tested was installed on the motor shaft, and the tunnel was checked to ensure it was clear of any obstructions. After the test section was closed the power to the motor was then powered on. With the tunnel controls powered on, the LabVIEW software was started and the appropriate propeller diameter being tested was entered to be used in the calculations. Figure 28 shows the location where the propeller test stand is mounted (model location). This is the high-speed test section of the ODU low-speed wind tunnel. The user then designates the name and location of the test data file. Before the motor was turned on, all residual values of thrust and torque were zeroed out using the tare control knobs on the front panel. After those initial steps were completed the user

then entered the desired speed of the motor using the slider on the front panel. The tunnel was turned on, and the tunnel velocity was set and maintained using the closed loop feature from the front panel. Once the tunnel has stabilized, the user then turns on the take data button which triggers the software to collect a user-designated number of samples (45 shown). Each sample takes about one second to obtain. After the completion of the data collection, data is retrieved from the file location designated by the user.

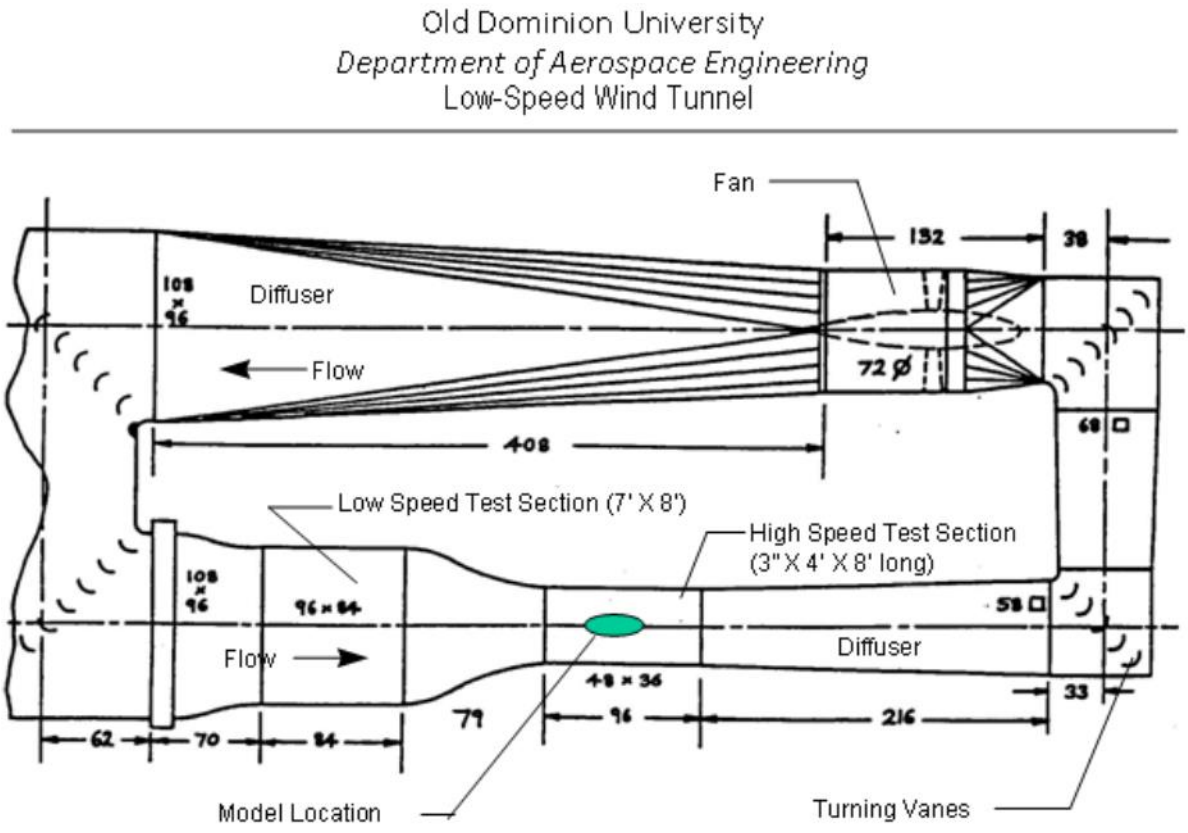

Figure 28 - ODU Low-Speed Wind Tunnel Diagram (Dimension in Feet/Inches)

CHAPTER 6 – RIGOROUS TEST DESIGN USING STATISTICAL ENGINEERING

A statistical engineering methodology was followed using the principles of Design of Experiments (DOE) and Response Surface Methods (RSM). A completely randomized run order was chosen, one of the guiding principles for DOE. Other principles include replication of data and blocking which deals with nuisance factors [11]. The basic building blocks of DOE are factorial designs, where all possible combinations of factor levels are tested. DOE was first seen in agriculture starting around 1918 where Sir Ronald A. Fisher and his co-workers made a profound impact on agricultural science using factorial designs and ANOVA [12]. In a designed experiment the engineer makes deliberate or purposeful changes in the controllable variables of the system or process, observes the resulting system output data, and then makes an inference or decision about which variables are responsible for the observed changes in output performance [13].

The experiment design chosen for this experiment was a factorial multilevel design which is also known as a general factorial. In this thesis, two factors were chosen one for RPM and the other for the advance ratio. Five levels were chosen for the advance ratio in order to cover the design space, support up to quartic models, and provide adequate power with a good prediction variance distribution. RPM levels were chosen as either one, two or three levels depending on the objective of the experiment, comparison or characterization. The design was replicated with one block per replicate in order to isolate any run to run variability. The regression model representation of the general factorial experiment with main effects, two-factor interactions, and pure quadratics can be seen in equation 7. Here x_1 represents advance ratio and x_2 RPM. Higher order terms up to fourth order in advance ratio are supported.

$$y = \beta_0 + \beta_1 x_1 + \beta_2 x_2 + \beta_{12} x_1 x_2 + \beta_{11} x_{11}^2 + \varepsilon \qquad (7)$$

In the equation above y is the response, β are the fitted regression coefficients, x represents the independent variables, and ε is the random error term. A general factorial design is shown in Table 1 for the APC 12 x 8 propeller. There are two factors involved in the design, RPM and J. The RPM contains three levels while J contains five levels. The design was assigned one replicate, it contained 30 runs with one block per replicate in order to account for nuisance factors. The experiment was then carried out in the random run order generated by Design Expert.

Std	Run	Factor 1 A:RPM	Factor 2 B:J
29	1	5000	0.65
23	2	5000	0.38
27	3	6000	0.51
18	4	6000	0.10
10	5	4000	0.51
13	6	4000	0.65
20	7	5000	0.24
16	8	4000	0.10
7	9	4000	0.38
8	10	5000	0.38
15	11	6000	0.65
3	12	6000	0.10
28	13	4000	0.65
1	14	4000	0.10
21	15	6000	0.24
6	16	6000	0.24
9	17	6000	0.38
25	18	4000	0.51
17	19	5000	0.10
30	20	6000	0.65
5	21	5000	0.24
22	22	4000	0.38
11	23	5000	0.51
19	24	4000	0.24
24	25	6000	0.38
26	26	5000	0.51
4	27	4000	0.24
14	28	5000	0.65
12	29	6000	0.51
2	30	5000	0.10
31	**31**	**4500**	**0.55**
32	**32**	**5500**	**0.30**
33	**33**	**4500**	**0.30**
34	**34**	**5500**	**0.55**

Table 1- General Factorial Design for APC Thin Electric 12 x 8 Propeller.

Figure 29 indicates the design space created for the model and shows the actual achievable values of factor combination.

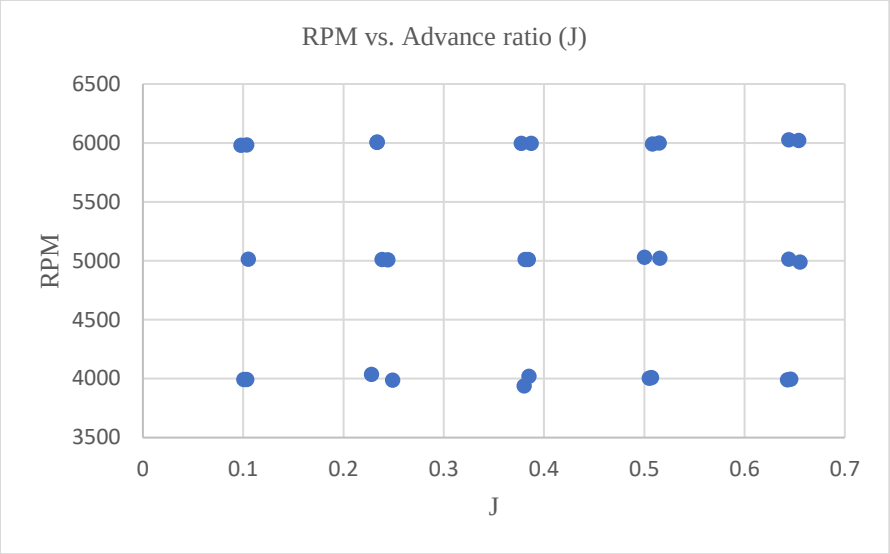

Figure 29 – RPM vs. Advance Ratio (J) for APC 12 x 8

A response surface is the regression model predictions in response to changes in the factors. The response surface is shown (figure 30) for the efficiency of one propeller used in this study. It can be used to show the optimum and minimum efficiency with the corresponding RPM value.

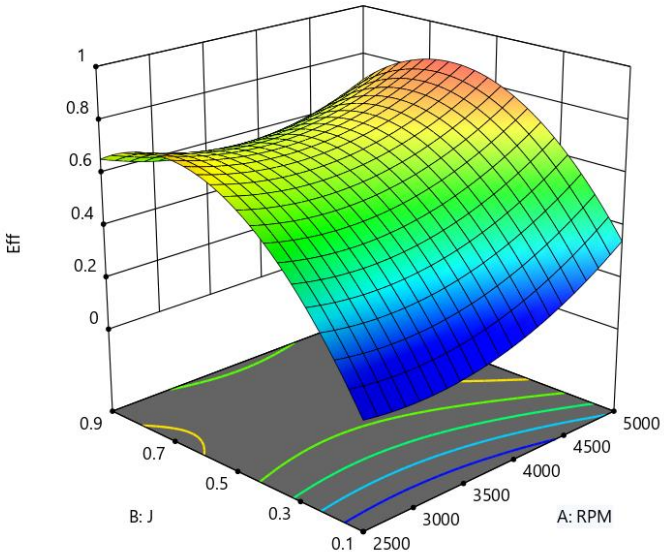

Figure 30- Efficiency Response Surface for APC Thin Electric 14 x 12 propeller

6.1 PROPELLER CHARACTERIZATION EXPERIMENT DESIGN AND ANALYSIS DETAILS

The randomized run order shown in Table 2 represents the design used to carry out the experimentation for the 16 in straight blade aluminum propeller. This design has RPM at two levels and J at 5 levels with four responses C_T, C_Q, C_P and η observed. The design has one replicate and contains a total of 20 runs with one block assigned per replicate. Run number 14 was omitted from the model because it was an outlier in efforts to help improve the model fit. Runs 21 through 24, shown in bold, are the confirmation points which are not used in the analysis but are used to determine the prediction capability of the model.

Std	Block	Run	Factor 1 A:RPM	Factor 2 B:J	Response 1 Ct	Respone 2 Cq	Response 3 Cp	Response 4 Eff
3	Block 1	1	3525.38	0.38501	0.0704193	0.00656729	0.0412635	0.657046
9	Block 1	2	3505.84	0.654431	0.0240268	0.00353754	0.022227	0.70756
6	Block 1	3	4987.48	0.477265	0.0536914	0.00555987	0.0349337	0.733553
1	Block 1	4	3503.51	0.291125	0.0800913	0.0068329	0.0429324	0.543105
4	Block 1	5	4995.23	0.372223	0.0692766	0.00626408	0.0393584	0.65518
2	Block 1	6	4989.96	0.290956	0.0789659	0.00655105	0.0411614	0.558182
10	Block 1	7	5022.3	0.649454	0.0224966	0.00327229	0.0205604	0.710616
8	Block 1	8	4983.65	0.568606	0.0382852	0.00453451	0.0284912	0.764074
5	Block 1	9	3535.31	0.468186	0.0575459	0.00606033	0.0380782	0.707623
7	Block 1	10	3524.2	0.563031	0.0414764	0.00505748	0.0317771	0.735024
16	Block 2	11	4985.8	0.465834	0.055791	0.00563531	0.0354077	0.734015
12	Block 2	12	4977.65	0.292897	0.079116	0.00647637	0.0406922	0.569468
14	Block 2	13	4983.19	0.378157	0.068644	0.00619834	0.0389453	0.666542
~~19~~	~~Block 2~~	~~14~~	~~3512.34~~	~~0.656023~~	~~0.0220159~~	~~0.00349505~~	~~0.02196~~	~~0.657818~~
18	Block 2	15	4991.23	0.557028	0.040456	0.00468992	0.0294676	0.764768
13	Block 2	16	3486.53	0.386689	0.0686656	0.00646451	0.0406177	0.653723
17	Block 2	17	3496.93	0.556568	0.0424263	0.00511614	0.0321456	0.734664
15	Block 2	18	3495.95	0.466193	0.0571979	0.00600142	0.0377081	0.707185
20	Block 2	19	5002.31	0.65264	0.0221637	0.00321264	0.0201856	0.716632
11	Block 2	20	3499.23	0.286217	0.0804335	0.00672554	0.0422578	0.544795
21	**Block 1**	**21**	**3770.06**	**0.328429**	**0.0775221**	**0.0064142**	**0.0403017**	**0.631766**
22	**Block 1**	**22**	**4766.91**	**0.599512**	**0.0328134**	**0.0040416**	**0.0253939**	**0.774782**
23	**Block 1**	**23**	**3760.25**	**0.609365**	**0.03285**	**0.0040966**	**0.0257398**	**0.77776**
24	**Block 1**	**24**	**4751.28**	**0.344779**	**0.0731286**	**0.0063167**	**0.039689**	**0.635279**

Table 2- Actual Design for 16 in Straight Blade Aluminum Propeller

Figures 31 through 34 show the normal probability plots for C_T, C_Q, C_P, and η. The plots were used in the validation of the normality assumption. All the residuals lie along a straight line passing the "fat pencil" test except for one outlier for run number 14 in the efficiency plot. Even though there was one outlier, every other residual was normally distributed, and the normality assumption was validated. The outlier could have been caused by many factors to include increased operating temperature or residual torque and thrust forces being present on the balance during that run.

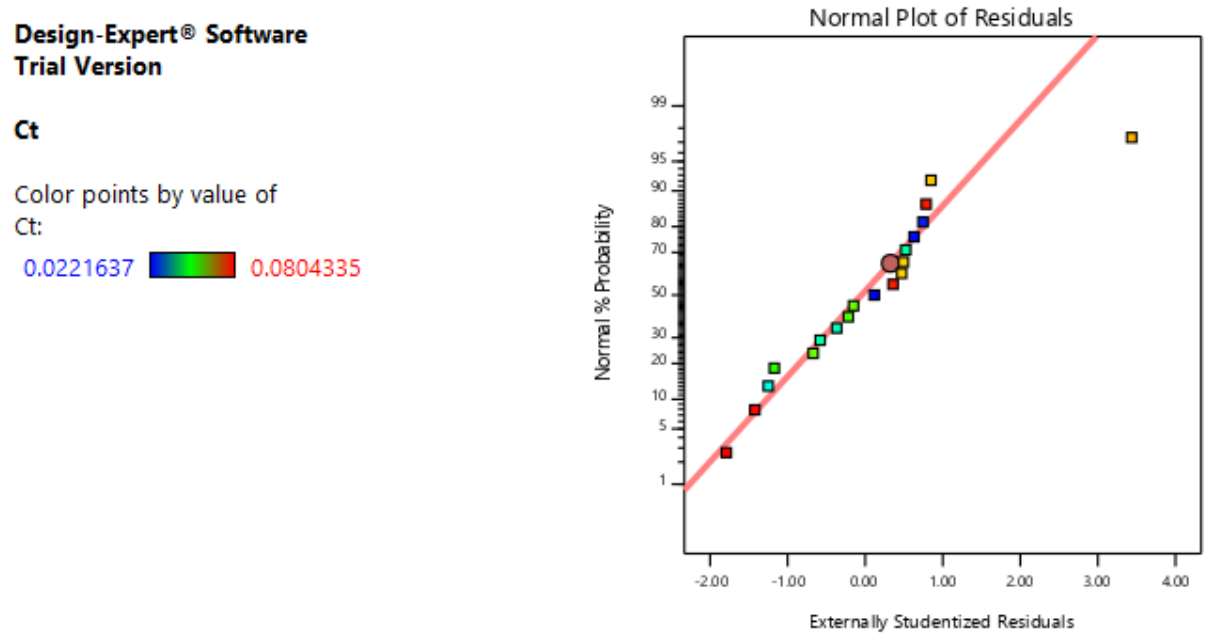

Figure 31- Normal Probability Plot of C_T for 16 in Straight Blade Aluminum Propeller

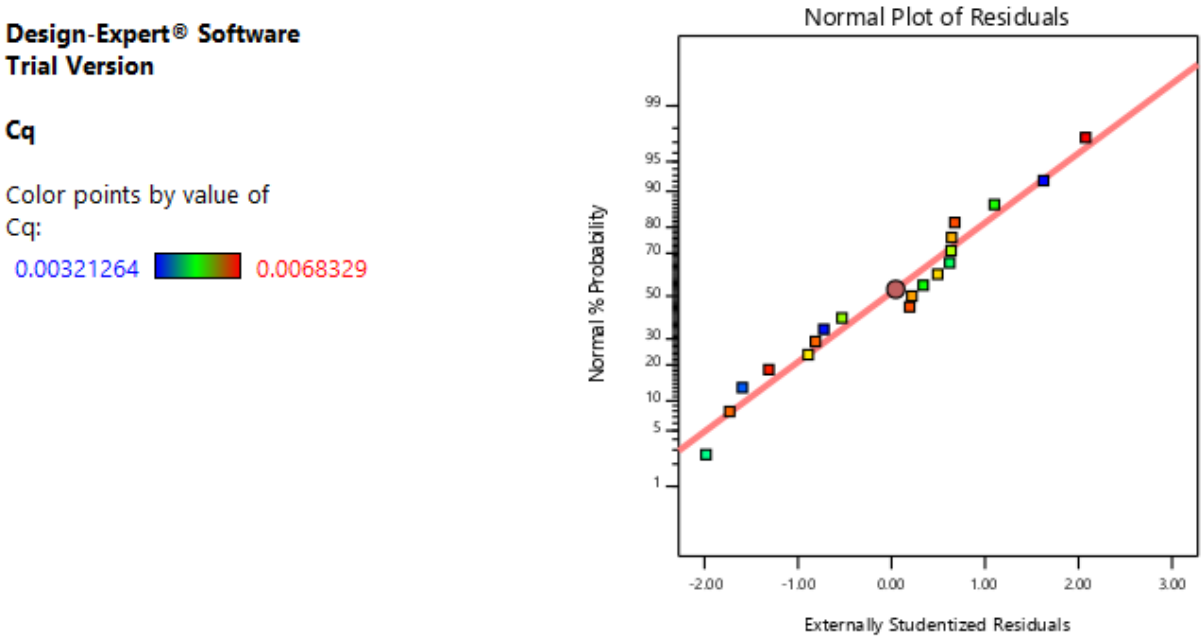

Figure 32- Normal Probability Plot of C_Q for 16 in Straight Blade Aluminum Propeller

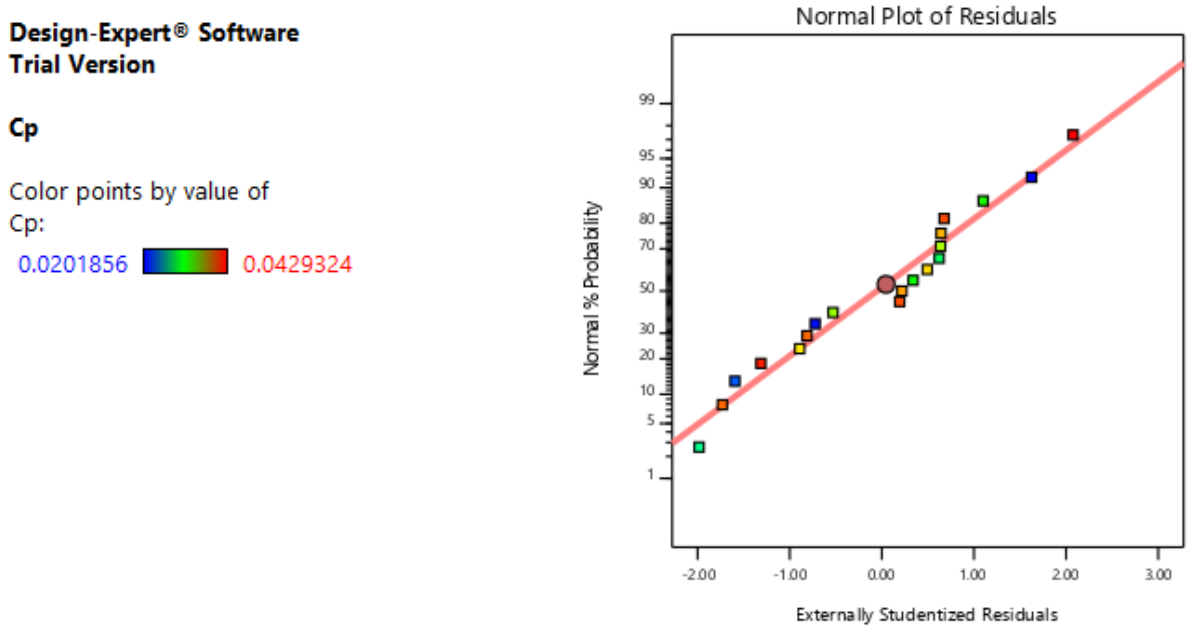

Figure 33- Normal Probability Plot of C_P for 16 in Straight Blade Aluminum Propeller

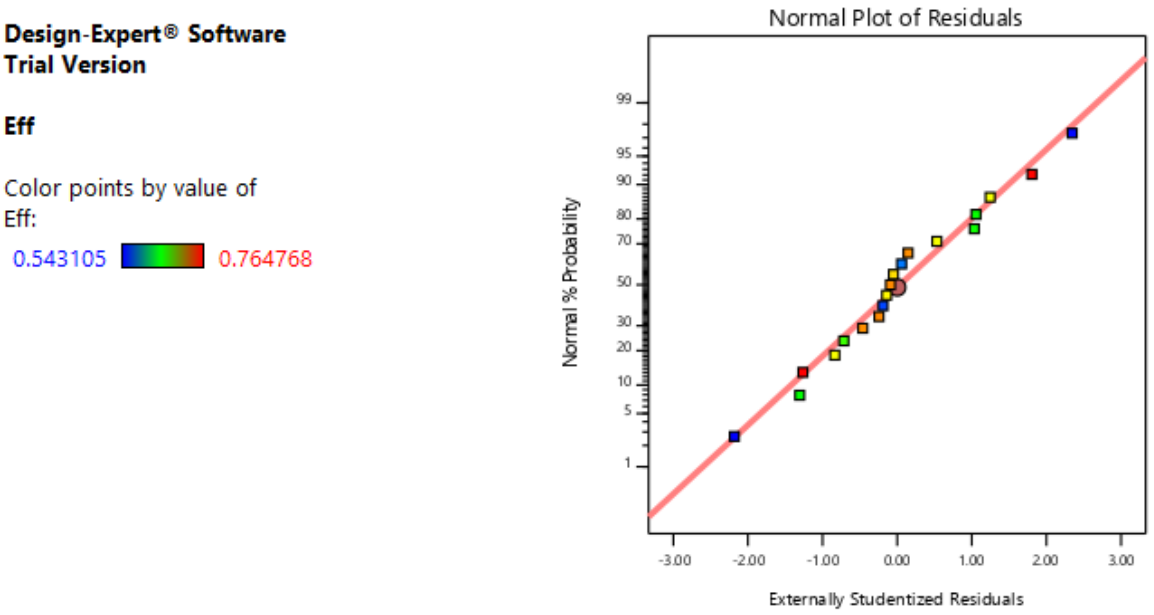

Figure 34- Normal Probability Plot of η for 16 in Straight Blade Aluminum Propeller

The following plots (Figures 35 through 38) shows the residual versus predicted analysis which is used to validate the constant variance assumption. No coning nor barreling shape was observed, and all residuals are bounded within the normal limits. The constant variance assumption is therefore satisfied.

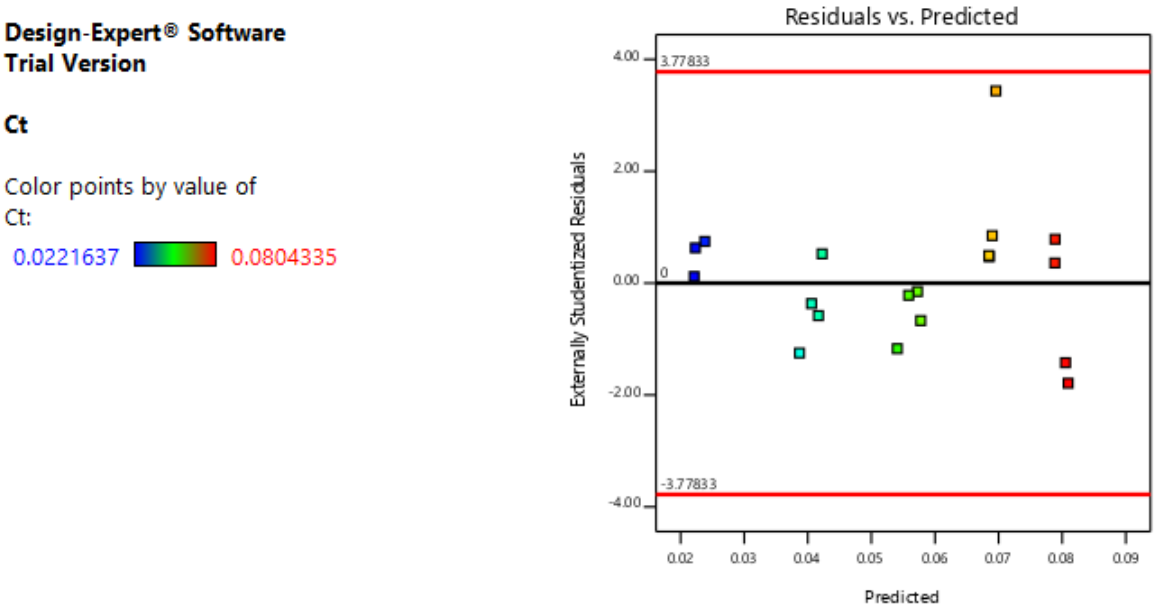

Figure 35- Residuals vs. Predicted Plots of C_T for 16 in Straight Blade Aluminum Propeller

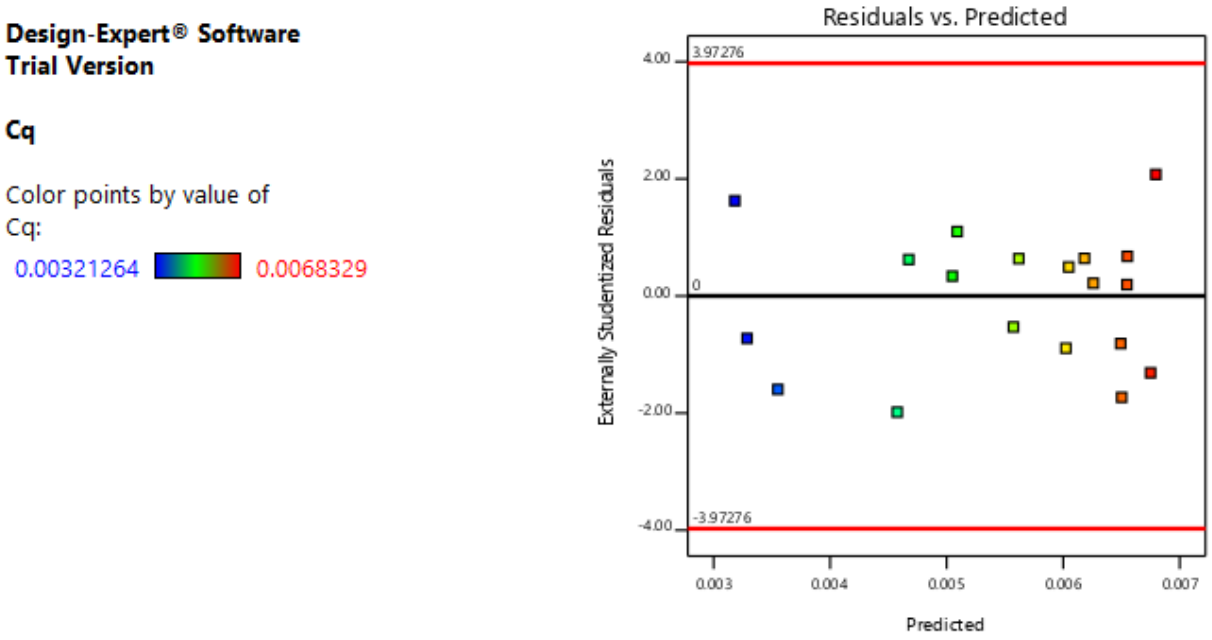

Figure 36- Residuals vs. Predicted Plots of C_Q for 16 in Straight Blade Aluminum Propeller

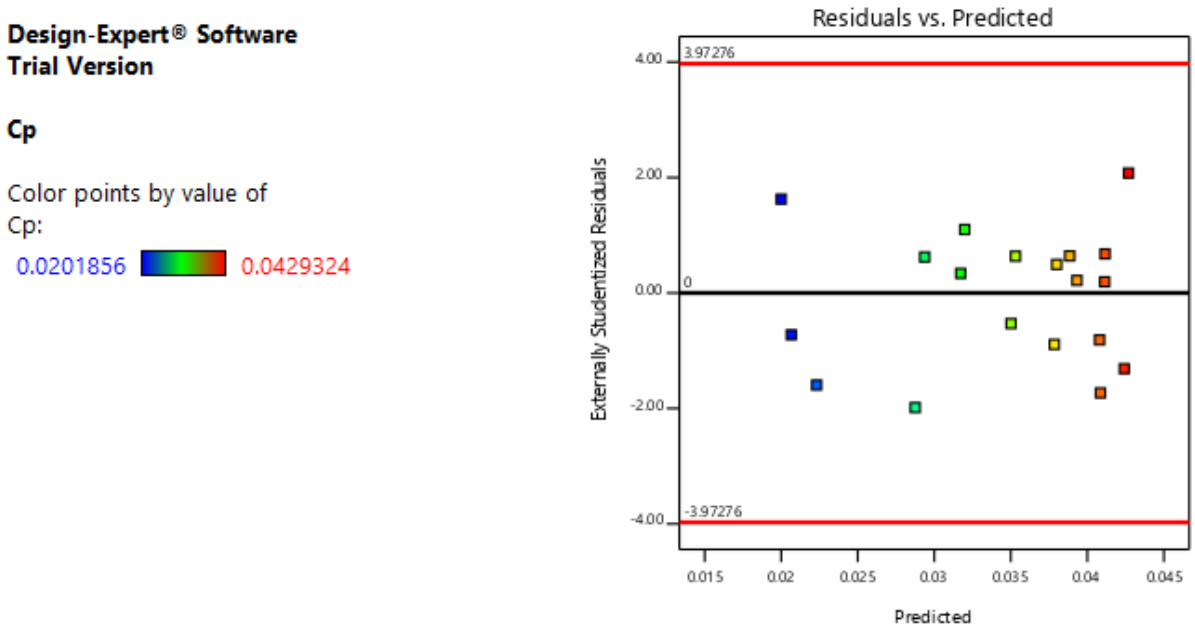

Figure 37- Residuals vs. Predicted Plots of C_P for 16 in Straight Blade Aluminum Propeller

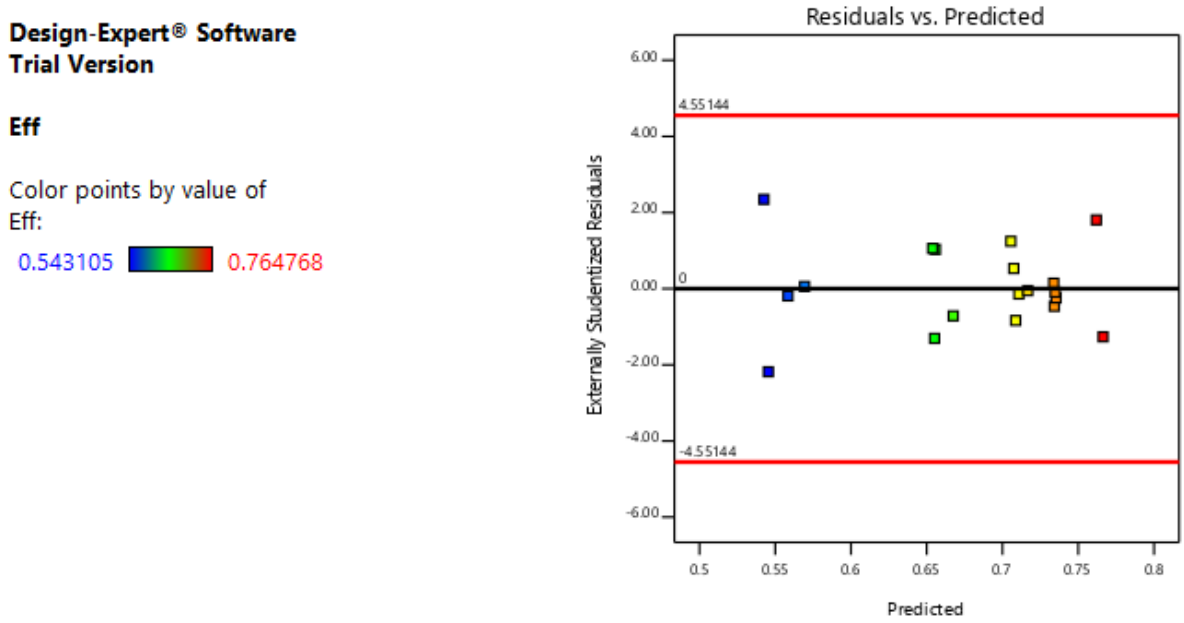

Figure 38- Residuals vs. Predicted Plots of η for 16 in Straight Blade Aluminum Propeller

Figures 39 through 42 show the Residual vs. Run plots of C_T, C_Q, C_P and η. These plots were used to identify the independence of the responses with time. The plots show a random oscillation around the zero line with no trends. This validates the independence assumption. The independence assumption is tested to discover if any time-dependent trends exist. Thermal shifts are a good example of a violation.

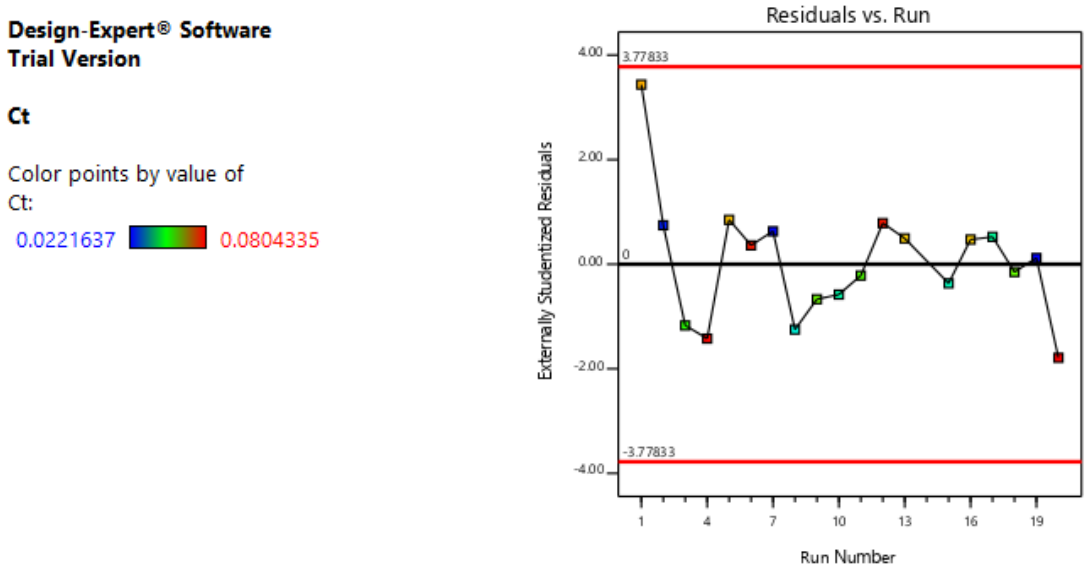

Figure 39- Residuals vs. Run Plots of C_T for 16 in Straight Blade Aluminum Propeller

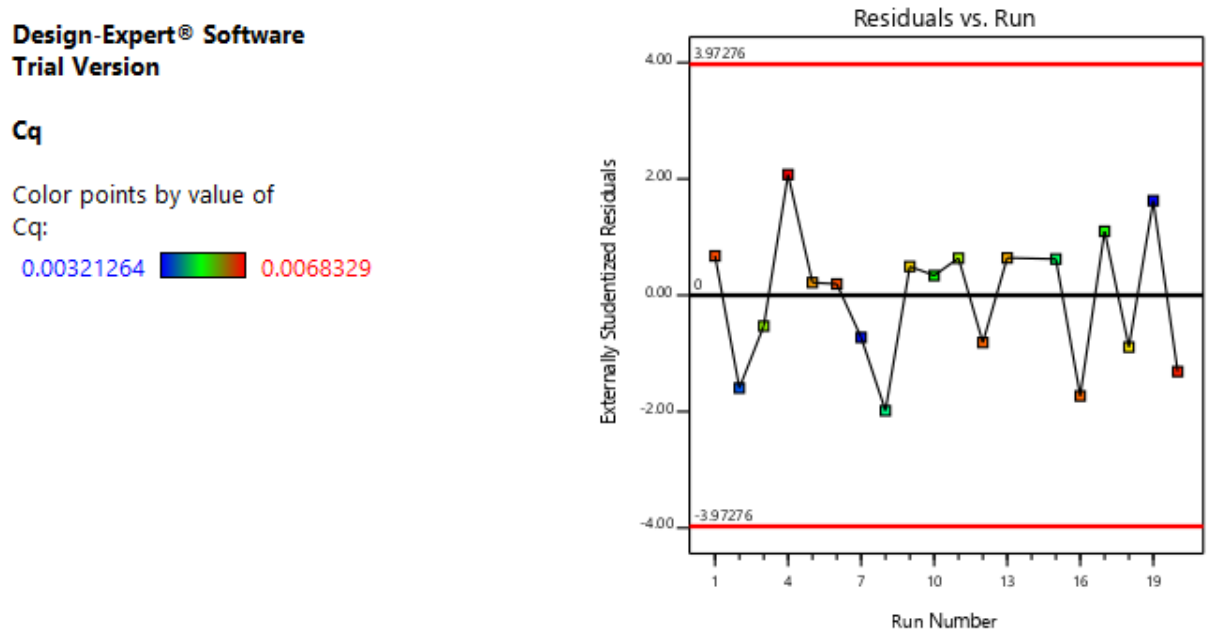

Figure 40- Residuals vs. Run Plots of C_Q for 16 in Straight Blade Aluminum Propeller

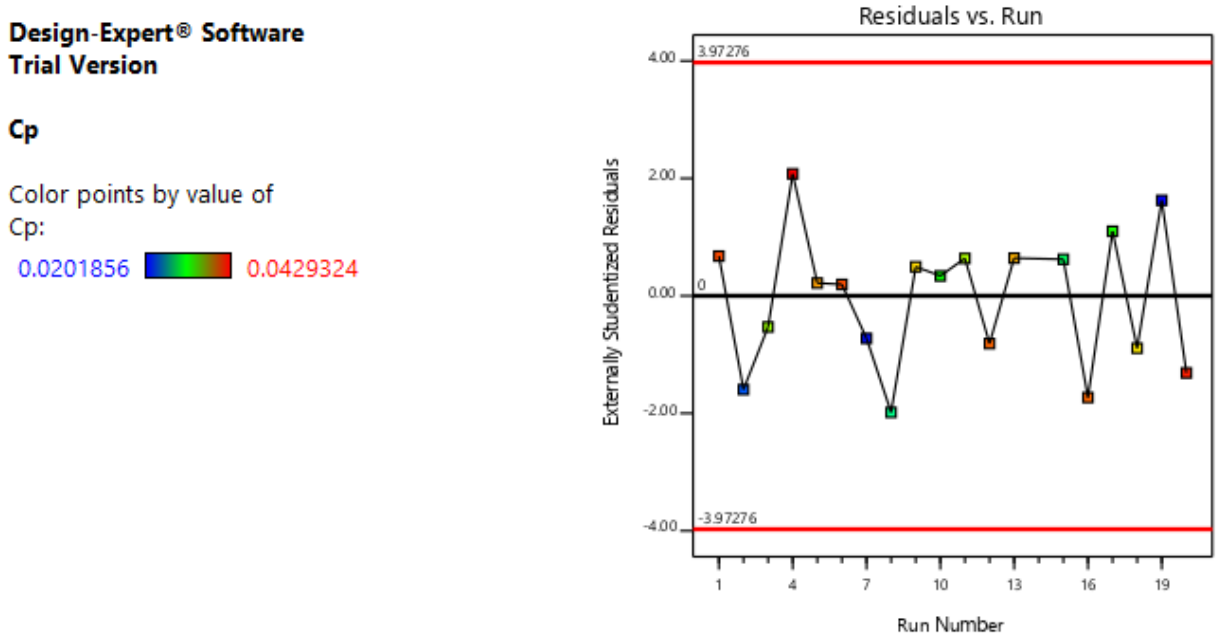

Figure 41- Residuals vs. Run Plots of C_P for 16 in Straight Blade Aluminum Propeller

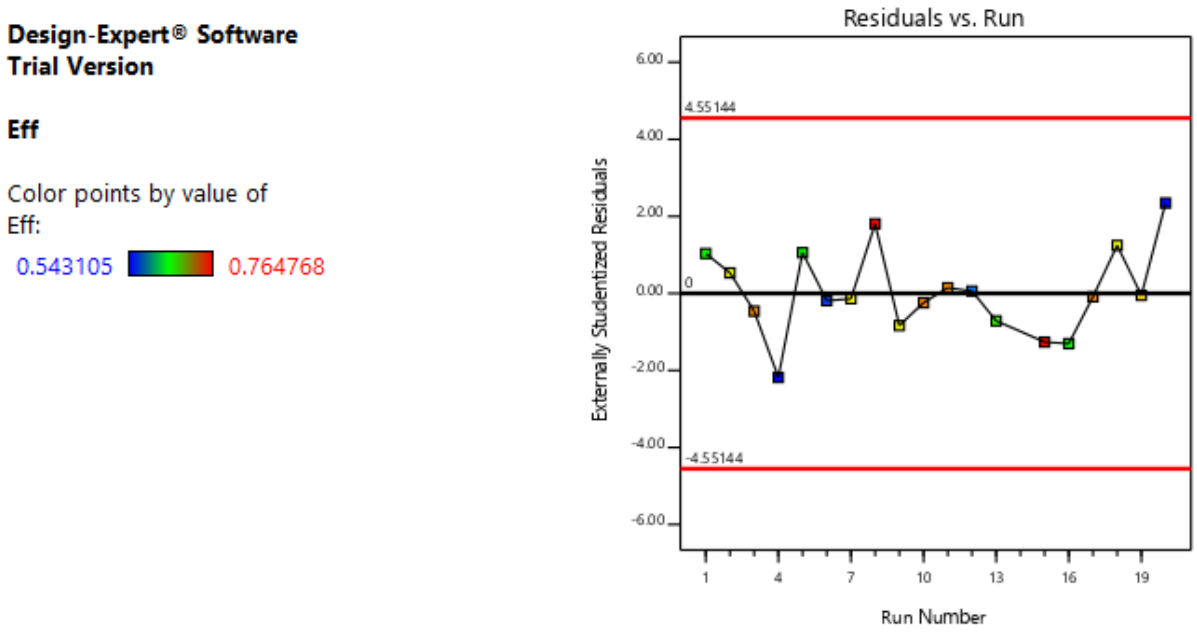

Figure 42- Residuals vs. Run Plots of Efficiency for 16 in Straight Blade Aluminum Propeller

The ANOVA for the Reduced Quadratic models is shown in Table 3 through 6. The ANOVA was used to determine the significant terms in the model. All terms in the model were significant at $\alpha = 0.05$ significance level which indicates a confidence of 95%. A p-value of less than 0.05 will yield a significant term. Here J is the most significant term in the model which is as expected from first principles. There were 14 degrees of freedom available to account for error within the model, well above recommended minimums.

Source	Sum of Squares	df	Mean Square	F-value	p-value	
Block	0.0001	1	0.0001			
Model	0.0071	3	0.0024	10657.12	< 0.0001	significant
A-RPM	0.0000	1	0.0000	66.32	< 0.0001	
B-J	0.0070	1	0.0070	31304.78	< 0.0001	
B^2	0.0001	1	0.0001	289.53	< 0.0001	
Residual	3.118E-06	14	2.227E-07			
Cor Total	0.0072	18				

Table 3- ANOVA of response C_T for 16 in Straight Blade Aluminum Propeller

Source	Sum of Squares	df	Mean Square	F-value	p-value	
Block	1.70E-07	1	1.70E-07			
Model	2.4859E-05	6	4.14317E-06	4824.193	< 0.0001	significant
A-RPM	3.34728E-07	1	3.34728E-07	389.74834	< 0.0001	
B-J	2.4223E-06	1	2.4223E-06	2820.4586	< 0.0001	
AB	6.11074E-09	1	6.11074E-09	7.1151775	0.0219	
B^2	1.87522E-06	1	1.87522E-06	2183.4507	< 0.0001	
AB^2	9.07939E-09	1	9.07939E-09	10.571791	0.0077156	
B^3	1.48307E-08	1	1.48307E-08	17.268473	0.0016014	
Residual	9.45E-09	11	8.59E-10			
Cor Total	2.50388E-05	18				

Table 4- ANOVA of response C_Q for 16 in Straight Blade Aluminum Propeller

Source	Sum of Squares	df	Mean Square	F-value	p-value	
Block	6.72E-06	1	6.72E-06			
Model	0.000981394	6	0.000163566	4824.4981	< 0.0001	significant
A-RPM	1.32147E-05	1	1.32147E-05	389.77805	< 0.0001	
B-J	9.5629E-05	1	9.5629E-05	2820.6522	< 0.0001	
AB	2.41223E-07	1	2.41223E-07	7.1150516	0.0219	
B^2	7.40305E-05	1	7.40305E-05	2183.5872	< 0.0001	
AB^2	3.58456E-07	1	3.58456E-07	10.572937	0.0077156	
B^3	5.8545E-07	1	5.8545E-07	17.268317	0.0016014	
Residual	3.73E-07	11	3.39E-08			
Cor Total	0.000988491	18				

Table 5- ANOVA of response C_P for 16 in Straight Blade Aluminum Propeller

Source	Sum of Squares	df	Mean Square	F-value	p-value	
Block	5.17E-07	1	5.17E-07			
Model	0.0964	8	0.0121	1035.88	< 0.0001	significant
A-RPM	0.0013	1	0.0013	115.64	< 0.0001	
B-J	0.0101	1	0.0101	869.59	< 0.0001	
AB	0.0001	1	0.0001	10.87	0.0093	
B^2	0.0004	1	0.0004	33.77	0.0003	

AB^2	0.0002	1	0.0002	19.96	0.0016	
B^3	0.0002	1	0.0002	17.91	0.0022	
AB^3	0.0002	1	0.0002	14.58	0.0041	
B^4	0.0001	1	0.0001	7.51	0.0228	
Residual	0.0001	9	0.0			
Cor Total	0.0965	18				

Table 6- ANOVA of response Efficiency for 16 in Straight Blade Aluminum Propeller

Table 7 shows the fit statistics that were used to examine the prediction capabilities and how well the model captures the data. An R^2 value of one is desired, with the lowest R^2 of 0.9996 observed this indicates that 99.96% of the variability in the response is explained by the model. This also indicates that the quadratic model is an ideal solution for the results. The adjusted R^2 value is used to compare the goodness-of-fit for regression models that contain differing numbers regression model terms, while predicted R^2 is used to determine how well a regression model makes predictions. As seen below values obtained show good model fit and prediction capability. The efficiency model has the lowest valued family of R^2 statistics and while generally good, shows that a higher order model could improve the metrics.

Response	**C_T**	**C_Q**	**C_P**	**η**
Std. Dev.	0.0005	2.931E-05	0.0001841	0.0034
Mean	0.0553	0.0055136	0.0346427	0.6770
R^2	0.9996	0.9996201	0.9996201	0.9989
Adjusted R^2	0.9995	0.9994129	0.9994129	0.9980
Predicted R^2	0.9992	0.9981263	0.9981265	0.9942

Table 7- Fit Statistics of C_T, C_Q, C_P, and η for 16 in Straight Blade Aluminum Propeller

Table 8 shows the model term coefficients for each of the responses observed. This was obtained from DE and used in the final equation in terms of actual factors to plot all the regression models seen in chapter 7 of this thesis.

	C_T	C_Q	C_P	η
Factor	**Coefficient Estimate**			
Intercept	+0.104182	0.005390129	0.033866586	-1.85299
RPM	-1.20055E-06	3.12E-07	1.96E-06	+0.000234
J	-0.026608	0.009209711	0.057870485	+17.92002
RPM*J	-	-2.29E-06	-1.44E-05	-0.001712
J^2	-0.137840	-0.001992562	-0.012528016	-48.06756
RPM * J^2	-	2.22772E-06	1.39975E-05	+0.004171
J^3	-	-0.02216625	-0.139269557	+56.63169
RPM * J^3	-	-	-	-0.003211
J^4	-	-	-	-24.26531

Table 8- Model term coefficients of C_T, C_Q, C_P, and η for 16 in Straight Blade Aluminum Propeller

Table 9 shows results from verification points used for run 24 to determine the prediction capability of the model. These points were chosen outside the design space, and they were not used in the analysis of the data or for model building. The results from all the verification points are included in Appendix J.3. Overall, the point prediction gave acceptable results and run 24 showed C_Q, and C_P falling slightly outside the prediction interval.

Verification Run 24 Response	**Predicted Mean**	**Observed**	**95% PI low**	**95% PI high**
C_T	0.0729189	**0.0731286**	0.0718448	0.0739931
C_Q	0.00640219	**0.0063167**	0.0063312	0.00647319
C_P	0.0402262	**0.039689**	0.0397801	0.0406722
η	0.627835	**0.635279**	0.618564	0.637106

Table 9- Prediction Capability for 16 in Straight Blade Aluminum Propeller (run 24)

CHAPTER 7 – PROPELLER PERFORMANCE CHARACTERIZATION RESULTS AND DISCUSSION

7.1 RESULTS

Sections 7.1.1 through 7.2.4 show the analysis results for the 12 x 8, 14 x 12, 17 x 12, 16 in swept, and 16 in straight blade propeller. Section 7.1.1 gives a detailed look for the 17 x 12, whereas the other props tested have detailed information in the Appendix. In order to validate the data collected throughout the experimentation, tests were necessary to compare to published results. Three APC Thin Electric propellers were tested and compared to the literature. Finally, a prototype swept and straight blade propeller were tested to help quantify uncertainty. The data collected on all propellers were tabulated and plotted with C_T, C_P, C_Q, and η vs. J. The comparison plots are shown overlaying experimental data for C_T, C_Q, and η. It is more desirable to select propellers of 16 inches or larger diameter to produce thrust force within the design range of the balance. With the 12 x 8 propeller, the comparison RPM was not known, but this comparison was used to check the test stand initial performance. Based on the plots it can be seen that the test stand is performing correctly as the comparison data follows the experimental data trend. For all propellers tested the plotted regression model was obtained from the designed general factorial experiment. Model building and significance testing were performed using ANOVA and regression modeling from Design Expert.

7.1.1 17 x 12 DETAILED RESULTS

As expected, the best comparison experiment was made using the 17 x 12 propeller. For clarity, details of the 17 x 12 analysis are included. The ODU 15 x 15 is best suited for the larger propellers of the ones tested. Since uncertainty values are based on a percentage of full-scale loads, loads highest in the allowable range give the most accurate results. Appendix D.2 shows the randomly generated run order of the test matrix created by DE that was used to carry out the experiment. The design had two factors; RPM and J, with RPM at three levels and J at five levels. The four responses C_T, C_Q, C_P, and η were observed. The experiment was performed with two replicates, each in its own block for a total of 30 runs. The points shown in bold represent the verification points that were chosen outside the design space. These points were not used in the analysis of the data but for the prediction capability of the model. The following assumptions were verified:

- Appendix G.2 shows the normal probability of the residuals for the four responses. The normality assumption is validated as all responses pass the “fat pencil” test.

- Appendix H.2 shows the Residual vs. Run plots for the responses observed. These plots were used to identify the independence of the responses with time. The random oscillation around the zero line with no trends validates the independence assumption.
- Appendix I.2 shows the Residuals vs. Predicted plots which verifies the assumption of constant variance. There is no coning or barreling shape observed within the plots.

The prediction capability of this model was excellent. As seen in Appendix J.2 for runs 32, 33, and 34 all points fell within the predicted range. For run 31 only two points fell outside that range for C_Q and C_P however the difference between the predicted range and the observed was noticeably small with the highest difference being 0.00141 for C_P. This model showed the best prediction capability out of all the propellers used in the comparison study.

The ANOVA shown in Table 10 through 13 indicates that all the terms were significant except for the RPM in the efficiency table. The second order quadratic model was used in this analysis. However, a higher order model could have been chosen that would yield higher R^2 values but would raise the VIF values above acceptable regions. The lowest R^2 value observed in the fit statistics was 99.58%. This is close to the desired value of 100% which indicates that the model captures the data well. The model term coefficients for the responses shown in Appendix F.2 were used to obtain the regression models in section 7.1.3 of this thesis.

Source	Sum of Squares	df	Mean Square	F-value	p-value	
Block	0.0119	1	0.0119			
Model	0.0136	4	0.0034	2544.19	< 0.0001	significant
A-RPM	0	1	0	15.83	0.0006	
B-J	0.0009	1	0.0009	701.83	< 0.0001	
AB	0	1	0	12	0.002	
B^2	0.0004	1	0.0004	324.26	< 0.0001	
Residual	0	24	1.34E-06			
Cor Total	0.0255	29				

Table 10- ANOVA of response C_T for APC 17 x 12 propeller

Source	Sum of Squares	df	Mean Square	F-value	p-value	
Block	0	1	0			
Model	0.0001	4	0	1438.01	< 0.0001	significant
A-RPM	1.74E-07	1	1.74E-07	17.37	0.0003	
B-J	7.13E-07	1	7.13E-07	71.18	< 0.0001	
AB	2.87E-07	1	2.87E-07	28.59	< 0.0001	
B^2	0	1	0	1675.23	< 0.0001	
Residual	2.41E-07	24	1.00E-08			
Cor Total	0.0001	29				

Table 11- ANOVA of response C_Q for APC 17 x 12 propeller

Source	Sum of Squares	df	Mean Square	F-value	p-value	
Block	0.0019	1	0.0019			
Model	0.0023	4	0.0006	1438	< 0.0001	significant
A-RPM	6.87E-06	1	6.87E-06	17.37	0.0003	
B-J	0	1	0	71.18	< 0.0001	
AB	0	1	0	28.59	< 0.0001	
B^2	0.0007	1	0.0007	1675.23	< 0.0001	
Residual	9.50E-06	24	3.96E-07			
Cor Total	0.0042	29				

Table 12- ANOVA of response C_P for APC 17 x 12 propeller

Source	Sum of Squares	df	Mean Square	F-value	p-value	
Block	0.000148188	1	0.000148188			
Model	0.267189273	8	0.033398659	985.056581	< 0.0001	significant
A-RPM	2.09768E-05	1	2.09768E-05	0.618687349	0.440756624	
B-J	0.004380292	1	0.004380292	129.1918682	< 0.0001	
AB	2.94928E-05	1	2.94928E-05	0.869857928	0.362118188	
B^2	0.000323286	1	0.000323286	9.534972758	0.005802167	
AB^2	1.01388E-05	1	1.01388E-05	0.299032057	0.590539654	
B^3	0.00016946	1	0.00016946	4.998048133	0.036937889	
AB^3	0.000194823	1	0.000194823	5.746089252	0.026409569	
B^4	0.001973325	1	0.001973325	58.20103576	< 0.0001	
Residual	0.000678106	20	3.39053E-05			
Cor Total	0.268015568	29				

Table 13- ANOVA of response Efficiency for APC 17 x 12 propeller

Figure 51 shows the fit statistics for the model. The model fits the data extremely well with the lowest observed R^2 value of 99.58%.

Response	C_T	C_Q	C_P	η
Std. Dev.	0.001155287	0.0001001	0.000629	0.0058228
Mean	0.056672769	0.0061018	0.0383384	0.651899
R^2	0.997647234	0.9958449	0.9958449	0.9974685
Adjusted R^2	0.997255106	0.9951524	0.9951524	0.9964559
Predicted R^2	0.996278735	0.9936427	0.9936427	0.9933127

Table 14 - Fit Statistics for APC 17 x 12 Propeller

The plots generated in Figures 43 through 46 were obtained from the data tables generated in Appendix B.2. The regression models were obtained from the model term coefficients in Appendix F.2.

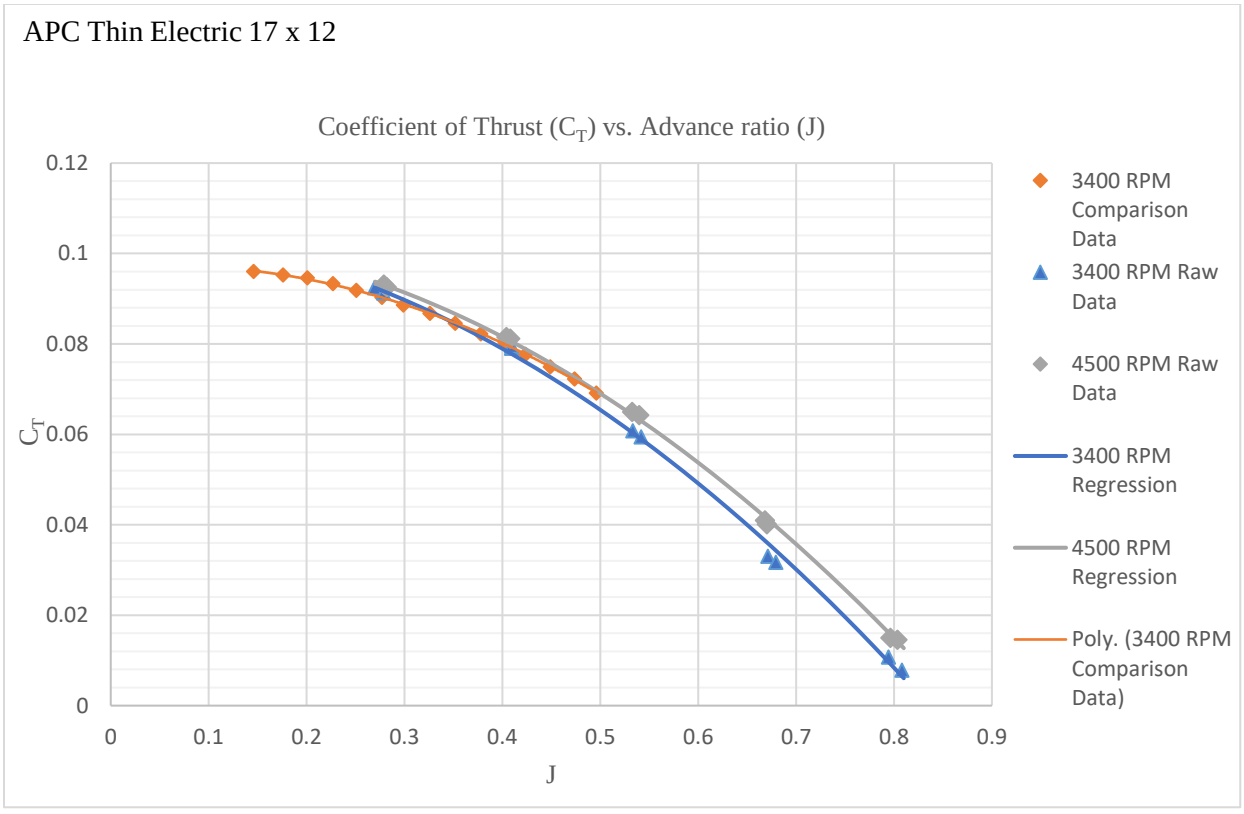

Figure 43- Coefficient of Thrust vs. Advance ratio regression model, raw data points, and comparison data Selig [6]

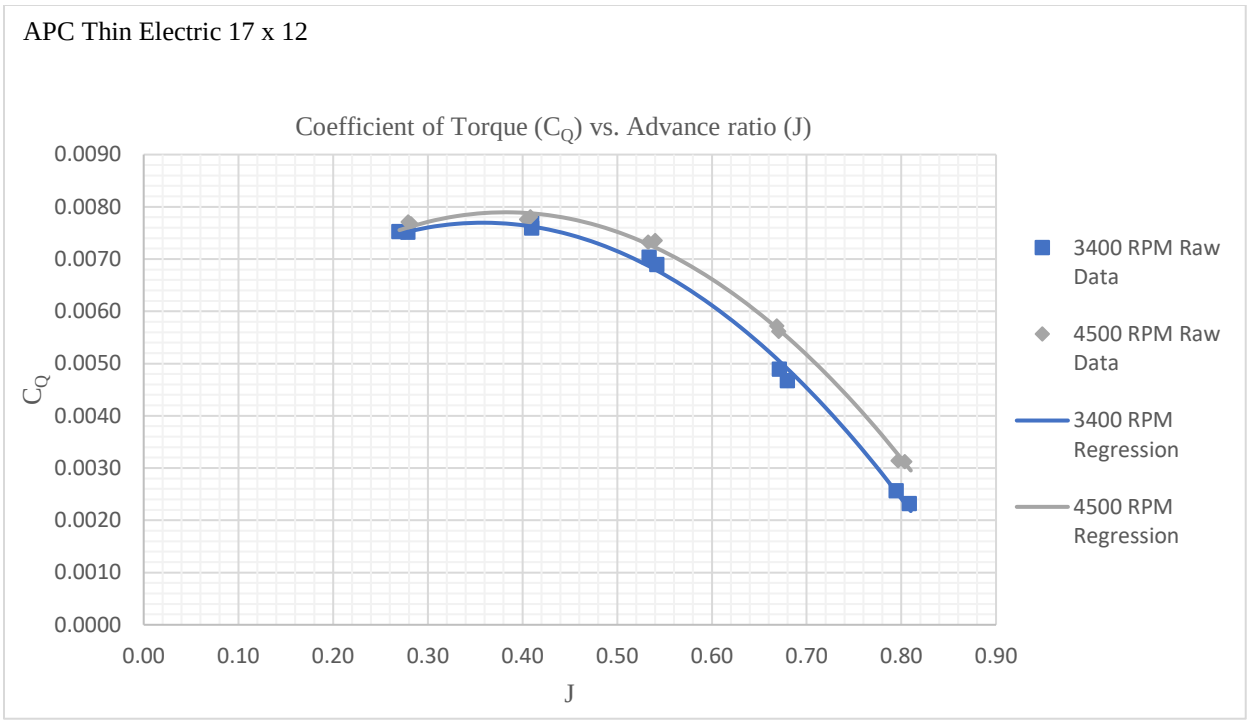

Figure 44- Coefficient of Torque vs. Advance ratio regression model and raw data

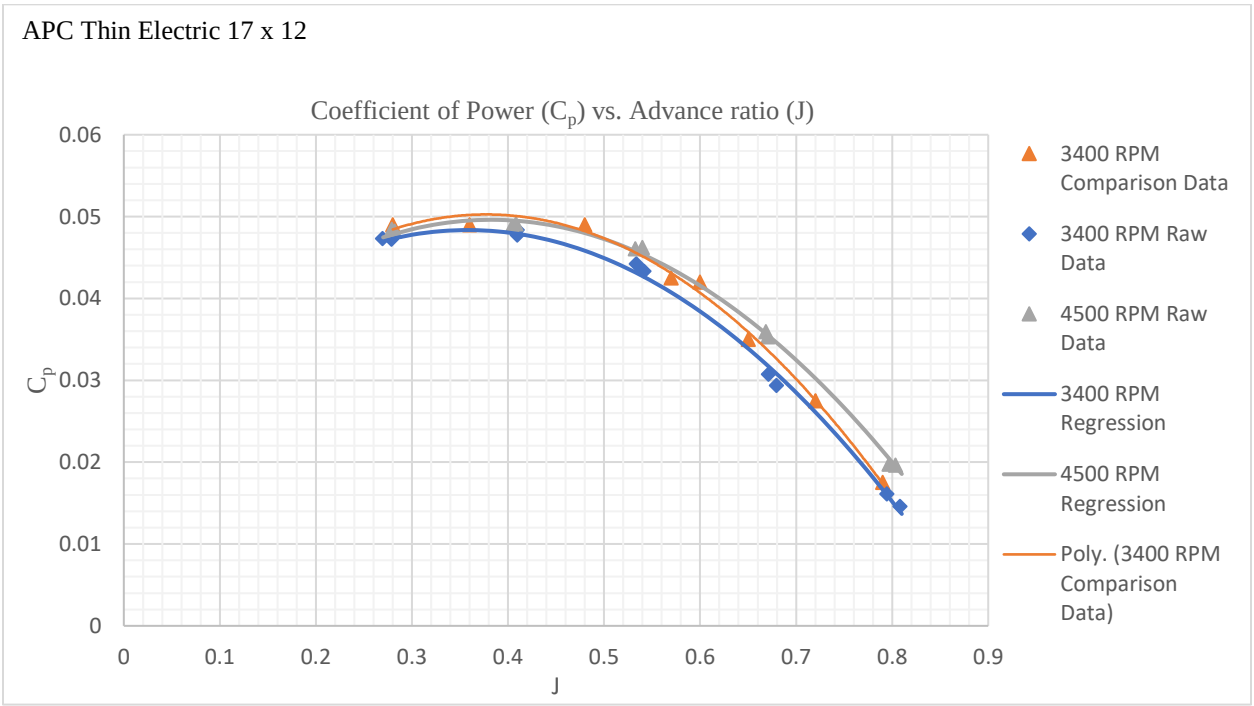

Figure 45- Coefficient of Power vs. Advance ratio regression model, raw data points, and comparison data Selig [6]

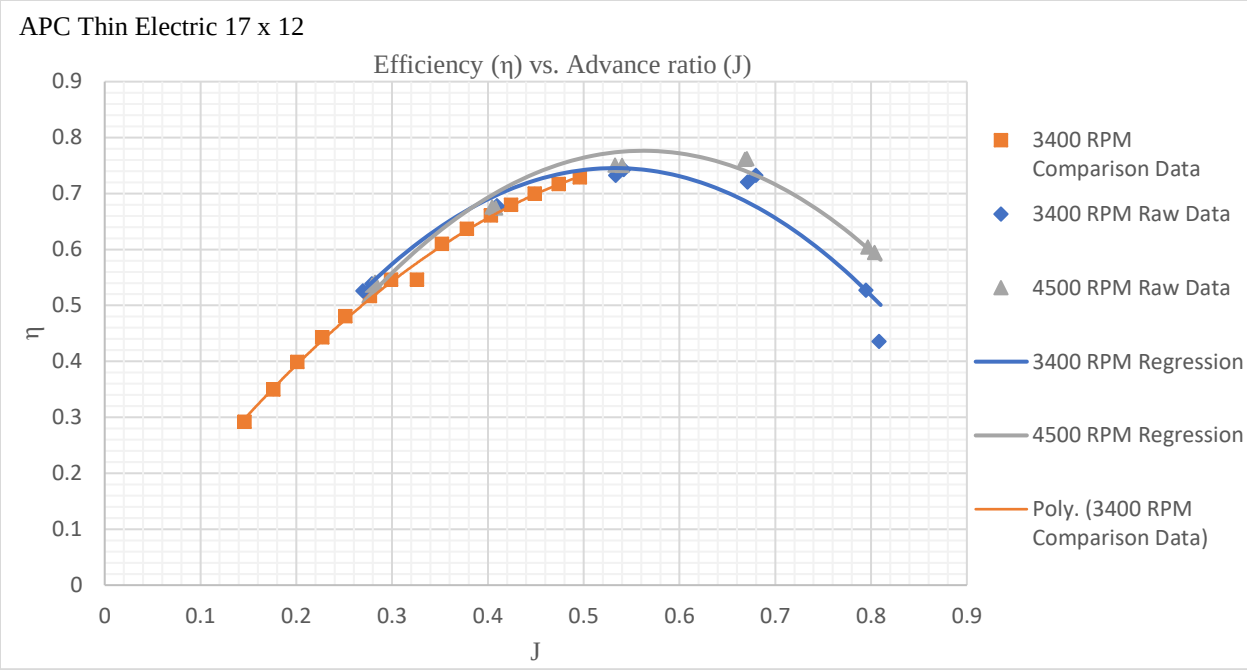

Figure 46- Efficiency vs. Advance ratio regression model, raw data points, and comparison data Selig [6]

7.1.2 APC THIN-ELECTRIC 12 X 8 PROPELLER

The 12 x 8 propeller was chosen as the lower bound for size and range of the torque and thrust values. The data table used to obtain Figures 47 through 50 are shown in Appendix B. The RPM of the comparison data is unknown however this was the first propeller tested and was used to validate the functionality of the system [14]. The plots obtained showed the expected general shape of C_P, C_T, C_Q, and η. The comparison data shown on the raw data points trend closely with each other. The model term coefficients shown in Appendix F were used to create the regression models in the following plots.

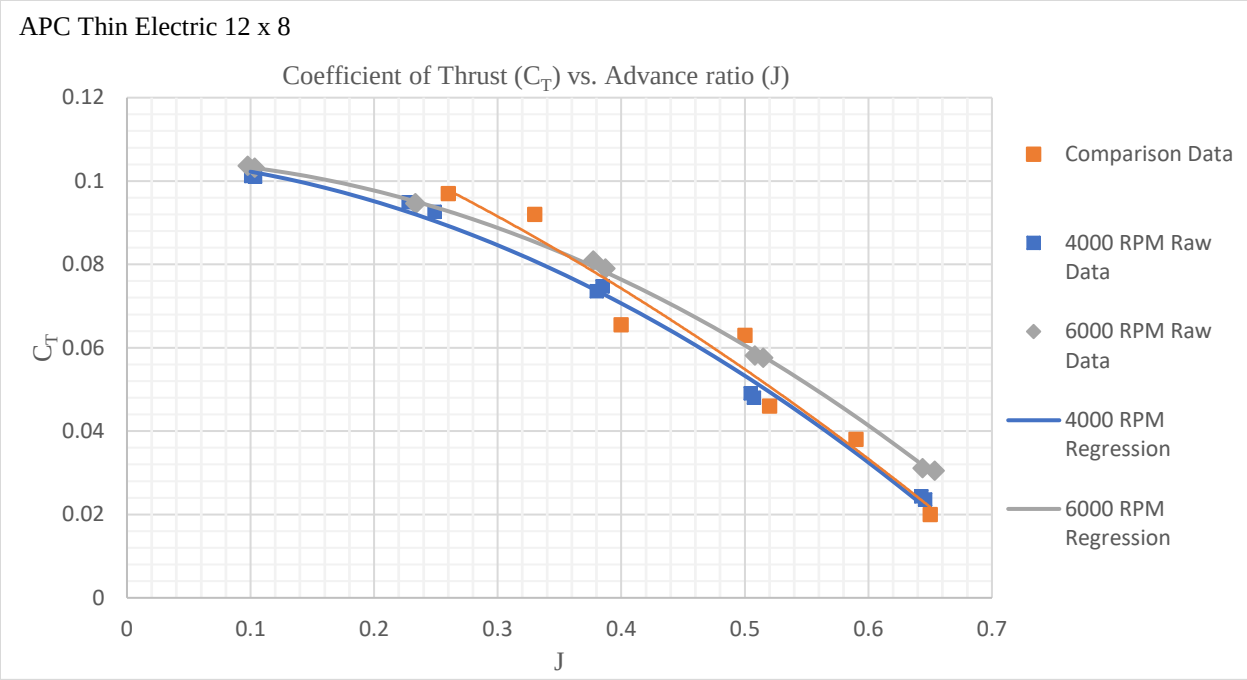

Figure 47- Coefficient of Thrust vs. Advance ratio regression model, raw data points and comparison data [14]

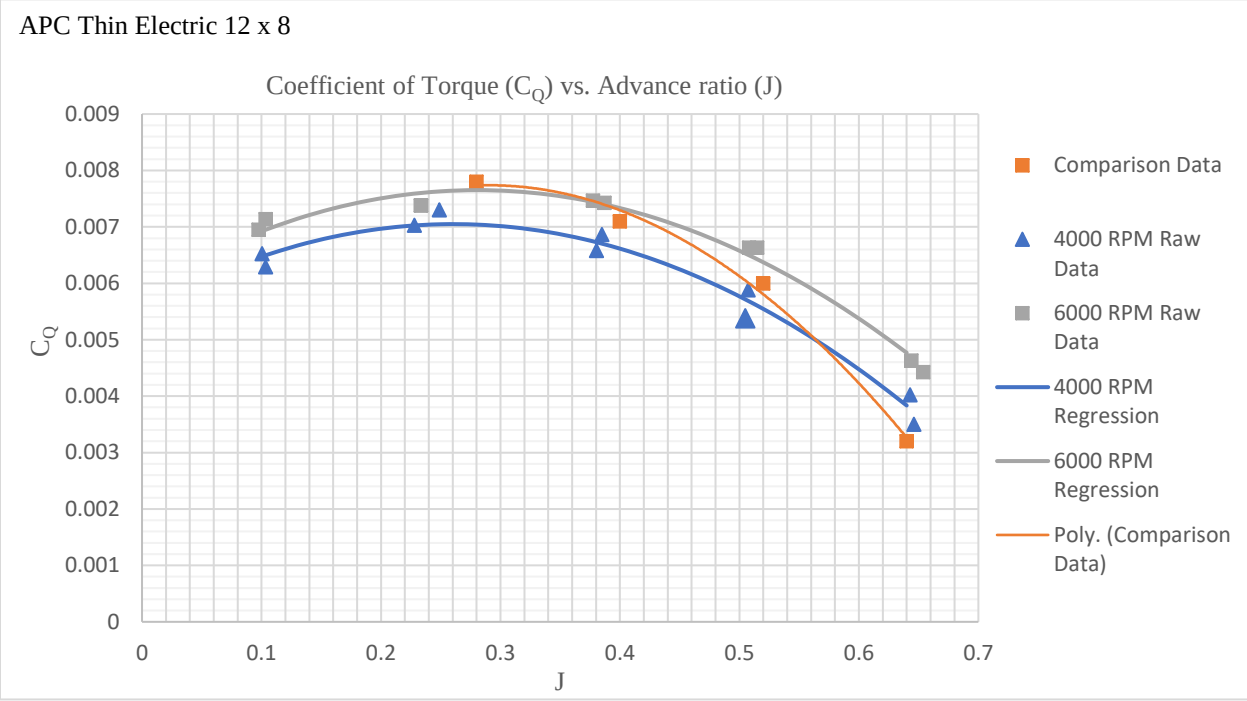

Figure 48- Coefficient of Torque vs. Advance ratio regression model, raw data points and comparison data [14]

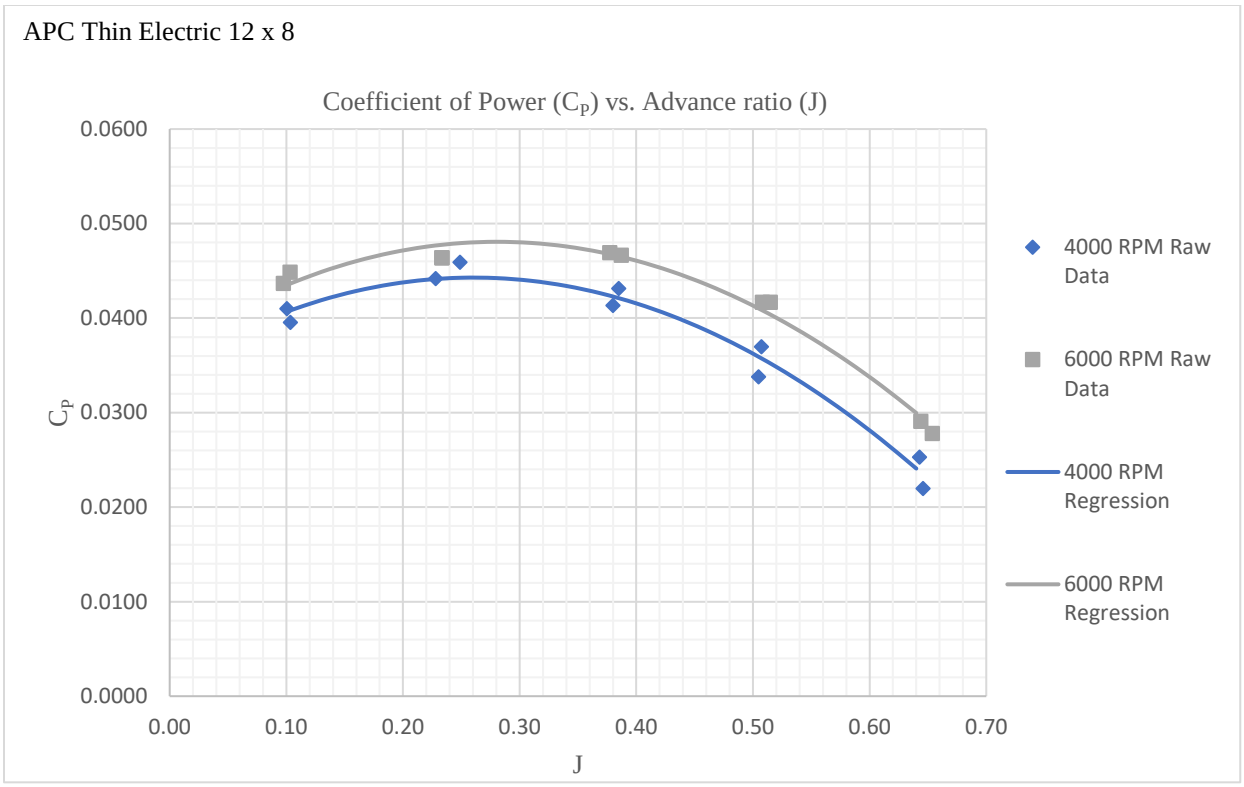

Figure 49- Coefficient of Power vs. Advance ratio regression model and raw data

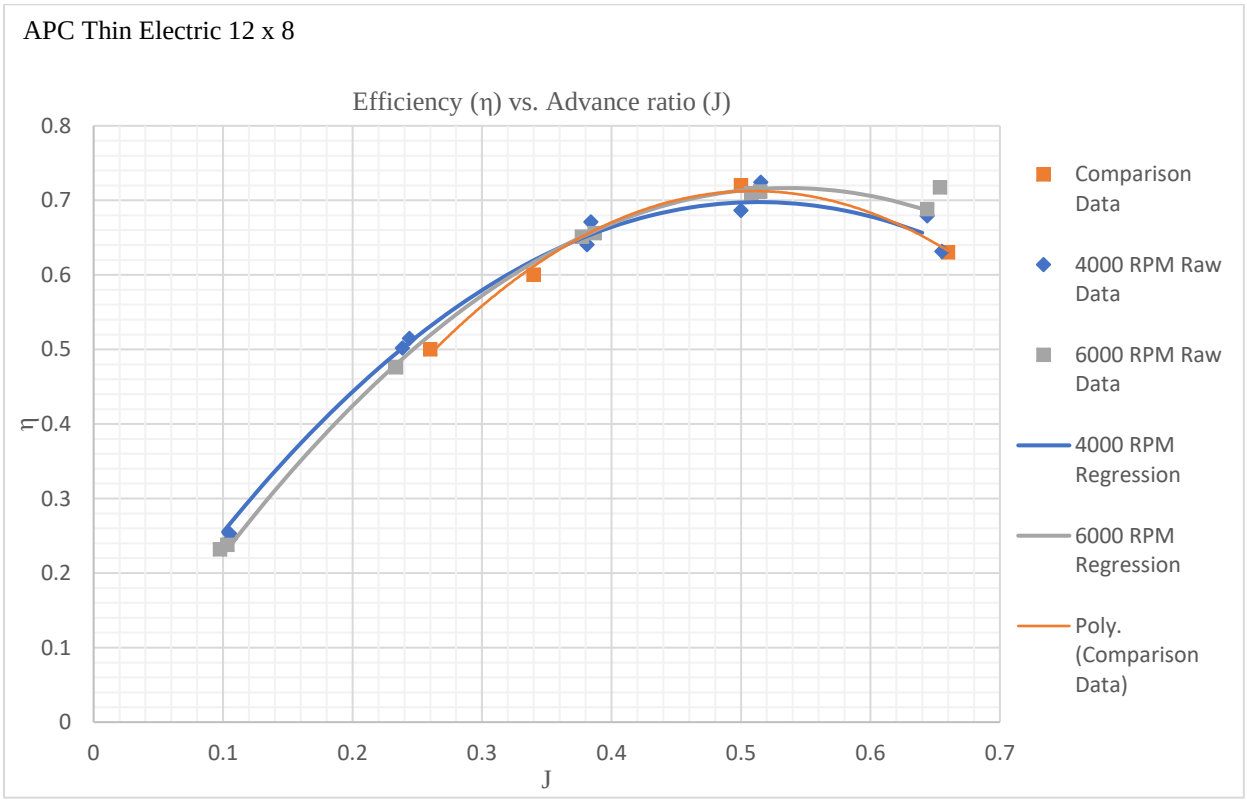

Figure 50- Efficiency vs. Advance ratio ratio regression model, raw data points and comparison data [14]

7.1.3 APC THIN-ELECTRIC 14 x 12 PROPELLER

The plots generated in Figures 51 through 54 were obtained from the data tables generated in Appendix B.1. The regression models were obtained from the model term coefficients in Appendix F.1. Based on the results obtained, the comparison data was close to the actual experimental data points. The comparison data was obtained from Selig and Brandt [6]. A more detailed analysis will be carried out in sections 7.2.2 to determine if the comparison data falls within the confidence interval of the experimental data.

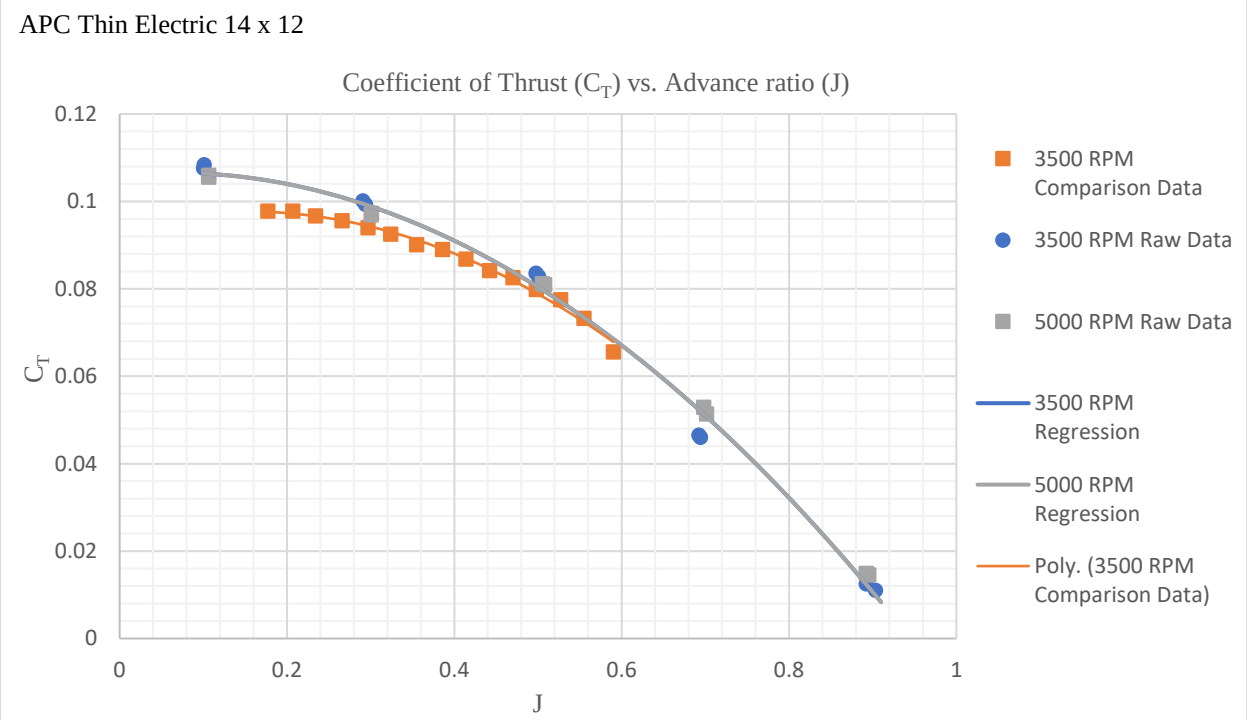

Figure 51- Coefficient of Thrust vs. Advance ratio regression model, raw data points and comparison data Selig [6]

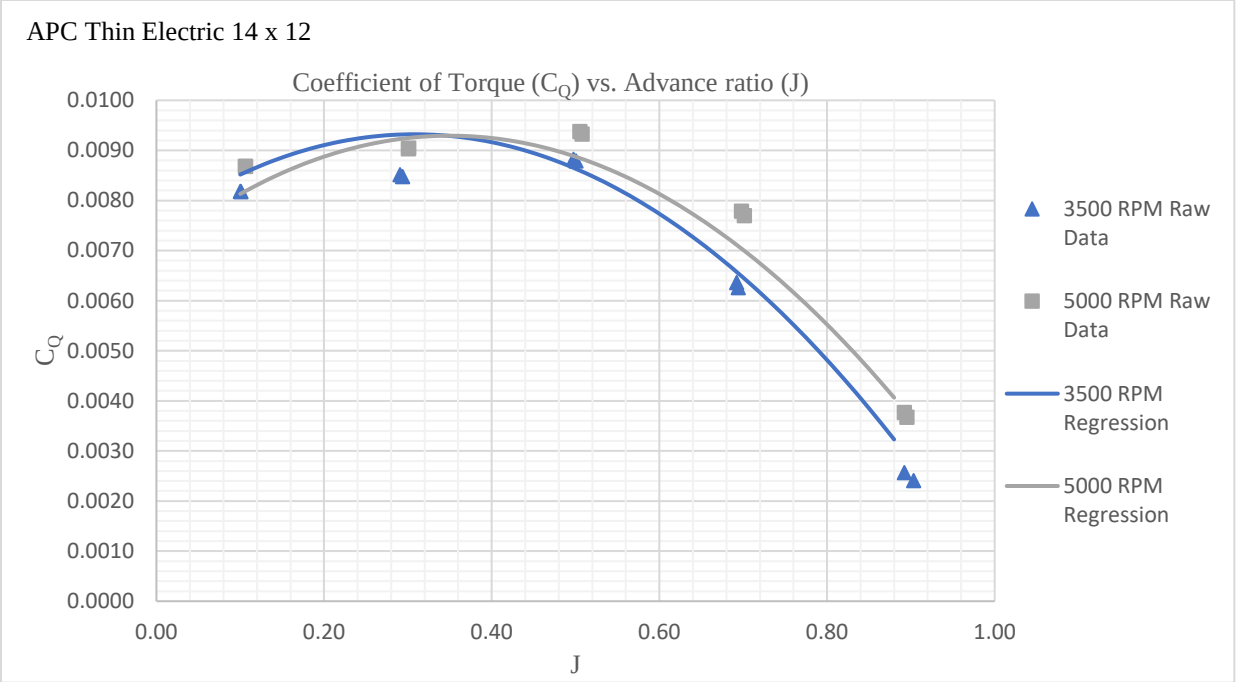

Figure 52- Coefficient of Torque vs. Advance ratio regression model and raw data

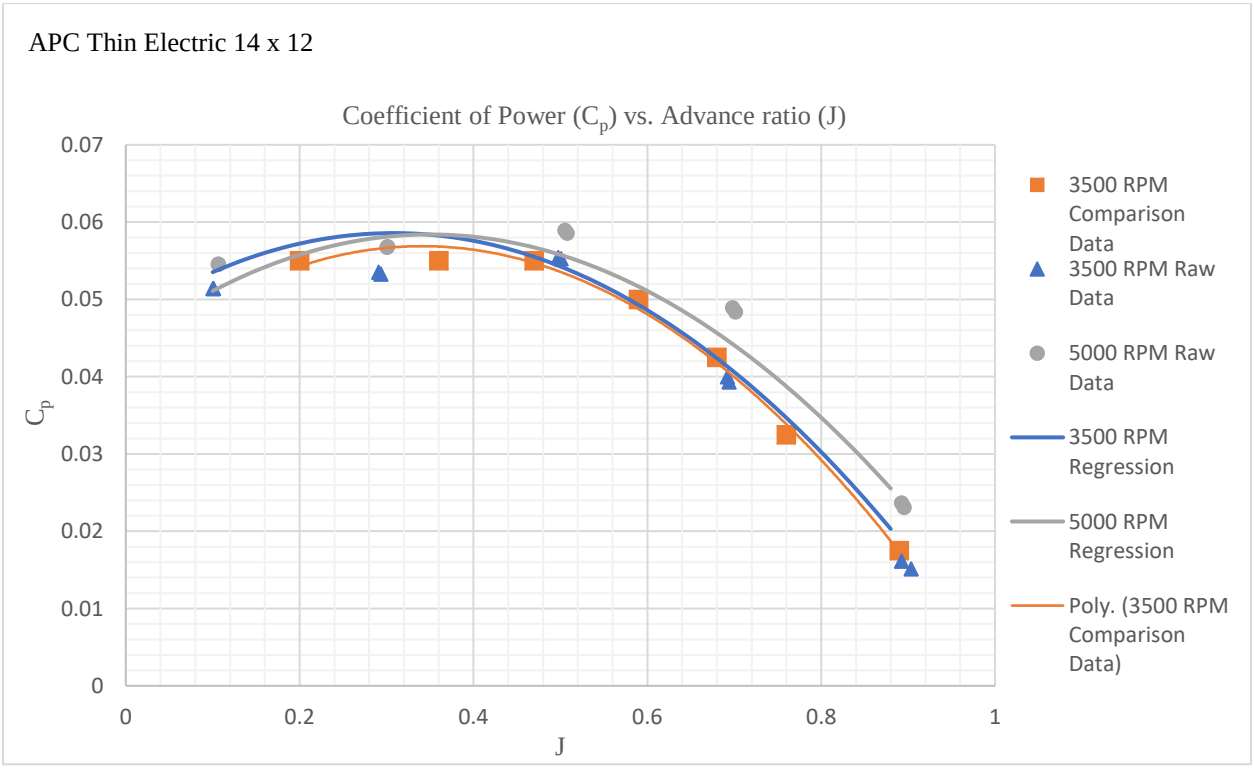

Figure 53- Coefficient of Power vs. Advance ratio regression model, raw data points and comparison data Selig [6]

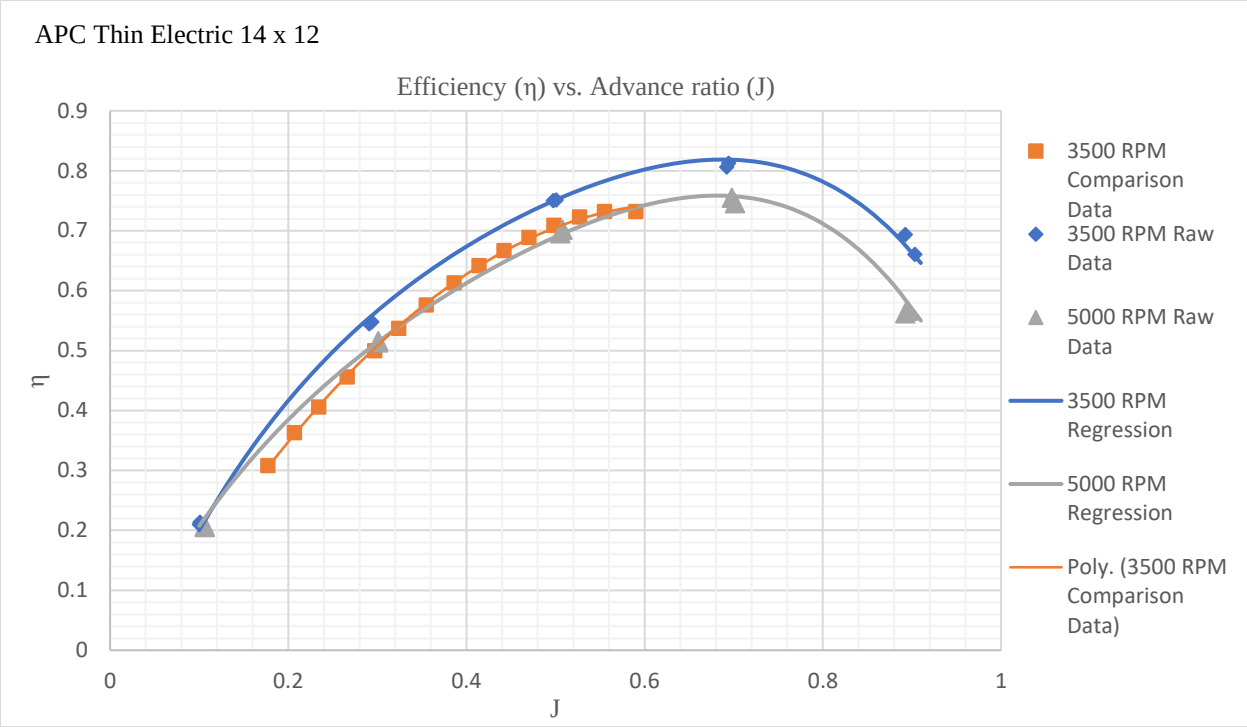

Figure 54- Efficiency vs. Advance ratio regression model, raw data points, and comparison data Selig [6]

7.1.4 16 IN STRAIGHT AND SWEPT BLADE ALUMINIUM PROPELLER

The plots generated in Figures 55 through 58 were obtained from the data tables generated in Appendix B.3. The regression models were obtained from the model term coefficients in Appendix F.3 for the swept blade propeller and Table 8 for the straight blade propeller.

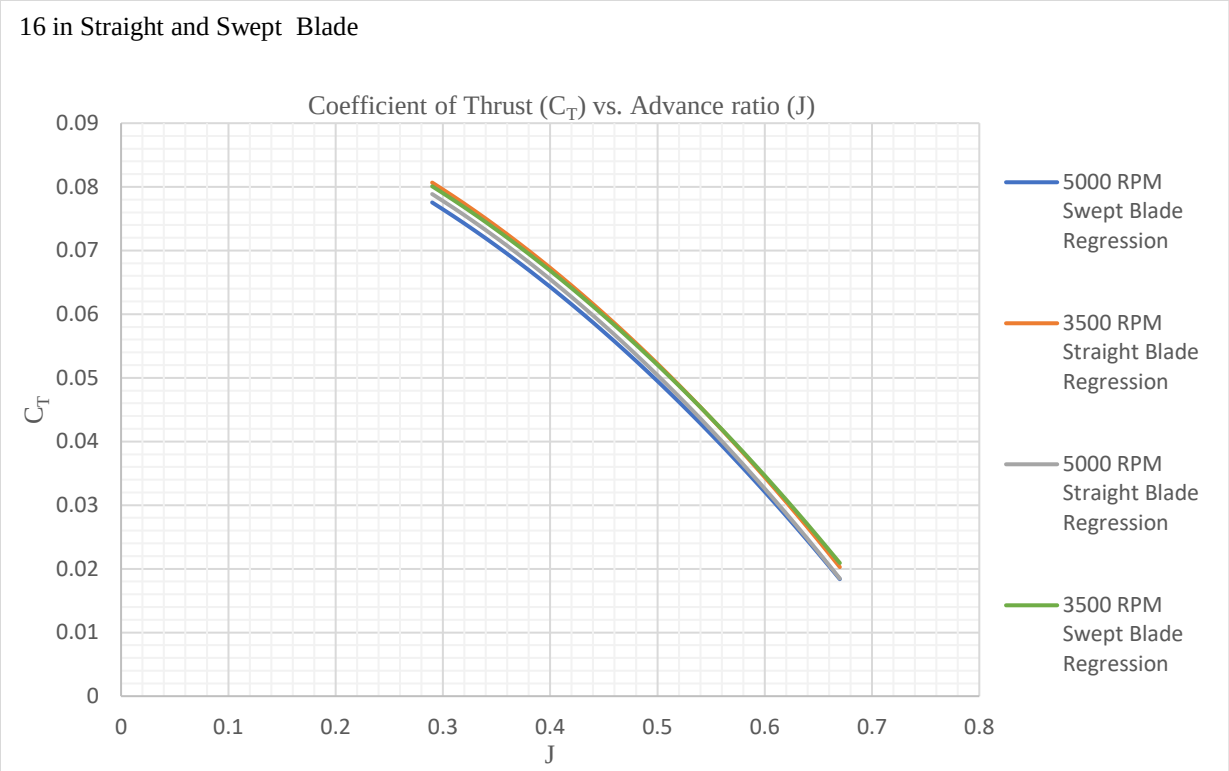

Figure 55- Coefficient of Thrust vs. Advance ratio regression model

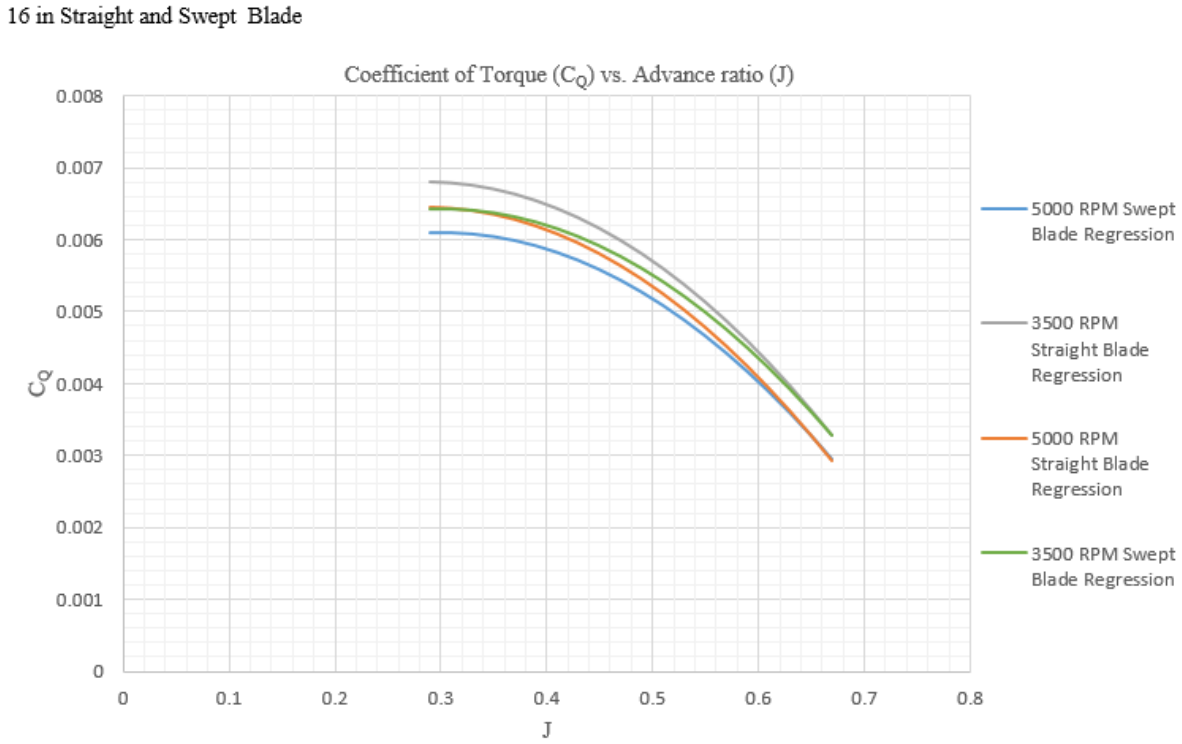

Figure 56- Coefficient of Torque vs. Advance ratio regression model

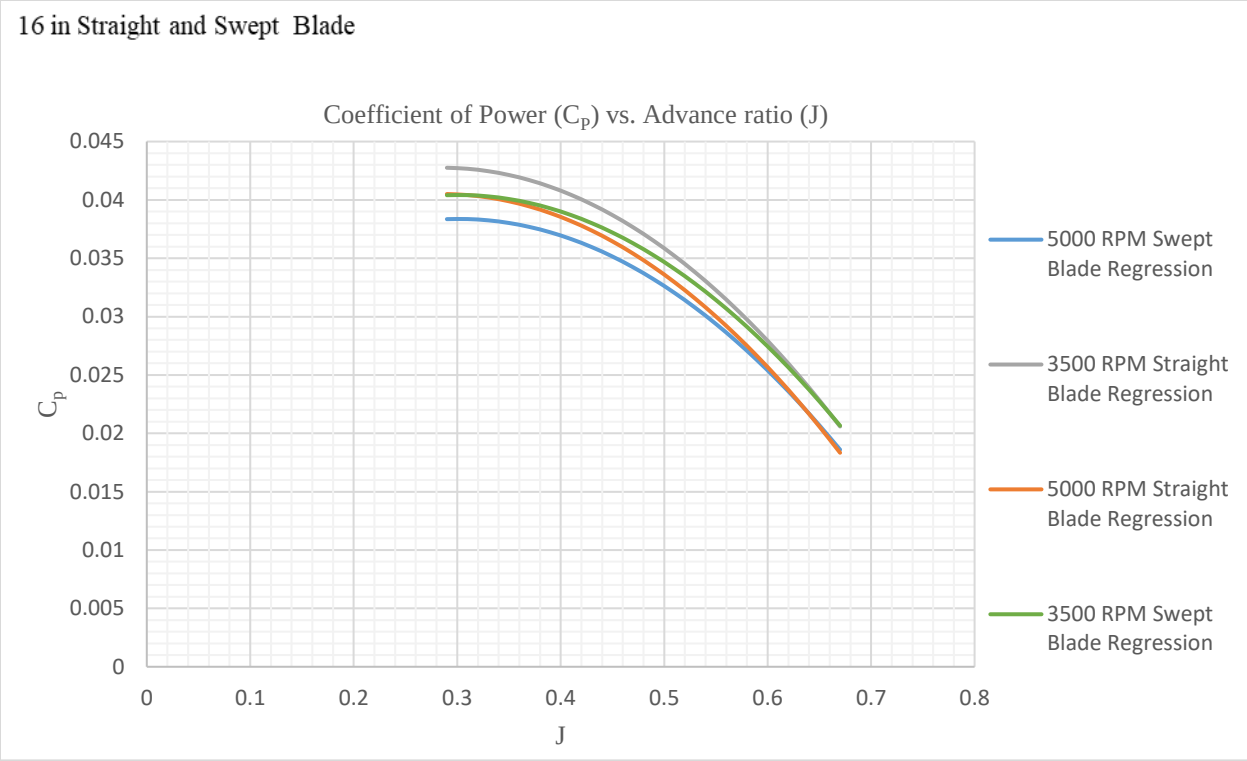

Figure 57- Coefficient of Power vs. Advance ratio regression model

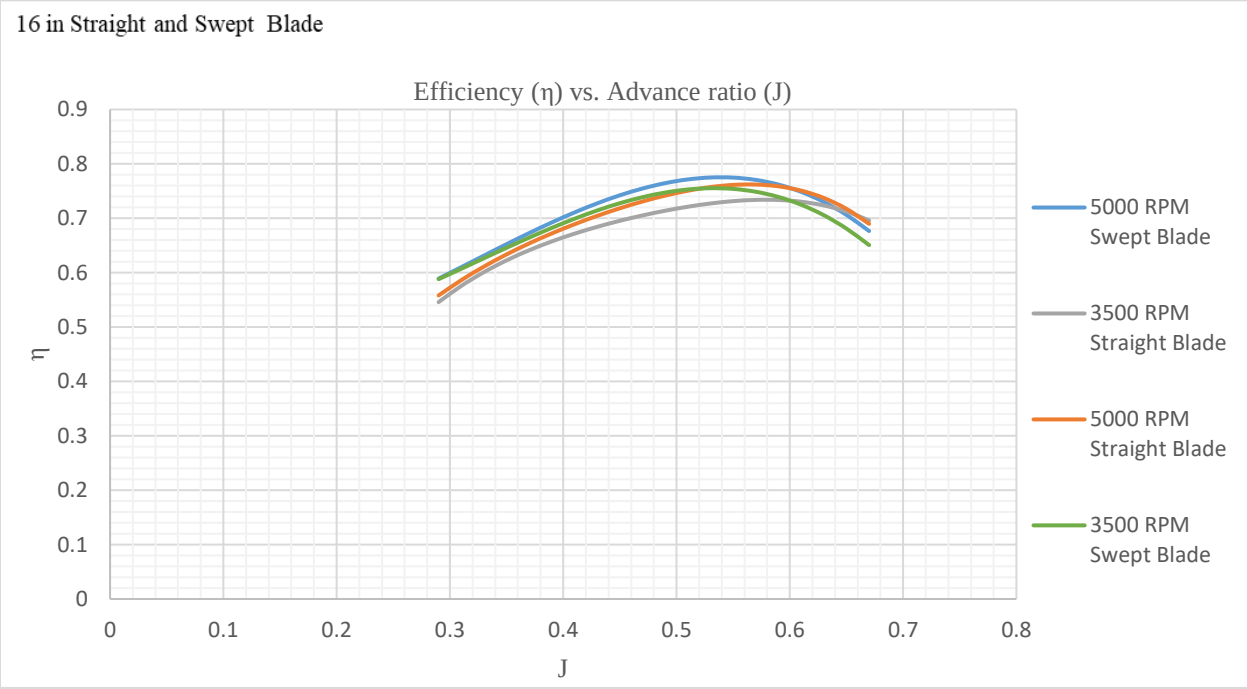

Figure 58- Efficiency vs. Advance ratio regression model

7.2 UNCERTAINTY

The high and low confidence intervals were obtained from Design-Expert and plotted for selected RPMs for C_T, C_Q, C_P and η for comparison. The 95% confidence interval bands are shown for all RPMs selected, and the comparison data was plotted on the same graph in order to judge the accuracy and if there was any difference. While not a formal comparison, this study helps shed some light on expected uncertainties. The RPM used for comparison on the APC 12 x 8 is not known. This propeller was tested as the initial check of the system in order to obtain and ensure proper operations at low thrust and torque. The uncertainty percentage for efficiency was obtained from Selig's data [4]. With the uncertainty known (0.595%) and using a coverage factor of 2, the +/- error bars were calculated and plotted on the efficiency plots below.

7.2.1 APC THIN ELECTRIC 12 X 8 PROPELLER

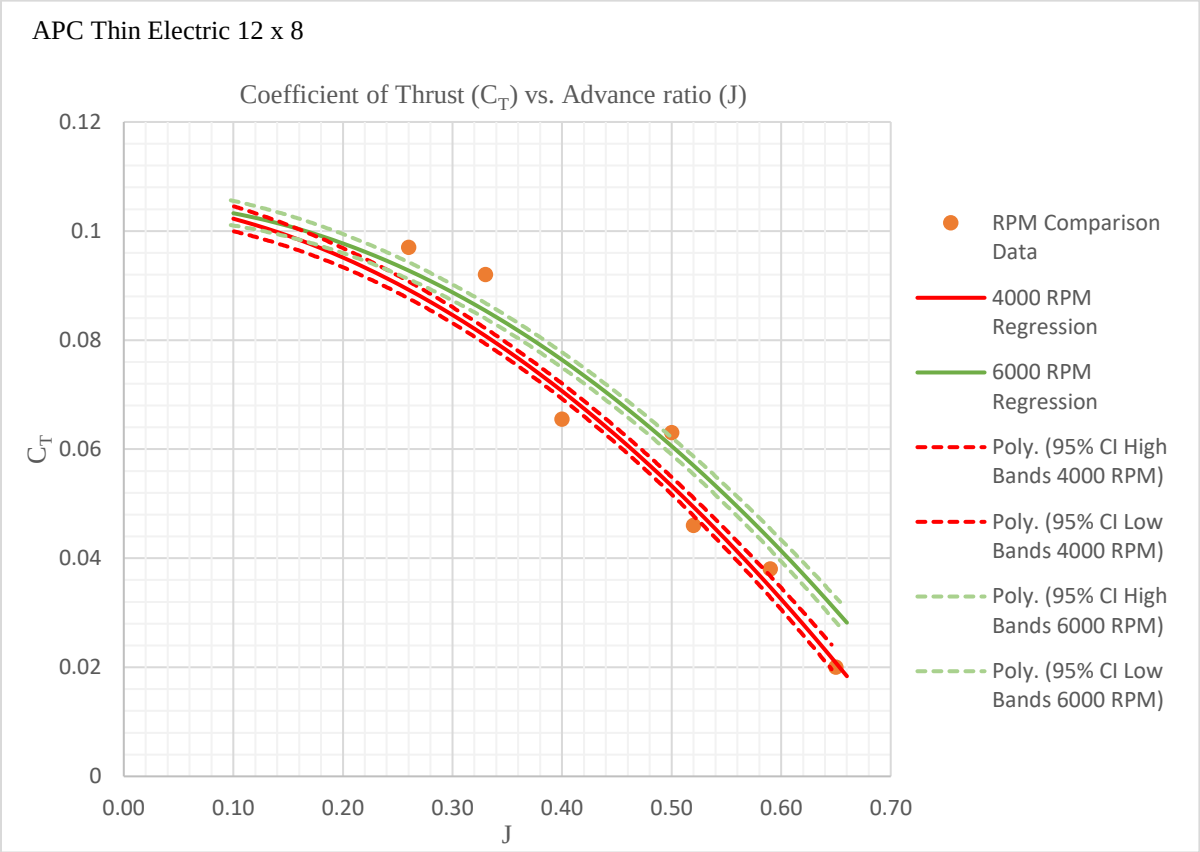

Figure 59- Coefficient of Thrust with 95% confidence interval band comparison data [14]

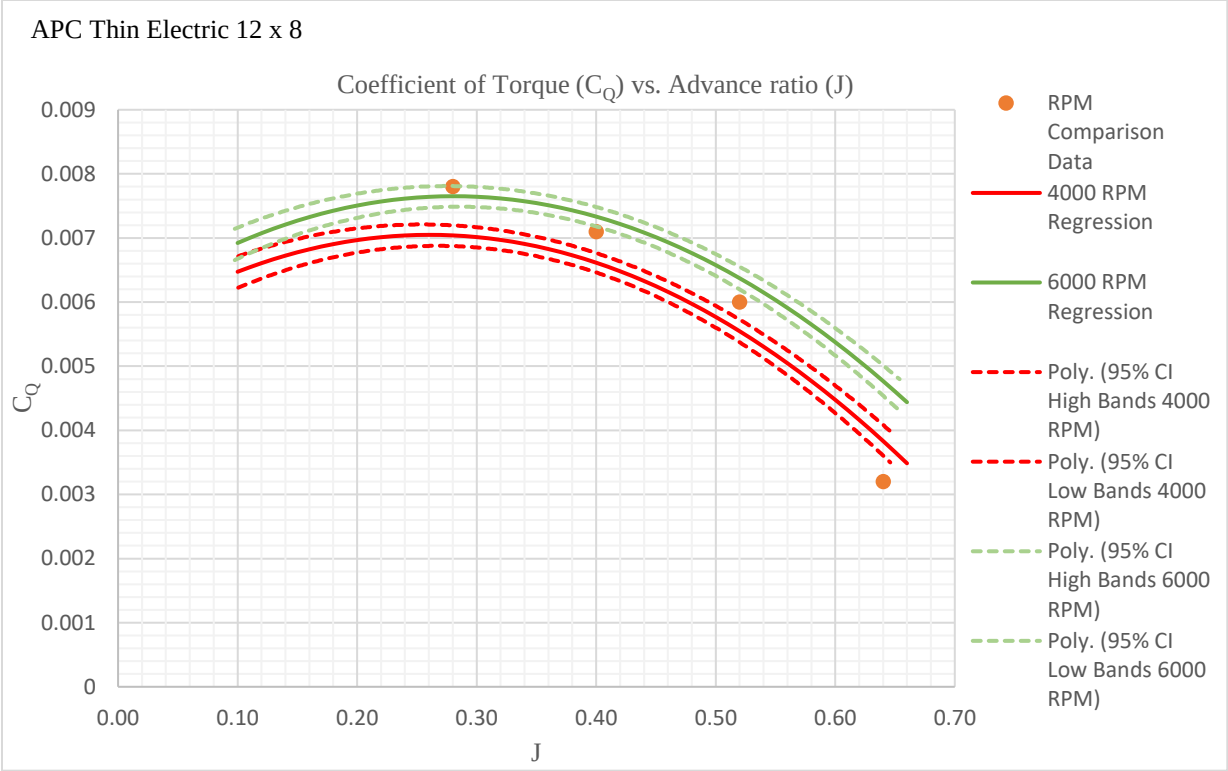

Figure 60- Coefficient of Torque with 95% confidence interval bands and comparison data [14]

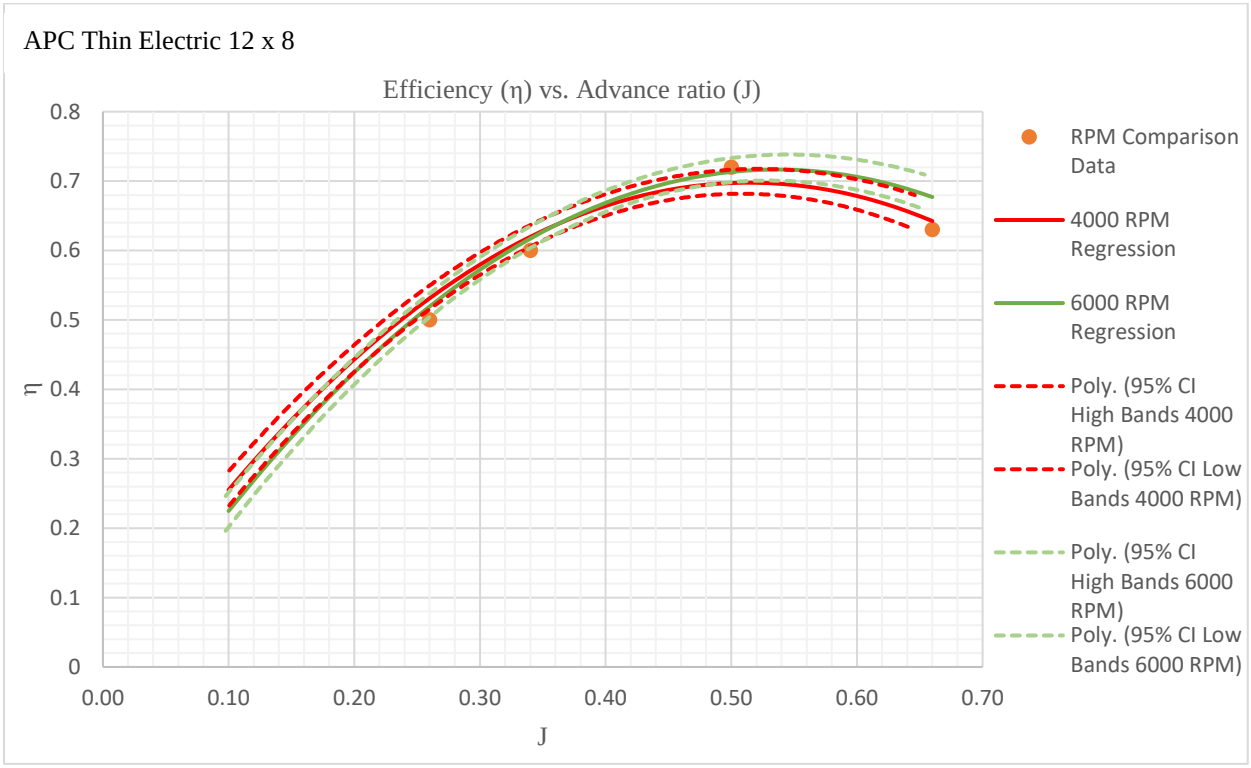

Figure 61- Efficiency with 95% confidence interval bands and comparison data [14]

7.2.2 APC THIN ELECTRIC 14 X 12 PROPELLER

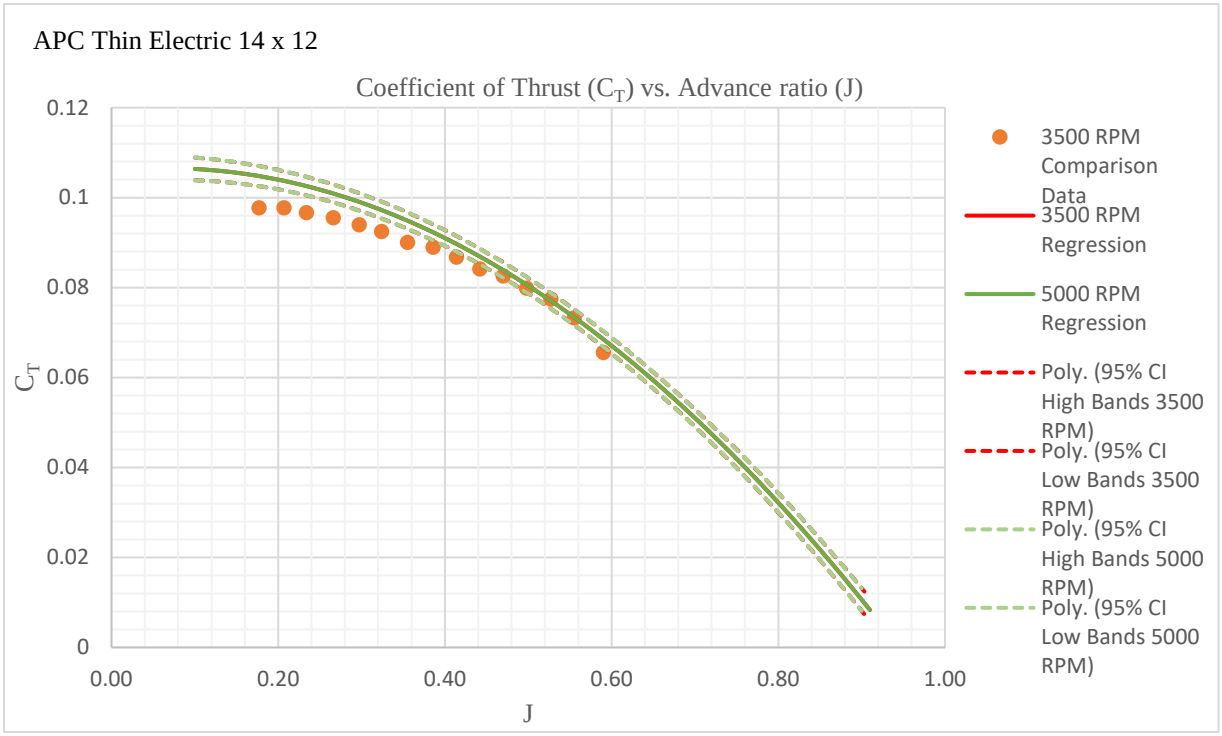

Figure 62- Coefficient of Thrust with 95% confidence interval bands and comparison data Selig [6]

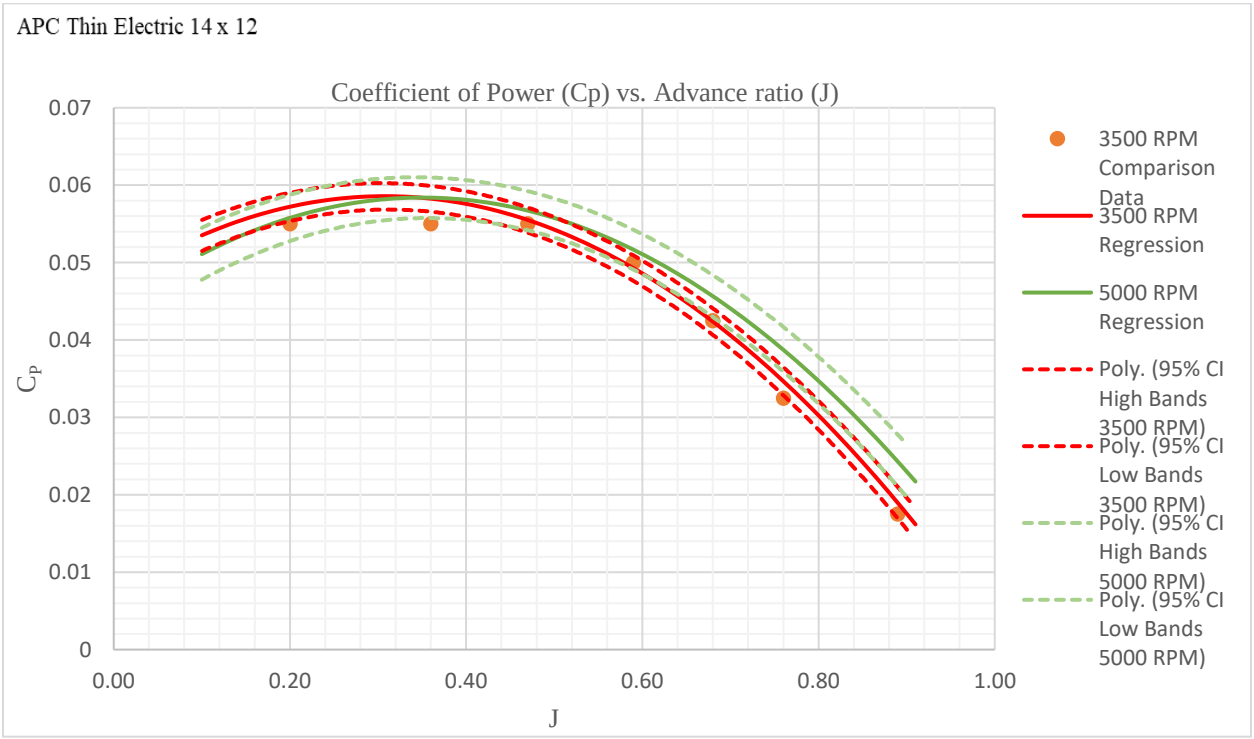

Figure 63- Coefficient of Power with 95% confidence interval bands and comparison data Selig [6]

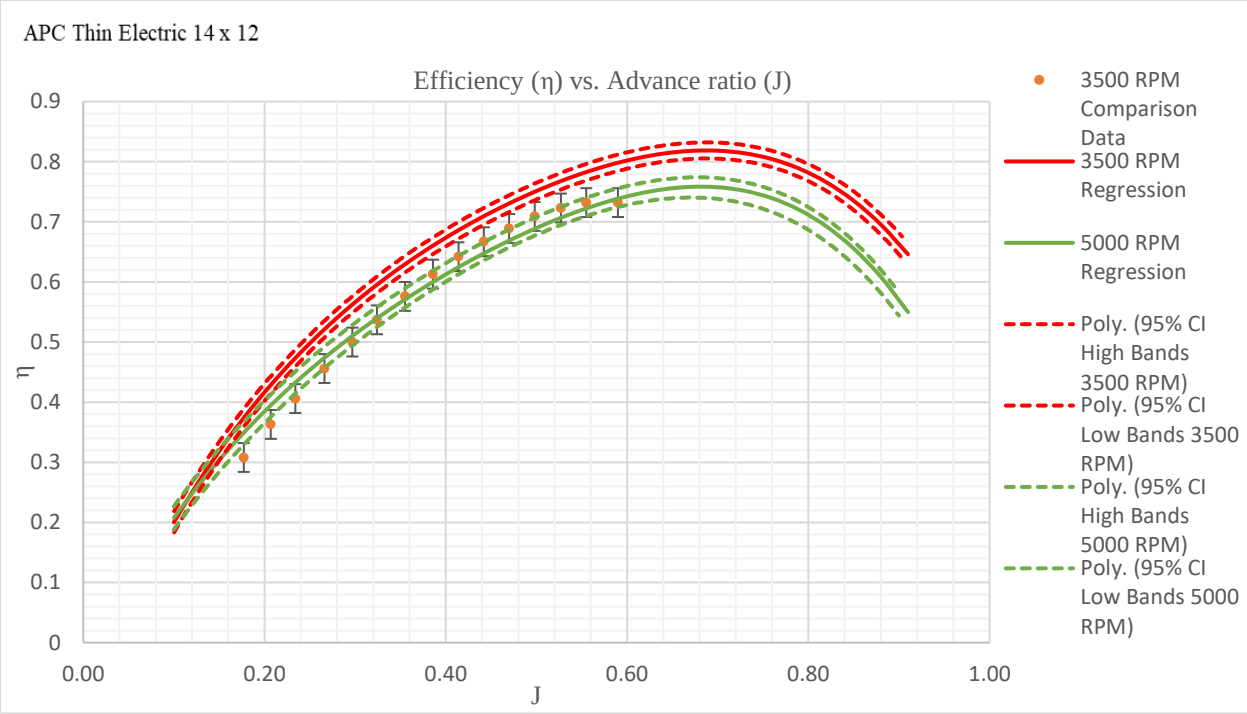

Figure 64- Efficiency with 95% confidence interval bands and comparison data with error bars Selig [6]

7.2.3 APC THIN ELECTRIC 17 X 12

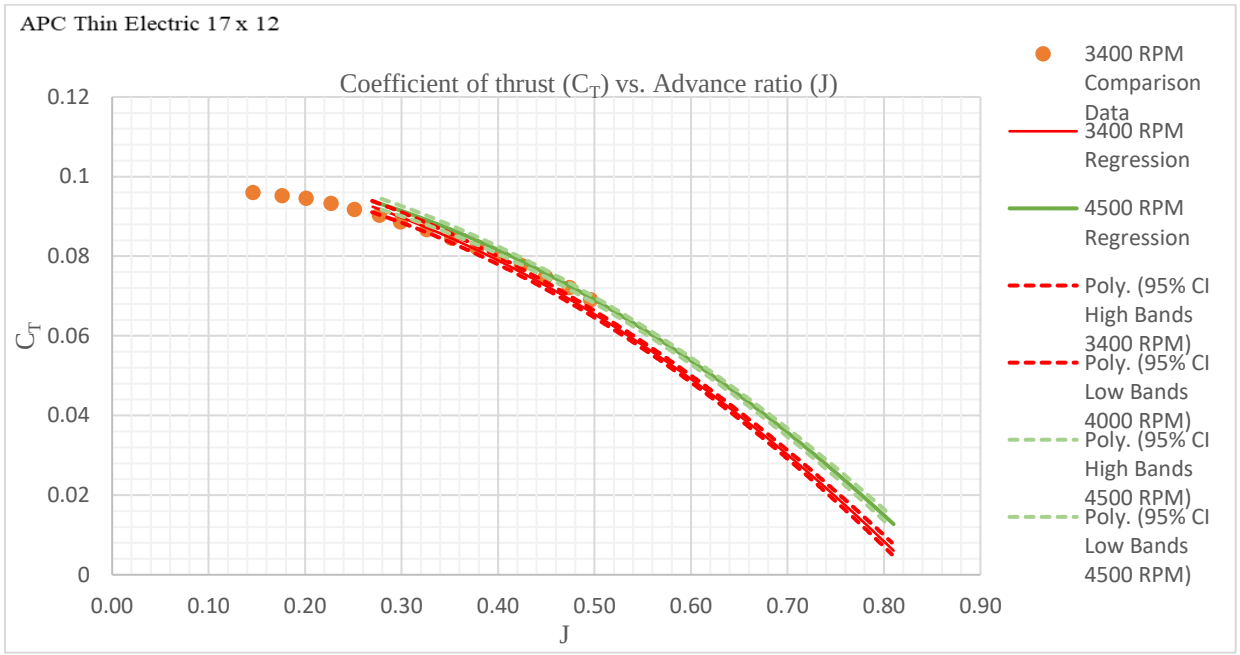

Figure 65- Coefficient of Thrust with 95% confidence interval bands and comparison data Selig [6]

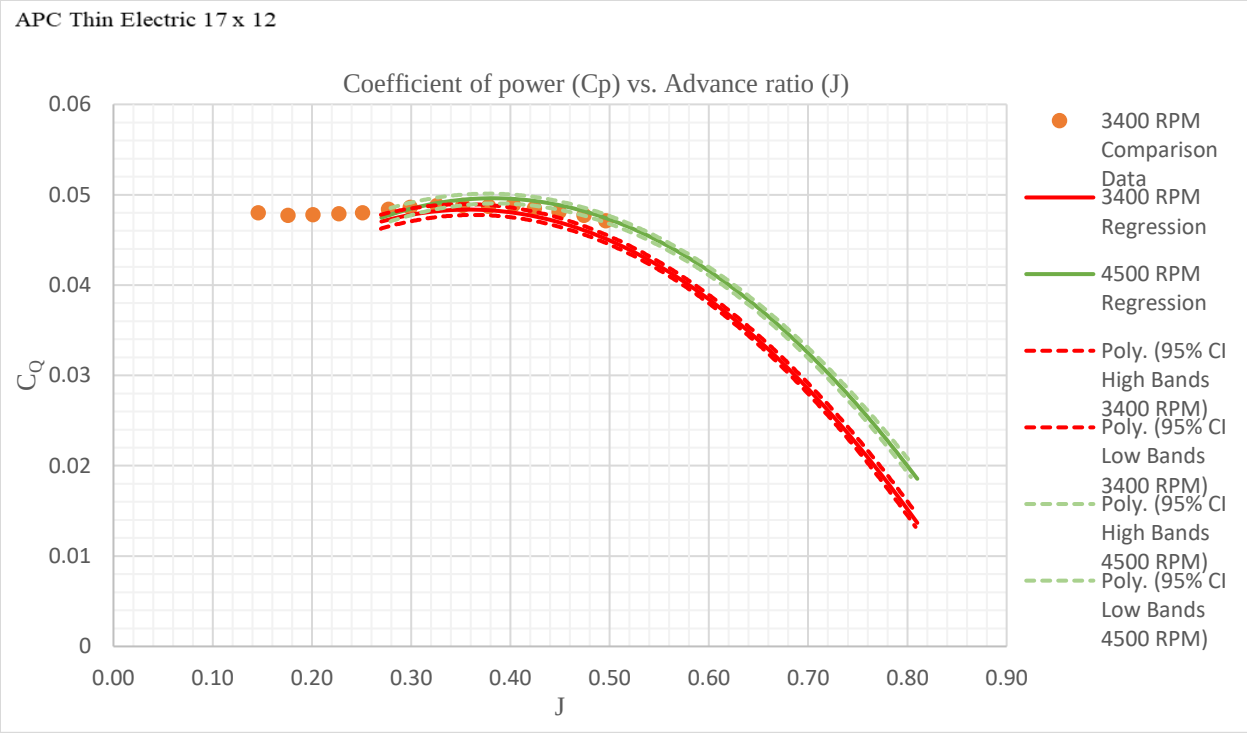

Figure 66- Coefficient of Power with 95% confidence interval bands and comparison data Selig [6]

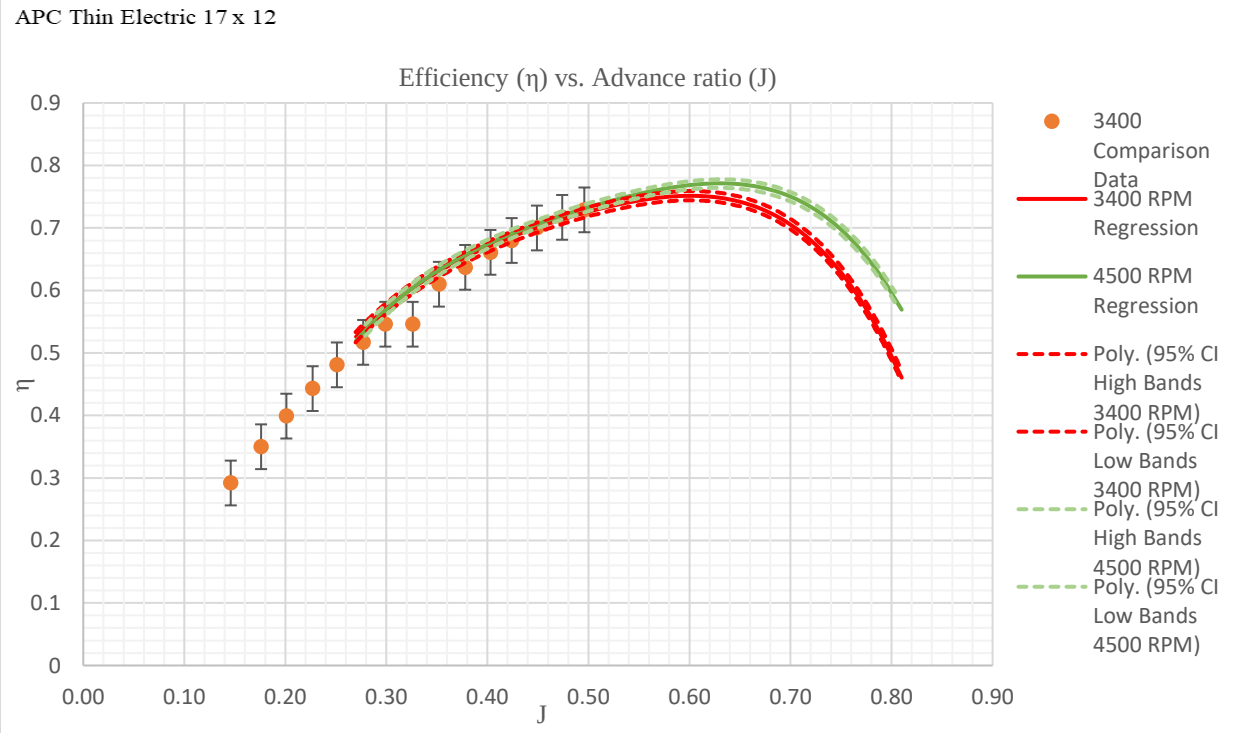

Figure 67- Efficiency with 95% confidence interval bands and comparison data with error bars Selig [6]

7.2.4 16 IN STRAIGHT AND SWEPT BLADE ALUMINIUM PROPELLER

A straight and swept blade aluminum propeller were machined at ODU with the intent to investigate the effect blade geometry has on the acoustic levels produced by the propeller. However, before venturing into the acoustic analysis, it was necessary first to investigate how the blade geometry affects its aerodynamic performance. This led to a comparison experiment between the swept and straight blade propeller. Both propellers were tested at a low and high RPM. A similar comparison study was performed by Wiedemann and Benjamin as a DOE class project in November 2018 before all improvements were made to the propeller test stand. A comparison was made between that project and this current experimentation to see how well the results improved in precision. The CI for both experiments were compared to each other in this study. Figures 68 through 75 were used to compare the results obtained at 3500 RPM for the project and this thesis for the swept and straight blade propeller. The 95% CI bands are shown for each propeller.

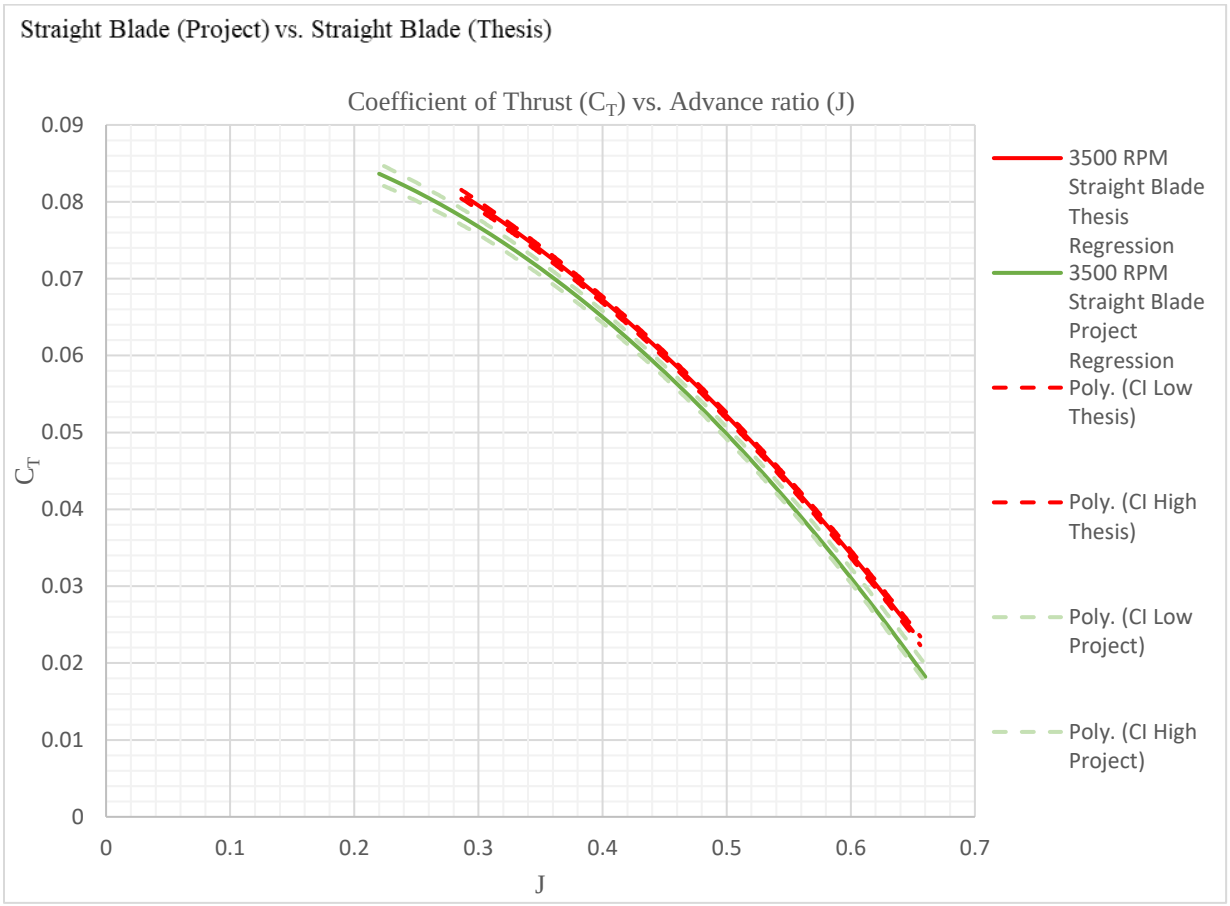

Figure 68- Coefficient of Thrust vs. Advance ratio for 16 in Straight Blade Propeller

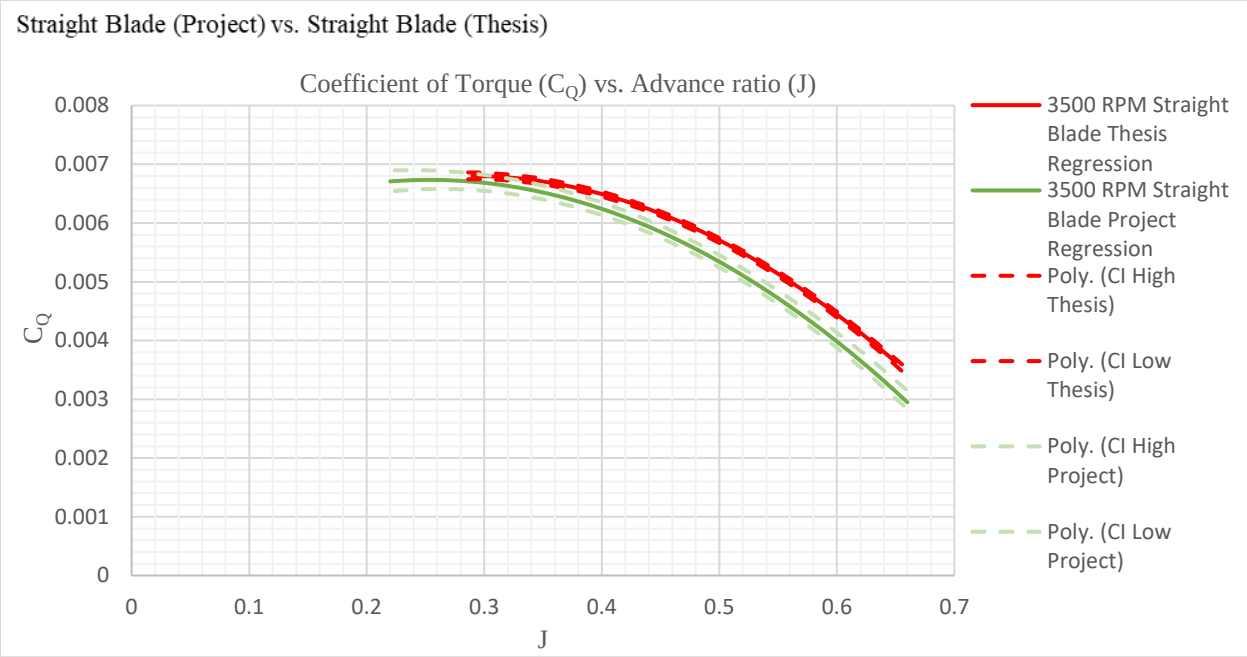

Figure 69- Coefficient of Torque vs. Advance ratio for 16 in Straight Blade Propeller

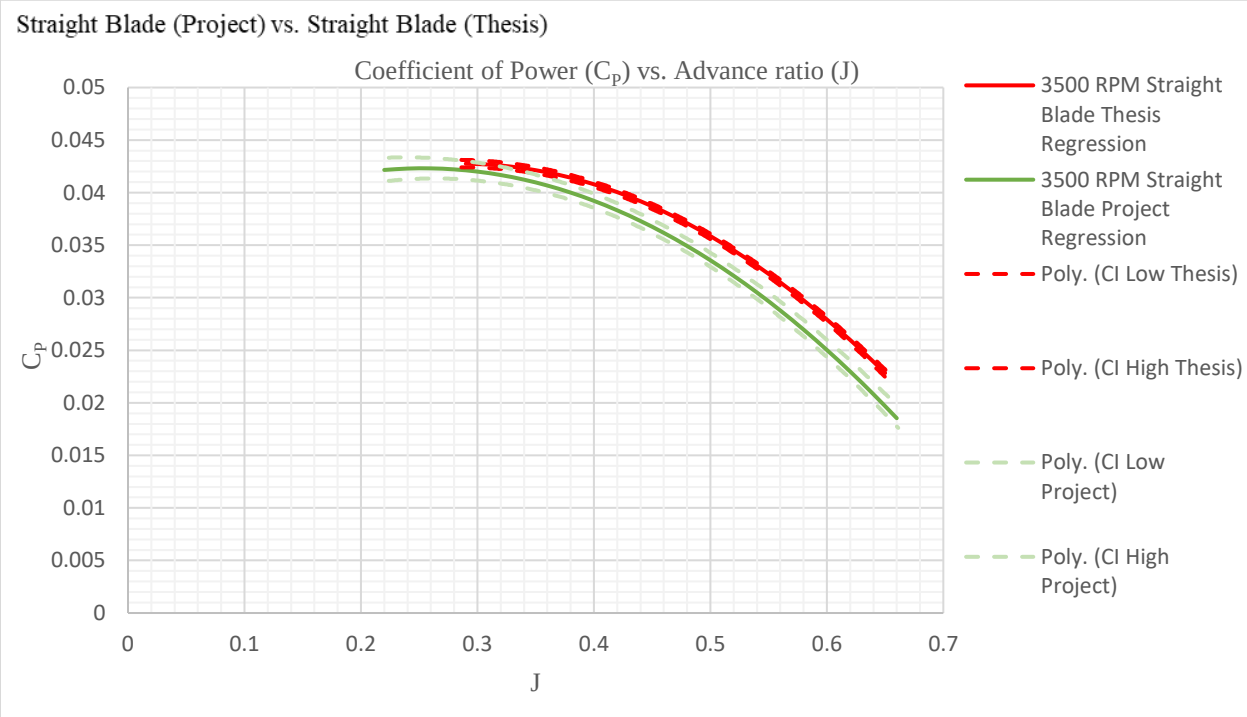

Figure 70- Coefficient of Power vs. Advance ratio for 16 in Straight Blade Propeller

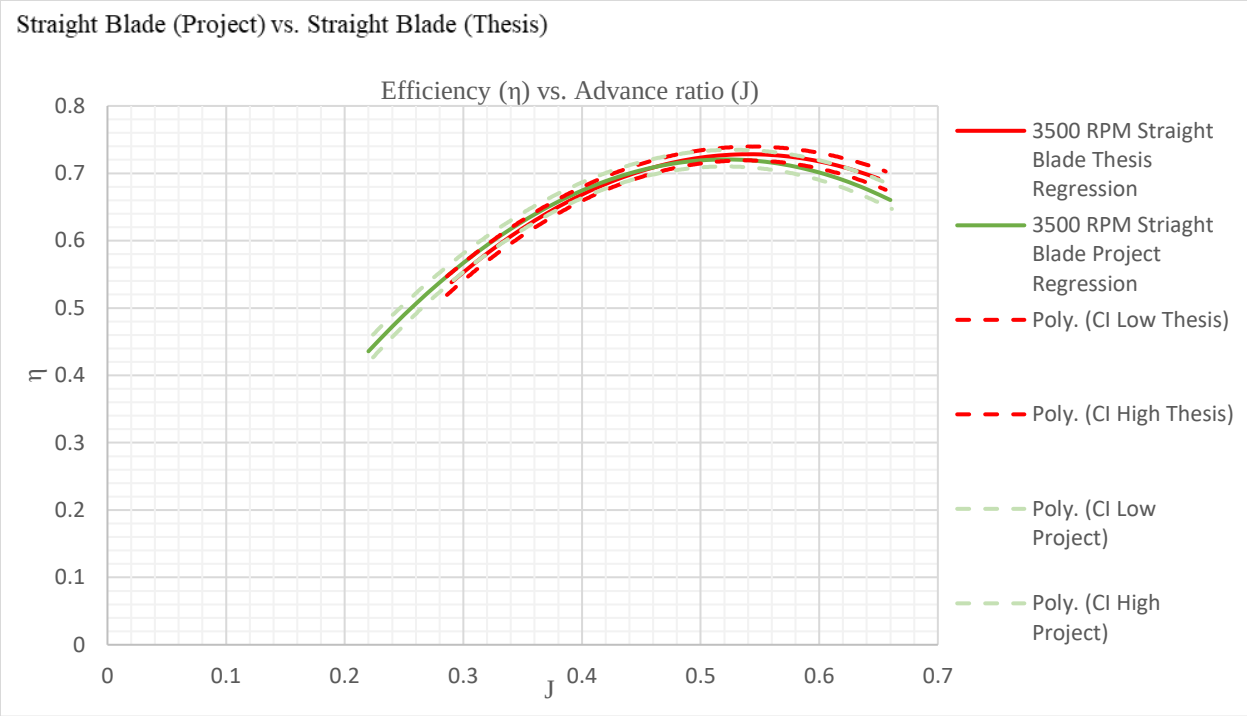

Figure 71- Efficiency vs. Advance ratio for 16 in Straight Blade Propeller

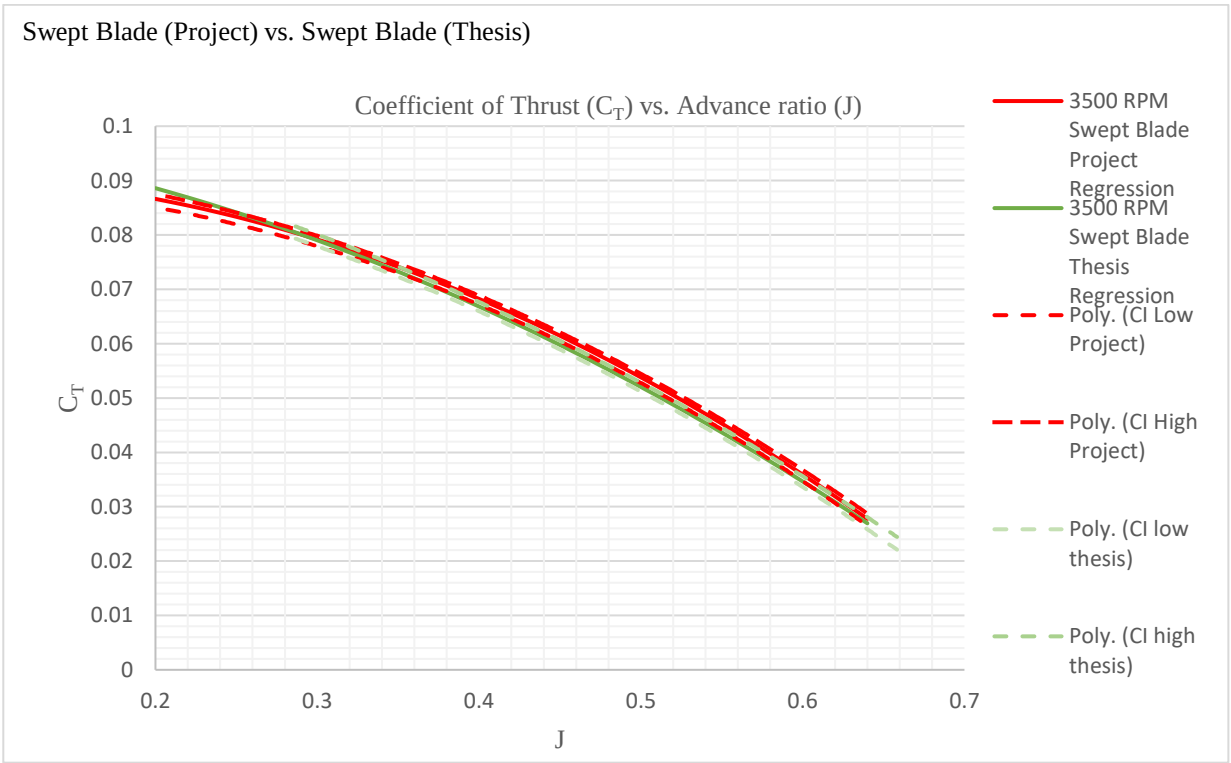

Figure 72- Coefficient of Thrust vs. Advance ratio for 16 in Swept Blade Propeller

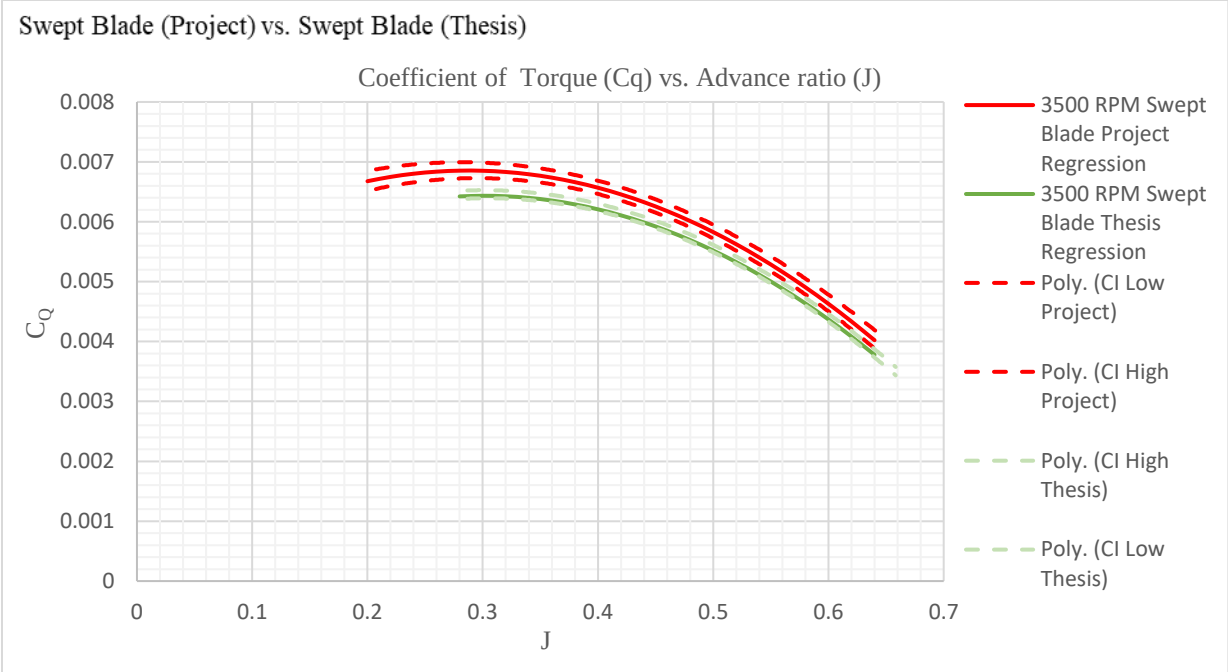

Figure 73- Coefficient of Torque vs. Advance ratio for 16 in Swept Blade Propeller

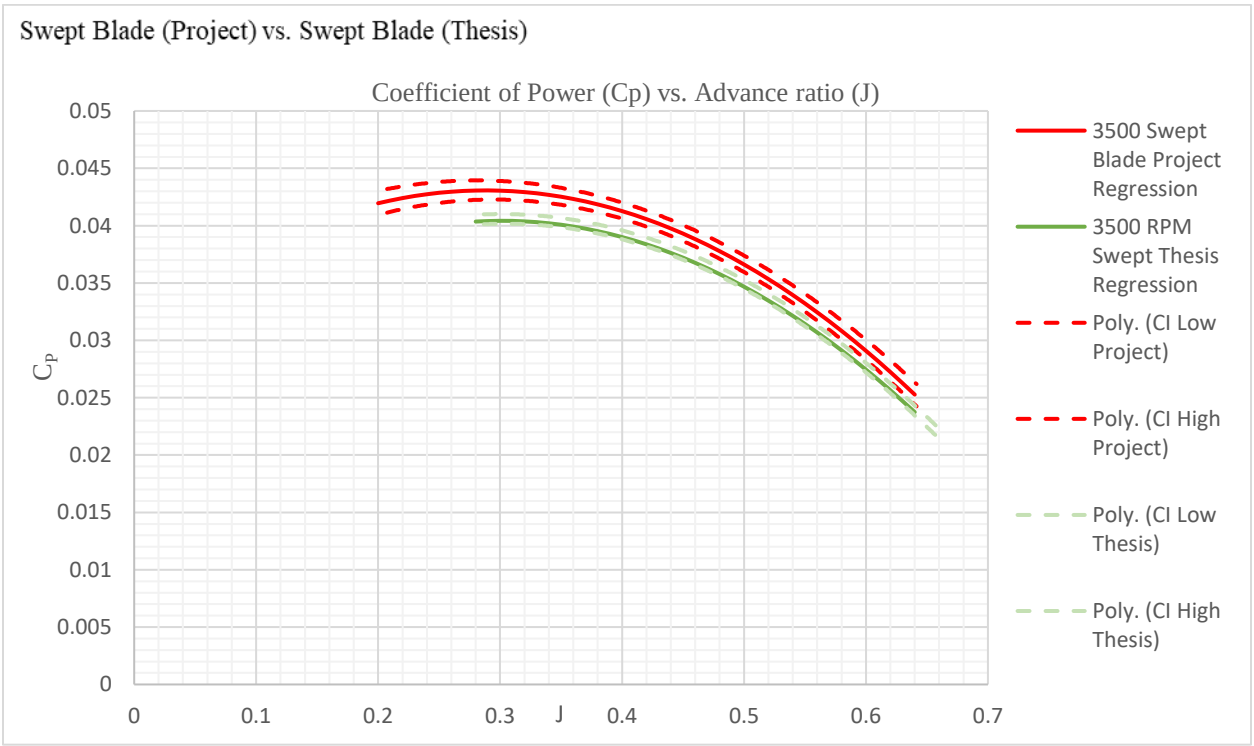

Figure 74- Coefficient of Power vs. Advance ratio for 16 in Swept Blade Propeller

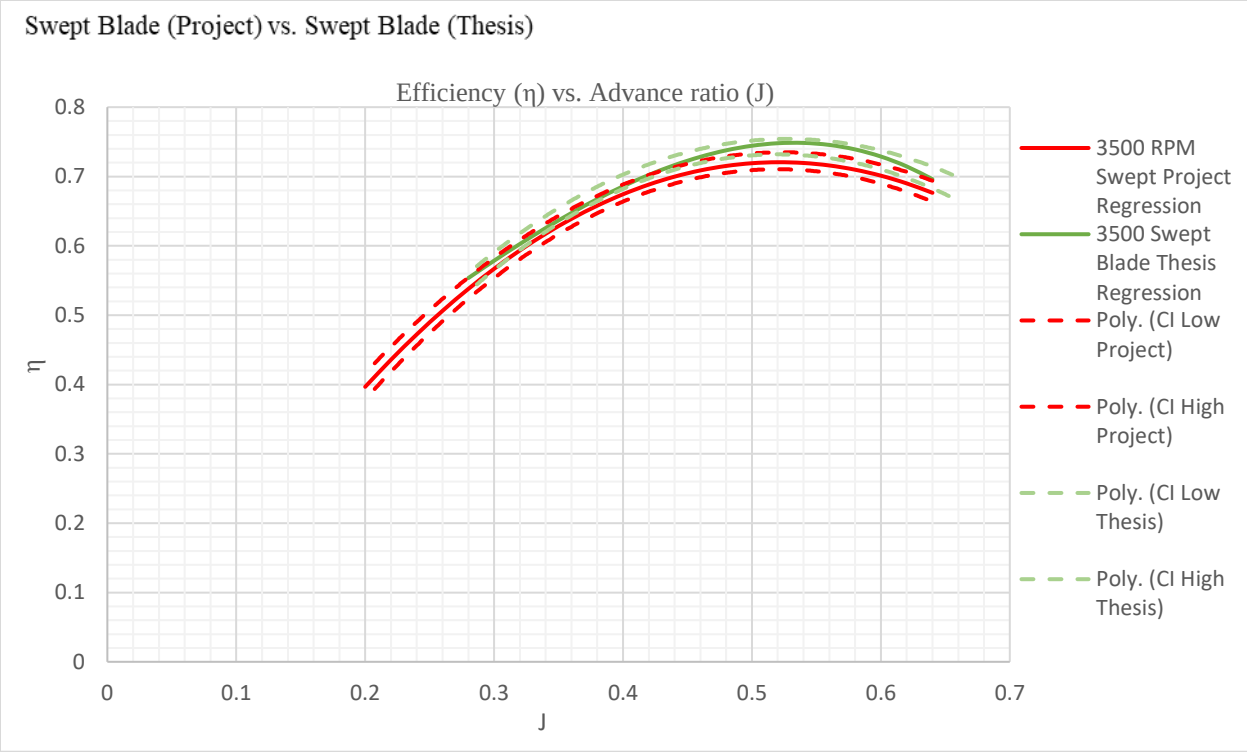

Figure 75- Efficiency vs. Advance ratio for 16 in Swept Blade Propeller

The performance characteristics of the swept and straight blade propeller were compared to each other with the data obtained throughout this thesis. Figure 76 through 79 show the results with the 95% CI bands.

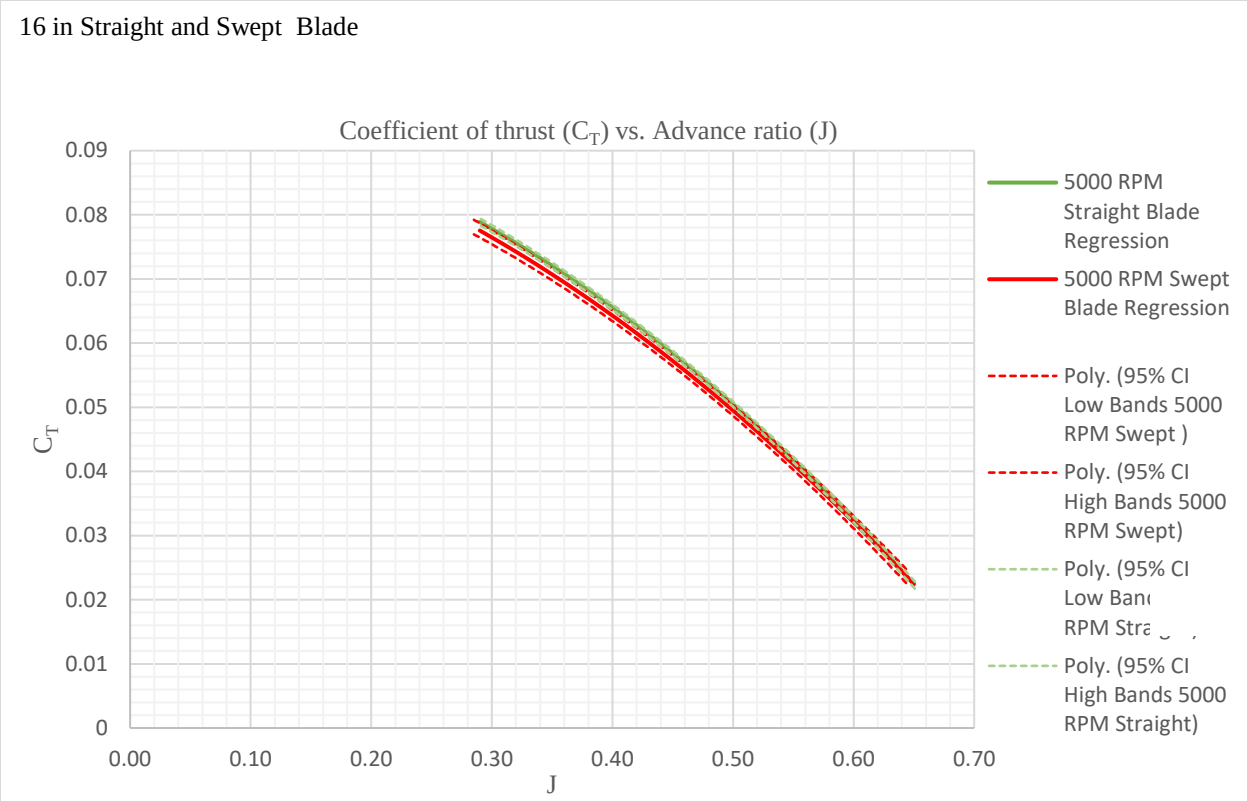

Figure 76- Coefficient of Thrust with 95% confidence interval bands

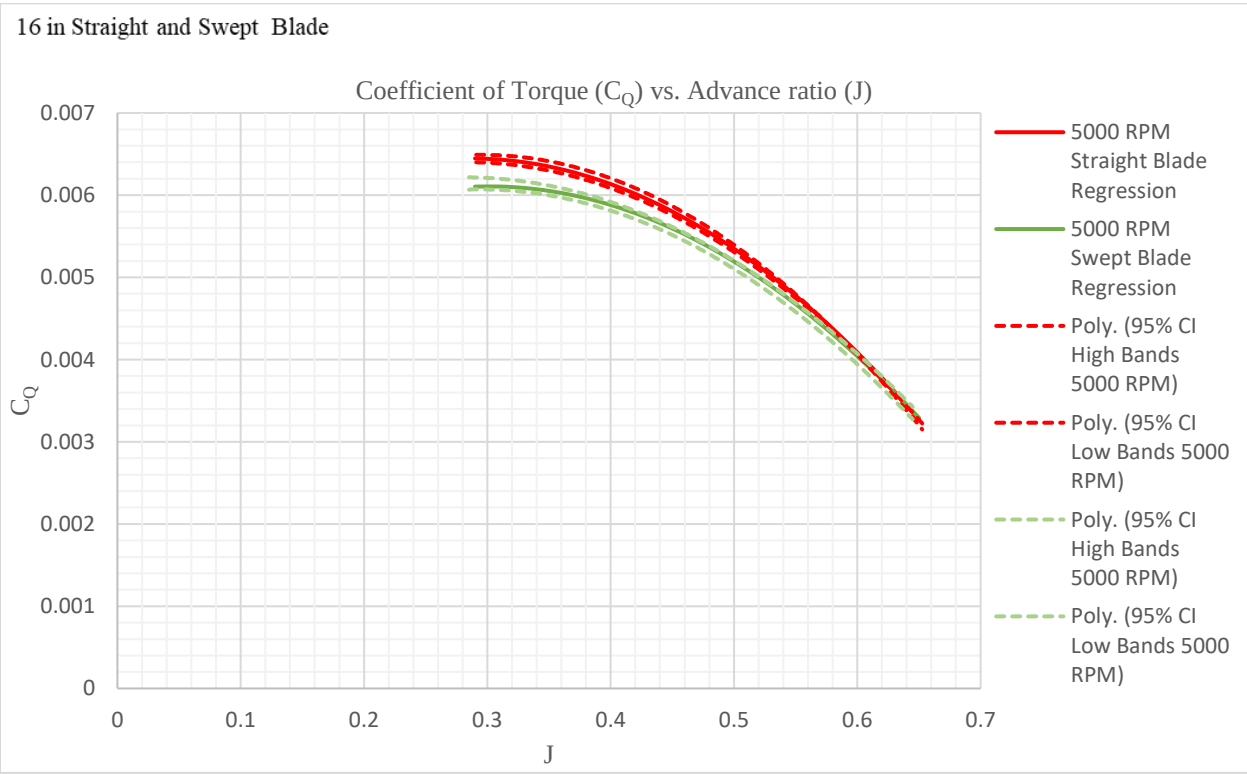

Figure 77- Coefficient of Torque with 95% confidence interval bands

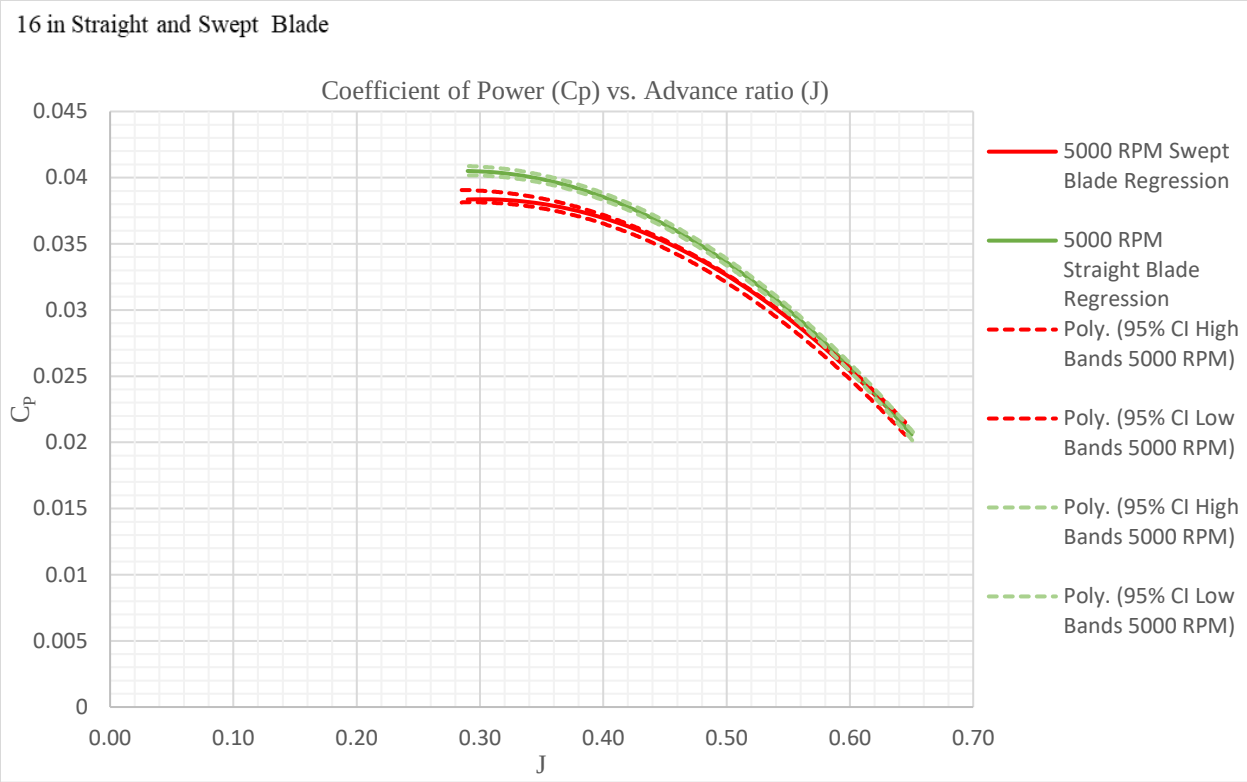

Figure 78- Coefficient of Power with 95% confidence interval bands

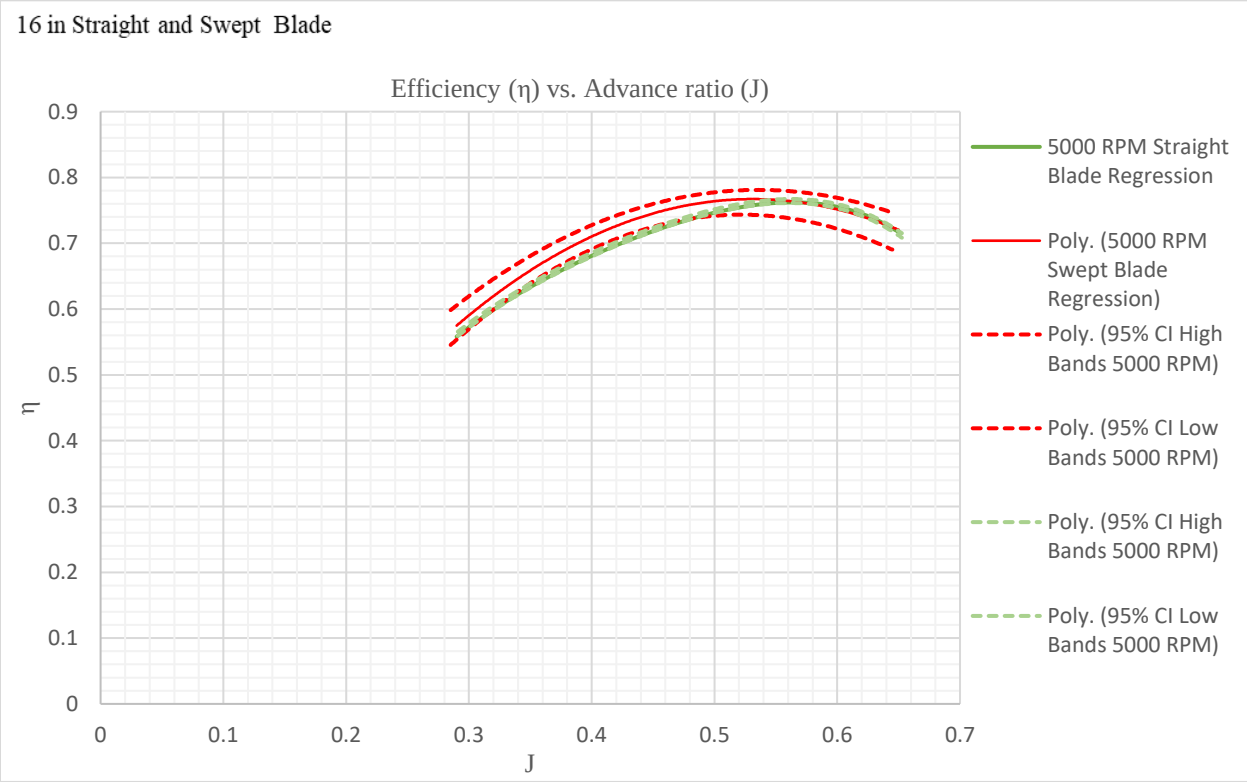

Figure 79- Efficiency with 95% confidence interval bands

7.3 DISCUSSION

The focus of this study was to characterize the propeller test stand and optimize it for the best precision and accuracy. The three APC propellers tested were compared to literature. The initial test with the 12 x 8 prop verified the proper functionality of the system. In order to make an accurate comparison, error bars are shown for the efficiency plots for the 14 x 12 and 17 x 12 props (Figures 64 and 67 respectively), which showed how well the experimental data compared to literature. For the 17 x 12 plot, the bars overlapped with the experimental data CI indicating that there is no difference between the two. However, for the 14 x 12 plot, the error bars overlapped with the wrong experimental RPM data. Known issues with Reynolds number sensitivity may explain this. For the straight and swept blade props, a comparison was made in order to address how geometry affects the aerodynamic performance of the propellers (Figures 76 through 79). The data indicates that the geometry does not affect the aerodynamic performance and surprisingly the swept blade propeller showed slightly higher efficiency than the straight blade propeller. The comparison plots of the swept and straight blade propeller for this thesis and the DOE project from November 2018 (Figures 68 through 75) showed that the uncertainty in measurements has improved, comparing the CI between the two experiments gave these results. For the efficiency comparison, the project from November indicated that the test rig performed slightly better. However, all other comparisons made showed that the test rig performed better throughout this thesis. There was an outlier within the efficiency model that was removed in order to improve the results. However, this did not decrease the CI bands. This anomaly is an unexpected result and is subjected to further research. This improved the R^2 value significantly, resulting in a better model.

The design test matrix shown in Appendix D, D.1, D.2, and D.3 contains the completely randomized run order for the 12 x 8, 14 x 12, 17 x 12, and the 16 in straight blade propeller tested in this thesis. A second order quadratic model was used in order to predict the final actual equation used to obtain each response. However, a quartic model was chosen for the 14 x 12, 17 x 12, 16 in swept, and 16 in straight propeller efficiency response since it yields higher R^2 values.

The verification points shown in bold of each test matrix were independent of the design point locations. These points were not used in the analysis however they were used to assess the prediction capability of the model. Appendix J through J.3 represents the confirmation points for the 12 x 8, 14 x 12, 17 x 12, and the 16 in straight-

blade propeller. The values in red indicate the points that fell outside the acceptable PI range. The 17 x 12 propeller showed the best comparison data throughout this experiment.

Appendix E through E.2 shows the ANOVA tables which were used to determine the significant and insignificant model terms used for building the final response model. The fit statistics indicate how well the model fits and its prediction capabilities. An R^2 value of one is desired, which means all of the variability in the response is explained by the model. Fit statistics obtained for the all tested propellers showed the lowest R^2 value was 97.63% indicating that the chosen models fit the data extremely well.

Response	**C_T**	**C_Q**	**C_P**	**η**
Std. Dev.	0.001577781	0.0001985	0.0012473	0.0209725
Mean	0.070705638	0.0062749	0.0394266	0.5554472
R^2	0.997272171	0.9762577	0.9762575	0.987641
Adjusted R^2	0.996835719	0.9724589	0.9724587	0.9856636
Predicted R^2	0.996121602	0.9658892	0.965889	0.9802993

Table 15- Fit Statistics for APC 12x8 Propeller Fit Statistics for APC 14x12 Propeller

Response	**C_T**	**C_Q**	**C_P**	**η**
Std. Dev.	0.003693997	0.0003956	0.0024855	0.0133
Mean	0.068910193	0.0069667	0.0437733	0.5993
R^2	0.990228289	0.9775895	0.9775895	0.9977
Adjusted R^2	0.989685416	0.974953	0.974953	0.9966
Predicted R^2	0.988544919	0.9700688	0.9700687	0.9938

Table 16- Fit Statistics for APC 14x12 Propeller Fit Statistics for APC 14x12 Propeller

Response	**C_T**	**C_Q**	**C_P**	**η**
Std. Dev.	0.0009	0.0001	0.0004	0.0109
Mean	0.0551	0.0053	0.0336	0.6888
R^2	0.9984	0.9967	0.9967	0.9824
Adjusted R^2	0.9980	0.9960	0.9960	0.9770
Predicted R^2	0.9969	0.9938	0.9938	0.9613

Table 17- Fit Statistics for 16 in Swept Blade Aluminum Propeller

The final equation in terms of actual factors are also shown in Appendix F through F.3. These equations were used in order to plot the regression models seen in the graphs. The graphs show 95% confidence interval bands used to compare the experimental data to literature. The comparison points did not all fall within these bands; however, they were reasonably close to the CI of the experimental data indicating high agreement with the data obtained. As expected the highest accuracy was observed with the APC 17x12 propeller because it can produce the desired thrust which is best suited to load the internal balance. This propeller showed a great prediction model and the comparison data agreed with the experimental data. Approximate confidence intervals were computed for the comparison data when possible which shows good agreement with the present data.

Assumptions of error normality, independence, and constant variance were tested using residual diagnostics. Appendix G through G.3 shows the normal probability plot for the 12 x 8, 14 x 12, 17 x 12 and the 16 in swept-blade propeller. The “fat pencil” test was passed, which indicates a normal distribution of all residuals validating the normality assumption. Appendix I through I.3 shows the plots of residuals versus run order that was obtained for the 12 x 8, 14 x 12, 17 x 12, and the 16 in swept-blade propeller. These plots identify the independence of the responses from time. The plots showed a structureless form alternating across zero, which verified the independence assumption.

The final assumption to be verified was the constant variance. The plots shown in Appendix H through H.3 of residuals versus predicted values shows no sign of coning or barreling and are bounded within the normal limits. This indicates that the constant variance assumption is valid.

As a final check to see if the method developed is generally applicable over a broad range of advance ratios, a data set was obtained from another student that includes a complete performance range for the 16 in straight blade propeller. Additional performance plots for this data are shown in Appendix K. By increasing the polynomial order to match the increased number of levels for factor J, performance was well modeled. Regression models obtained are given in Appendix L. It should be noted that this data set was not randomized and hence no statistical testing was done. It did, however, showcase the methodology and looks promising going forward.

CHAPTER 8 – CONCLUSION AND FUTURE WORK

A total of five propellers were tested in the ODU low-speed wind tunnel over an average of three different rotational speeds and a wide range of advance ratios in order to validate the improvements made to the propeller test stand. In each test, a completely randomized test matrix was generated, and a detailed statistical analysis was performed on the resulting data. The validation of all results on the three APC propellers was done by comparing them to previous literature, while a direct comparison was made between the swept and straight blade aluminum propeller. In addition, a comparison was made between measurements on the swept and straight blade props from a DOE project completed in November 2018 and this thesis in order the determine if the uncertainty of measurements were improved. From the data obtained it can be concluded that the improvements made to the propeller test stand increased the accuracy and precision of the measurements obtained during experimentation. Accuracy was gauged by a favorable comparison to the literature. The precision of measurements was improved and shown by decreased confidence interval widths in the recent aluminum propeller data versus that of November 2018. From first principles, it is known that as a propeller's diameter and pitch increases so does the thrust and torque force it produces. Also, when within the limits of the balance, the relative precision improves and it is a percentage of the full-scale balance range.

The objectives of this thesis have been met, and the newly designed and upgraded features made to the propeller test stand showed improved performance, accuracy, and precision of the data collected. The system shows excellent repeatability of data with stable RPM and tunnel velocity settings. However, the results confirmed that a propeller which produces a low thrust value tends to have a high variation. The three APC propellers that were tested and compared to literature showed results with the comparison plots mainly falling within the confidence interval from the experimental data. This suggests good accuracy of the system and its ability to replicate previous data. Unfortunately, there is no real standard to compare for propeller performance. During the characterization of the two aluminum propellers, significant data was obtained with excellent repeatability. The system is capable of generating high-quality data suitable for research. This leaves room for the exploration of these types of designed propellers for UAVs. Interest in the acoustics of these propellers could be further explored since the swept geometry does not diminish the propeller's performance. For future comparisons, using larger propellers would be better in order to load the balance in a more desired range than the smaller propellers. Also obtaining acoustic data on the swept and straight propeller and comparing them to each other would be a useful exploration as minimal data set

exists on these propeller designs with acoustic characterization. Furthermore, it would be of interest to use DOE to characterize the uncertainties with the propeller test stand.

REFERENCES

[1] B.E. Duvall, “Development and Implementation of a Propeller Test Capability for GI-10” Greased Lightening “Propeller Design,” M.S. thesis, Dept. Aero. Eng., Old Dominion Univ., VA, USA, 2016. [Online]. Available:https://digitalcommons.odu.edu/mae_etds/12

[2] N.B. Sadowski, “A Cost Effective Design for a Propeller Thrust/Torque Balance,” M.S. thesis, Dept. Mech. and Aero. Eng., Old Dominion Univ., VA, USA, 2018. [Online]. Available: https://digitalcommons.odu.edu/mae_etds/39

[3] A.J. Brezina and S.K. Thomas, “Measurement of Static and Dynamic Performance Characteristics of Small Electric Propulsion Systems,” Ph.D. disser, Dept. Mech. and Mat. Eng., Wright State Univ., OH, USA,

[4] J.B. Brandt, “Small-Scale Propeller Performance at Low Speeds,” M.S. thesis, Dept. Aero. Eng., Univ. of Urbana-Champaign, IL, USA, 2005.

[5] “Recommended Practice: Calibration and Use of Internal Strain-Gage Balances with Application to Wind Tunnel Testing (AIAA R-091-2003),” in *Recomm. Prac.: Calib. and Use of Int. Strain-Gage Balances with Appl. To Wind Tunnel Testing (AIAA R-091-2003),* 2003, doi: 10.2514/4.476464.001

[6] J. B. Brandt and M. S. Selig, “Propeller Performance Data at Low Reynolds Numbers,” presented at 49 th AIAA Aero. Science Meeting, Orlando, FL, USA, Jan. 4-7, 2011.

[7] D. Verstraete and R. MacNeill, “The Effects of Blockage on the Performance of Small Propellers,” School of Aero., Mech. and Mechatronic Eng.

[8] “Fibre Glast – Fiberglass, Carbon Fiber, Resin, Composite Materials.” http://www.fibreglast.com/ (accessed Oct. 3, 2018).

[9] “Wire Gauges – Current Ratings.” Engineering ToolBox. https://www.engineeringtoolbox.com/wire-gauges-d_419.html (accessed Jun. 15, 2018).

[10] D. C. Giancoli, in *Physics for scientists & engineers*. Upper Saddle River, NJ, USA: Pearson Prentice Hall, 2008.

[11] D.C. Montgomery, in *Design and analysis of experiments*. Hoboken, NJ, USA: Wiley, 2017.

[12] D.Landman. (2018). Four Eras in the History of DOE [PowerPoint slides].

[13] D.C. Montgomery and G.C. Runger, in *Applied statistics and probability for engineers*. Hoboken, NJ, USA: Wiley, 2018.

[14] M. Ol, C. Zeune, and M. Logan, "Analytical-Experimental Comparison for Small Electric Unmanned Air Vehicle Propellers," AIAA 2008-7345, presented at 26th AIAA Applied Aerodynamics Conference, Honolulu, HI, August 18-21, 2008.

[15] R.H. Myers, D.C. Montgomery and C.M. Anderson-Cook, in *Response Surface Methodology*, 4th ed., Hoboken, NJ, USA: Wiley, 2016. [Online]. Available: //http://books.google.com.

[16] T.R. Yechout, S.L. Morris, D.E. Bossert, W.F. Hallgren and J.K. Hall, in *Introduction to Aircraft Flight Mechanics*, 2nd ed. AIAA, 2014.

[17] E. Baris, "An investigation Into the Potential Benefits of Distributed Electric Propulsion on Small UAVs at Low Reynolds Numbers," M.S. thesis, Dept. Mech. and Aero. Eng., Old Dominion Univ., VA, USA, 2017. [Online]. Available: https://digitalcommons.odu.edu/mae_etds/24

[18] M.P. Merchant and S.L. Miller, "Propeller performance Measurement for Low Reynolds Number UAV Applications," in *AIAA*, 2006.

[19] A.J. Brezina and S.K. Thomas, "Measurement of Static and Dynamic Performance Characteristics of Small Electric Propulsion Systems," Dept. Mech. and Mat. Eng., Wright State Univ. Ohio

[20] R.K. Tripathi, V. Tiwari, I. Khunger and P. Berwal, "Development of Propeller Test Rig and Evaluation of Propeller Performance."

[21] P.M. Creciun, "The Effects of Blockage Ratio and Distance from a Free Surface on the Performance of a Hydrokinetic Turbine," M.S. thesis, Dept. Mech. and Aero. Eng., 2013

[22] D. Landman, J. Simpson, R. Mariani, F. Ortiz and C. Britcher, "Hybrid Design for Aircraft Wind-Tunnel Testing Using Response Surface Methodologies," *Journal of Aircraft*, vol. 44, no.4, pp.1214-1221, 2007.

[23] D. Landman and D. Yodert, "Wind- Tunnel Balance Calibration with Temperature Using Design of Experiments," *Journal of Aircraft*, vol. 51, no.3, May-Jun. 2014, doi: 10.2514/1.c032416.

[24] D. Landman, J. Simpson, R. Mariani, F. Ortiz, and C. Britcher, "Hybrid Design for Aircraft Wind-Tunnel Testing Usng Response Surface Methodologies," Journal of Aircraft, vol. 44, no.4, pp. 1214 – 1221, Jul. – Aug. 2007, doi: 10.2514/1.25914.

APPENDIX A

LABVIEW BLOCK DIAGRAM OF OUTPUT FILE DOCUMENTATION

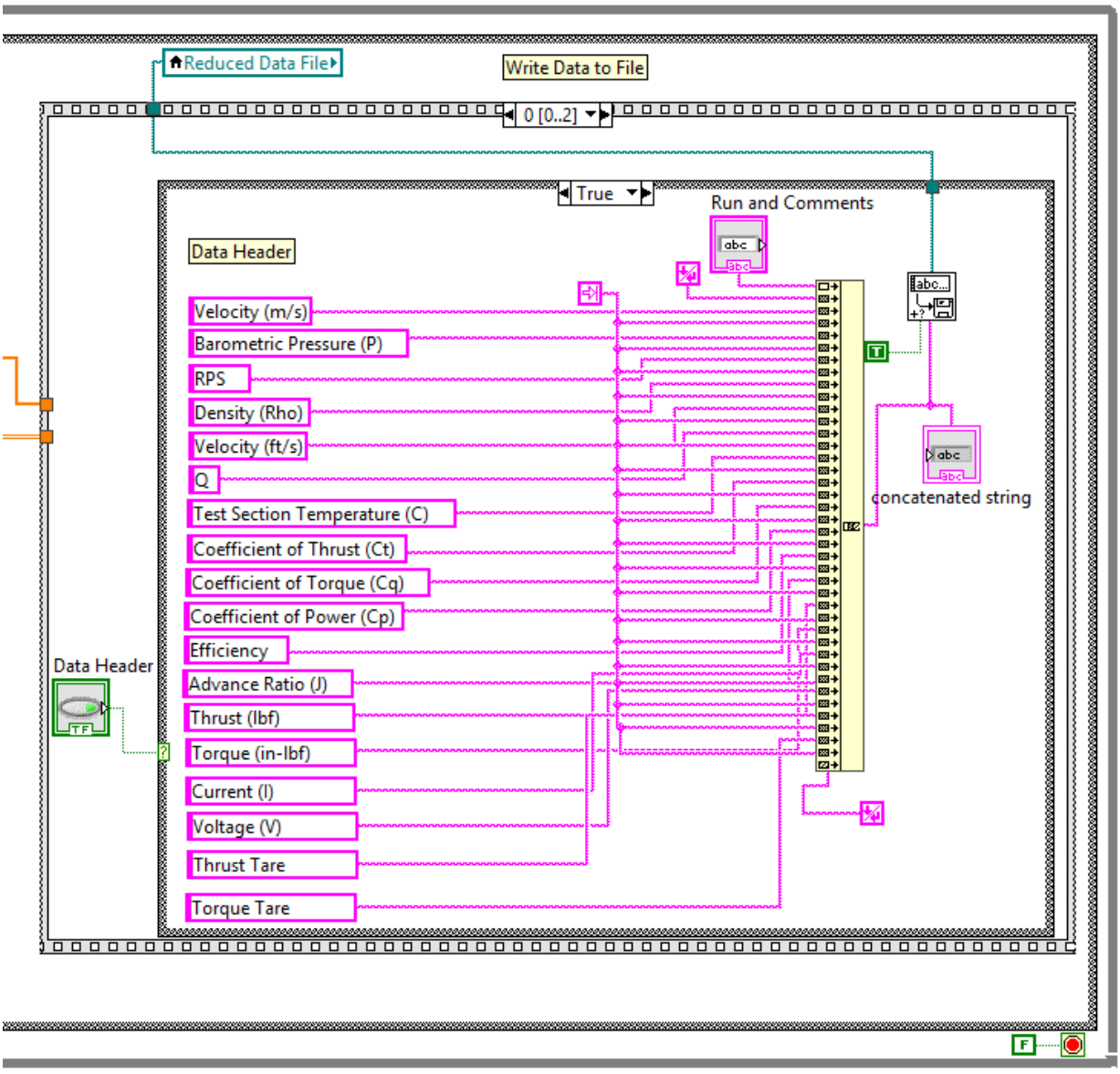

APPENDIX A.1

LABVIEW BLOCK DIAGRAM OF RPM SIGNAL INPUT, CURRENT AND VOLTAGE

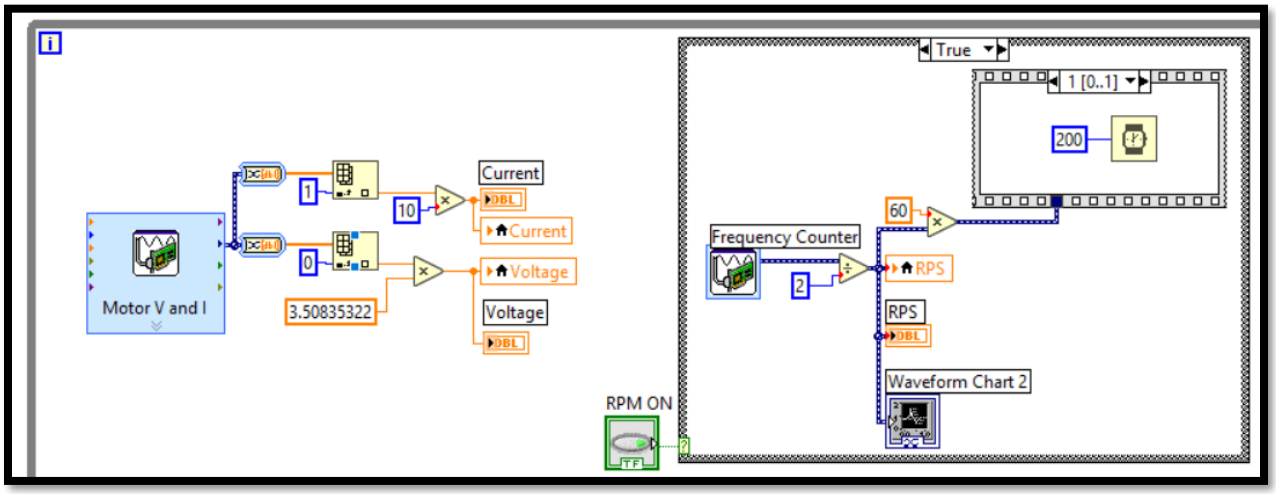

APPENDIX B

RESULTS OF APC THIN ELECTRIC 12 x 8 PROPELLER

Wind Tunnel Performance Results

APC Thin Electric 12x8 Propeller 4000 RPM

Velocity (m/s)	Barometric Pressure (Pa)	RPS	Density (slugs/ft³)	Velocity (ft/s)	Dynamic Pressure (q)	Test Section Temperature (°C)	Coefficient of Thrust (C_t)	Coefficient of Torque (C_q)	Coefficient of Power (C_p)	Efficiency	Advance Ratio (J)	Thrust (lbf)	Torque (in-lbf)	Current (I)	Voltage (V)	Thrust Tare	Torque Tare	RPM
7.61	101491.16	65.65	0.00233	24.96	2.50	21.0	0.1012	0.0065	0.0410	0.25	0.10	1.045	-0.808	2.97	20.85	-1.1807	-0.3639	3939.20
5.04	101474.00	66.48	0.00233	16.55	2.65	21.0	0.1011	0.0063	0.0395	0.26	0.10	1.043	-0.779	2.97	20.85	-1.1807	-0.4625	3988.62
13.03	101547.31	66.50	0.00233	42.74	13.12	21.0	0.0949	0.0070	0.0442	0.49	0.23	1.001	-0.890	3.14	20.85	-1.1807	-0.3639	3989.87
2.10	101502.09	66.53	0.00233	6.89	15.28	21.0	0.0926	0.0073	0.0459	0.50	0.25	0.953	-0.903	3.07	20.85	-1.1807	-0.1942	3991.65
2.04	101524.00	66.53	0.00233	6.69	34.78	21.0	0.0735	0.0066	0.0413	0.68	0.38	0.739	-0.793	2.90	20.85	-1.1807	-0.4625	3991.97
13.12	101506.20	66.61	0.00233	43.03	37.14	21.0	0.0747	0.0069	0.0431	0.67	0.39	0.782	-0.862	3.05	20.85	-1.1807	-0.3639	3996.49
10.27	101524.42	66.71	0.00233	33.68	63.34	21.0	0.0490	0.0054	0.0338	0.74	0.50	0.509	-0.670	2.59	20.85	-1.1807	-0.3639	4002.75
10.33	101547.09	66.80	0.00233	33.89	64.12	21.0	0.0480	0.0059	0.0370	0.66	0.51	0.500	-0.734	2.59	20.85	-1.1807	-0.4625	4007.87
7.86	101516.91	67.00	0.00233	25.79	102.02	21.0	0.0244	0.0040	0.0253	0.62	0.64	0.251	-0.498	1.94	20.85	-1.1807	-0.4625	4019.91
4.67	101504.62	67.25	0.00233	15.33	103.35	21.0	0.0236	0.0035	0.0220	0.69	0.65	0.244	-0.434	1.94	20.85	-1.1807	-0.3639	4034.95

APC Thin Electric 12x8 Propeller 5000 RPM

Velocity (m/s)	Barometric Pressure (Pa)	RPS	Density (slugs/ft³)	Velocity (ft/s)	Dynamic Pressure (q)	Test Section Temperature (°C)	Coefficient of Thrust (C_t)	Coefficient of Torque (C_q)	Coefficient of Power (C_p)	Efficiency	Advance Ratio (J)	Thrust (lbf)	Torque (in-lbf)	Current (I)	Voltage (V)	Thrust Tare	Torque Tare	RPM
16.61	101533.00	83.15	0.00233	54.49	4.30	21.0	0.1015	0.0067	0.0422	0.25	0.11	1.653	-1.313	5.10	20.85	-1.1807	-0.3639	4988.96
6.21	101531.69	83.45	0.00233	20.37	4.32	21.0	0.1022	0.0070	0.0440	0.25	0.11	1.662	-1.365	5.09	20.85	-1.1807	-0.1942	5007.04
9.78	101501.40	83.51	0.00233	32.09	22.16	21.0	0.0937	0.0071	0.0445	0.50	0.24	1.524	-1.383	5.28	20.85	-1.1807	-0.3639	5010.48
9.70	101529.02	83.51	0.00233	31.83	23.16	21.0	0.0926	0.0070	0.0441	0.51	0.24	1.504	-1.369	5.27	20.85	-1.1807	-0.4625	5010.64
2.68	101467.93	83.53	0.00233	8.80	56.56	21.0	0.0768	0.0073	0.0457	0.64	0.38	1.249	-1.420	5.27	20.85	-1.1807	-0.4625	5011.51
6.07	101520.47	83.53	0.00233	19.92	57.46	21.0	0.0771	0.0070	0.0441	0.67	0.38	1.253	-1.371	5.27	20.85	-1.1807	-0.4625	5011.60
2.68	101539.38	83.57	0.00233	8.78	98.00	21.0	0.0557	0.0065	0.0406	0.69	0.50	0.912	-1.269	4.66	20.85	-1.1807	-0.1215	5014.34
16.41	101476.53	83.57	0.00233	53.83	103.81	21.0	0.0526	0.0060	0.0374	0.72	0.52	0.859	-1.167	4.54	20.85	-1.1807	-0.3639	5014.47
13.15	101511.22	83.68	0.00233	43.13	161.68	21.0	0.0278	0.0042	0.0263	0.68	0.64	0.452	-0.818	3.40	20.85	-1.1807	-0.1942	5020.75
12.77	101463.78	83.81	0.00233	41.91	165.80	21.0	0.0246	0.0041	0.0256	0.63	0.66	0.397	-0.787	3.24	20.85	-1.1807	-0.4625	5028.58

APC Thin Electric 12x8 Propeller 6000 RPM

Velocity (m/s)	Barometric Pressure (Pa)	RPS	Density (slugs/ft³)	Velocity (ft/s)	Dynamic Pressure (q)	Test Section Temperature (°C)	Coefficient of Thrust (C_t)	Coefficient of Torque (C_q)	Coefficient of Power (C_p)	Efficiency	Advance Ratio (J)	Thrust (lbf)	Torque (in-lbf)	Current (I)	Voltage (V)	Thrust Tare	Torque Tare	RPM
2.97	101485.56	99.68	0.00233	9.73	5.29	21.0	0.1037	0.0070	0.0437	0.23	0.10	2.400	-1.931	8.11	20.85	-1.1807	-0.4625	5981.00
3.14	101534.42	99.69	0.00233	10.30	5.92	21.0	0.1032	0.0071	0.0449	0.24	0.10	2.392	-1.985	8.12	20.85	-1.1807	-0.4625	5981.60
7.12	101525.44	100.09	0.00233	23.35	30.43	21.0	0.0947	0.0074	0.0464	0.48	0.23	2.212	-2.069	8.54	20.85	-1.1807	-0.4625	6005.22
7.13	101532.00	100.10	0.00233	23.39	30.53	21.0	0.0945	0.0074	0.0464	0.48	0.23	2.208	-2.069	8.54	20.85	-1.1807	-0.4625	6006.19
11.49	101500.44	99.93	0.00233	37.71	79.35	21.0	0.0810	0.0075	0.0469	0.65	0.38	1.885	-2.086	8.56	20.85	-1.1807	-0.3639	5996.02
11.79	101512.84	99.94	0.00233	38.69	83.57	21.0	0.0790	0.0074	0.0467	0.66	0.39	1.840	-2.075	8.55	20.85	-1.1807	-0.3639	5996.50
15.47	101533.00	99.87	0.00233	50.75	143.77	21.0	0.0581	0.0066	0.0417	0.71	0.51	1.352	-1.850	7.64	20.85	-1.1807	-0.4625	5991.98
15.69	101476.00	99.99	0.00233	51.48	147.87	21.0	0.0576	0.0066	0.0417	0.71	0.51	1.342	-1.854	7.56	20.85	-1.1807	-0.1942	5999.38
19.72	101508.22	100.45	0.00233	64.69	233.58	21.0	0.0311	0.0046	0.0291	0.69	0.64	0.731	-1.307	5.73	20.85	-1.1807	-0.4625	6027.25
19.99	101533.56	100.33	0.00233	65.60	240.24	21.0	0.0305	0.0044	0.0278	0.72	0.65	0.716	-1.246	5.53	20.85	-1.1807	-0.3639	6020.03

APPENDIX B.1

RESULTS OF APC THIN ELECTRIC 14 x 12 PROPELLER

Wind Tunnel Performance Results

APC Thin Electric 14x12 Propeller 2500 RPM

Velocity (m/s)	Barometric Pressure (Pa)	RPS	Density (slugs/ft^3)	Velocity (ft/s)	Dynamic Pressure (q)	Test Section Temperature (°C)	Coefficient of Thrust (C_t)	Coefficient of Torque (C_q)	Coefficient of Power (C_p)	Efficiency	Advance Ratio (J)	Thrust (lbf)	Torque (in-lbf)	Current (I)	Voltage (V)	Thrust Tare	Torque Tare	RPM
13.26	100733.00	41.22	0.00232	43.51	105.02	20.5	0.0112	0.0019	0.0118	0.85	0.90462172	0.082	-0.192	0.94	20.85	-1.1807	-0.2905	2473.40
13.27	100713.00	41.25	0.00232	43.53	105.17	20.4	0.0117	0.0020	0.0127	0.81	0.90451106	0.085	-0.207	0.94	20.85	-1.1807	-0.2905	2475.24
4.42	100949.00	41.74	0.00232	14.49	11.68	20.3	0.1023	0.0084	0.0525	0.58	0.29759539	0.767	-0.877	2.25	20.85	-1.1807	-0.2905	2504.21
4.56	100948.00	41.75	0.00232	14.97	12.47	20.3	0.1022	0.0084	0.0528	0.59	0.30739441	0.767	-0.883	2.24	20.85	-1.1807	-0.2905	2505.13
7.51	100701.00	41.83	0.00232	24.63	33.64	20.6	0.0810	0.0087	0.0545	0.75	0.5047067	0.608	-0.912	2.24	20.85	-1.1807	-0.2905	2509.85
7.56	100988.00	41.84	0.00232	24.80	34.21	20.5	0.0804	0.0084	0.0528	0.77	0.50801219	0.606	-0.886	2.24	20.85	-1.1807	-0.2905	2510.55
1.43	100703.00	42.18	0.00232	4.69	1.22	20.4	0.1031	0.0088	0.0553	0.18	0.09524143	0.788	-0.941	2.32	20.85	-1.1807	-0.2905	2531.01
10.62	101019.00	42.23	0.00232	34.86	67.62	20.4	0.0411	0.0054	0.0337	0.86	0.70747392	0.316	-0.577	1.69	20.85	-1.1807	-0.2905	2533.90
1.42	100811.00	42.23	0.00232	4.66	1.21	20.3	0.1035	0.0086	0.0539	0.18	0.09463927	0.793	-0.922	2.32	20.85	-1.1807	-0.2905	2533.96
10.65	100746.00	42.25	0.00232	34.94	67.79	20.3	0.0415	0.0053	0.0335	0.88	0.70883704	0.318	-0.572	1.69	20.85	-1.1807	-0.2905	2535.05

APC Thin Electric 14x12 Propeller 3000 RPM

Velocity (m/s)	Barometric Pressure (Pa)	RPS	Density (slugs/ft^3)	Velocity (ft/s)	Dynamic Pressure (q)	Test Section Temperature (°C)	Coefficient of Thrust (C_t)	Coefficient of Torque (C_q)	Coefficient of Power (C_p)	Efficiency	Advance Ratio (J)	Thrust (lbf)	Torque (in-lbf)	Current (I)	Voltage (V)	Thrust Tare	Torque Tare	RPM
12.38	101010.00	49.51	0.00232	40.62	91.83	20.4	0.0423	0.0056	0.0352	0.84	0.70	0.446	-0.828	2.44	20.85	-1.1807	-0.2905	2970.60
1.70	100983.00	49.66	0.00232	5.57	1.73	20.4	0.1015	0.0085	0.0537	0.18	0.10	1.078	-1.269	3.36	20.85	-1.1807	-0.2905	2979.53
8.94	100701.00	49.67	0.00232	29.32	47.70	20.4	0.0824	0.0088	0.0551	0.76	0.51	0.872	-1.300	3.36	20.85	-1.1807	-0.2905	2980.02
8.95	101008.00	49.92	0.00233	29.36	47.98	20.3	0.0842	0.0087	0.0548	0.77	0.50	0.904	-1.310	3.48	20.85	-1.1807	-0.2905	2994.94
1.73	100764.00	50.09	0.00232	5.66	1.78	20.3	0.1035	0.0087	0.0549	0.18	0.10	1.116	-1.319	3.47	20.85	-1.1807	-0.2905	3005.57
5.56	100823.00	50.19	0.00232	18.24	18.47	20.4	0.1006	0.0086	0.0541	0.58	0.31	1.089	-1.306	3.45	20.85	-1.1807	-0.2905	3011.29
5.12	100830.00	50.28	0.00232	16.80	15.68	20.4	0.1027	0.0085	0.0536	0.55	0.29	1.116	-1.298	3.45	20.85	-1.1807	-0.2905	3016.76
16.33	100998.00	50.39	0.00232	53.57	159.70	20.4	0.0084	0.0018	0.0116	0.66	0.91	0.092	-0.283	1.30	20.85	-1.1807	-0.2905	3023.18
16.18	100751.00	50.49	0.00232	53.09	156.53	20.3	0.0100	0.0021	0.0129	0.70	0.90	0.110	-0.316	1.34	20.85	-1.1807	-0.2905	3029.60
12.75	101001.00	50.53	0.00232	41.82	97.34	20.4	0.0428	0.0058	0.0363	0.84	0.71	0.471	-0.889	2.61	20.85	-1.1807	-0.2905	3031.86

APC Thin Electric 14x12 Propeller 3500 RPM

Velocity (m/s)	Barometric Pressure (Pa)	RPS	Density (slugs/ft^3)	Velocity (ft/s)	Dynamic Pressure (q)	Test Section Temperature (°C)	Coefficient of Thrust (C_t)	Coefficient of Torque (C_q)	Coefficient of Power (C_p)	Efficiency	Advance Ratio (J)	Thrust (lbf)	Torque (in-lbf)	Current (I)	Voltage (V)	Thrust Tare	Torque Tare	RPM
18.38	100988.00	57.91	0.00233	60.29	202.43	20.2	0.0125	0.0026	0.0161	0.69	0.89	0.181	-0.519	1.97	20.85	-1.1807	-0.2905	3474.41
10.25	101000.00	57.95	0.00232	33.63	62.94	20.4	0.0836	0.0088	0.0554	0.75	0.50	1.208	-1.785	4.95	20.85	-1.1807	-0.2905	3476.88
14.30	100813.00	57.96	0.00232	46.93	122.35	20.4	0.0460	0.0063	0.0393	0.81	0.69	0.665	-1.265	3.72	20.85	-1.1807	-0.2905	3477.61
10.36	100732.00	58.18	0.00232	33.99	64.09	20.5	0.0829	0.0088	0.0552	0.75	0.50	1.204	-1.788	4.98	20.85	-1.1807	-0.2905	3490.88
6.10	100993.00	58.45	0.00232	20.02	22.32	20.3	0.0994	0.0085	0.0533	0.55	0.29	1.462	-1.746	4.89	20.85	-1.1807	-0.2905	3507.16
14.39	100820.00	58.47	0.00232	47.22	123.86	20.4	0.0466	0.0064	0.0400	0.81	0.69	0.684	-1.309	3.82	20.85	-1.1807	-0.2905	3508.26
2.11	100945.00	58.72	0.00232	6.92	2.67	20.3	0.1084	0.0082	0.0514	0.21	0.10	1.609	-1.699	4.82	20.85	-1.1807	-0.2905	3522.95
2.10	100950.00	58.76	0.00232	6.87	2.63	20.3	0.1076	0.0082	0.0514	0.21	0.10	1.599	-1.702	4.80	20.85	-1.1807	-0.2905	3525.32
18.94	100727.00	58.96	0.00232	62.14	214.20	20.5	0.0111	0.0024	0.0151	0.66	0.90	0.165	-0.503	1.95	20.85	-1.1807	-0.2905	3537.54
6.11	100984.00	59.13	0.00233	20.06	22.41	20.2	0.1002	0.0085	0.0535	0.54	0.29	1.508	-1.795	5.05	20.85	-1.1807	-0.2905	3548.07

APC Thin Electric 14x12 Propeller 5000 RPM

Velocity (m/s)	Barometric Pressure (Pa)	RPS	Density (slugs/ft^3)	Velocity (ft/s)	Dynamic Pressure (q)	Test Section Temperature (°C)	Coefficient of Thrust (C_t)	Coefficient of Torque (C_q)	Coefficient of Power (C_p)	Efficiency	Advance Ratio (J)	Thrust (lbf)	Torque (in-lbf)	Current (I)	Voltage (V)	Thrust Tare	Torque Tare	RPM
3.13	101332.27	82.93	0.00233	10.28	5.89	21.0	0.1060	0.0087	0.0546	0.21	0.11	3.142	-3.603	10.64	20.86	-1.1807	-0.4625	4975.61
3.14	101319.24	83.09	0.00233	10.31	5.92	21.2	0.1055	0.0087	0.0546	0.21	0.11	3.138	-3.615	10.64	20.87	-1.1807	-0.4625	4985.25
8.88	101330.16	83.07	0.00232	29.14	47.24	21.4	0.0970	0.0090	0.0568	0.51	0.30	2.880	-3.757	10.64	20.87	-1.1807	-0.4625	4984.13
8.89	101324.91	83.02	0.00233	29.16	47.42	20.8	0.0973	0.0090	0.0568	0.52	0.30	2.893	-3.765	10.64	20.87	-1.1807	-0.4625	4981.18
14.93	101320.93	83.08	0.00232	48.97	133.46	21.3	0.0812	0.0094	0.0589	0.70	0.51	2.412	-3.902	10.64	20.87	-1.1807	-0.4625	4984.67
14.96	101327.56	82.81	0.00232	49.07	133.97	21.4	0.0809	0.0093	0.0586	0.70	0.51	2.389	-3.853	10.64	20.87	-1.1807	-0.4625	4968.71
20.81	101329.49	83.87	0.00232	68.29	259.33	21.6	0.0529	0.0078	0.0489	0.75	0.70	1.601	-3.298	10.64	20.86	-1.1807	-0.4625	5032.19
20.75	101315.11	83.19	0.00233	68.08	258.11	21.1	0.0514	0.0077	0.0484	0.75	0.70	1.533	-3.213	10.64	20.86	-1.1807	-0.4625	4991.19
26.62	101317.11	83.88	0.00232	87.33	424.40	21.3	0.0149	0.0038	0.0237	0.56	0.89	0.452	-1.597	5.64	20.86	-1.1807	-0.4625	5033.08
26.73	101328.49	83.95	0.00232	87.68	427.68	21.5	0.0146	0.0037	0.0231	0.57	0.90	0.443	-1.559	5.57	20.86	-1.1807	-0.4625	5037.01

APPENDIX B.2

RESULTS OF APC THIN ELECTRIC 17 x 12 PROPELLER

Wind Tunnel Performance Results

APC Thin Electric 17x12 Propeller 3400 RPM																		
Velocity	Barometric Pressure	RPS	Density	Velocity	Dynamic Pressure	Test Section Temperature	Coefficient of Thrust	Coefficient of Torque	Coefficient of Power	Efficiency	Advance	Thrust	Torque	Current (I)	Voltage (V)	Thrust	Torque	RPM
(m/s)	(Pa)		(slugs/ft^3)	(ft/s)	(q)	(°C)	(C_t)		(C_p)		Ratio (J)	(lbf)	(in-lbf)			Tare	Tare	
10.01	102472.00	56.58	0.00235	32.83	60.63	21.5	0.0790	0.0076	0.0477	0.68	0.41	2.395	-3.912	10.31	20.85	-1.1807	-0.3088	3395.06
13.24	102417.36	56.61	0.00235	43.45	106.01	21.8	0.0594	0.0069	0.0433	0.74	0.54	1.798	-3.549	9.30	20.85	-1.1807	-0.3088	3396.83
13.06	102650.67	56.68	0.00235	42.84	103.39	21.5	0.0607	0.0070	0.0442	0.73	0.53	1.849	-3.643	9.47	20.85	-1.1807	-0.3088	3400.64
10.03	102765.09	56.72	0.00235	32.91	61.04	21.7	0.0795	0.0077	0.0483	0.67	0.41	2.427	-3.991	10.49	20.85	-1.1807	-0.3088	3403.28
6.61	102555.71	56.77	0.00235	21.67	26.44	21.6	0.0924	0.0075	0.0473	0.53	0.27	2.819	-3.906	10.31	20.85	-1.1807	-0.3088	3406.33
6.83	102389.98	56.79	0.00235	22.42	28.25	21.6	0.0913	0.0075	0.0472	0.54	0.28	2.782	-3.895	10.31	20.85	-1.1807	-0.3088	3407.48
16.46	102583.62	56.81	0.00235	54.01	164.16	21.7	0.0330	0.0049	0.0307	0.72	0.67	1.008	-2.540	6.57	20.85	-1.1807	-0.3088	3408.52
19.53	102487.31	56.94	0.00235	64.08	230.89	21.7	0.0107	0.0026	0.0161	0.53	0.79	0.328	-1.337	3.80	20.85	-1.1807	-0.3088	3416.12
19.90	102607.64	57.01	0.00235	65.28	239.86	21.7	0.0078	0.0023	0.0146	0.44	0.81	0.241	-1.213	3.44	20.85	-1.1807	-0.3088	3420.89
16.73	102513.60	57.02	0.00235	54.90	169.51	21.6	0.0317	0.0047	0.0294	0.73	0.68	0.974	-2.445	6.46	20.85	-1.1807	-0.3088	3421.30

APC Thin Electric 17x12 Propeller 4000 RPM																		
Velocity	Barometric Pressure	RPS	Density	Velocity	Dynamic Pressure	Test Section Temperature	Coefficient of Thrust	Coefficient of Torque	Coefficient of Power	Efficiency	Advance	Thrust	Torque	Current (I)	Voltage (V)	Thrust	Torque	RPM
(m/s)	(Pa)		(slugs/ft^3)	(ft/s)	(q)	(°C)	(C_t)		(C_p)		Ratio (J)	(lbf)	(in-lbf)			Tare	Tare	
7.96	102385.20	66.28	0.00235	26.12	38.35	21.6	0.0923	0.0076	0.0477	0.54	0.28	3.833	-5.352	10.64	20.86	-1.1807	-0.3088	3976.55
11.78	102566.31	66.35	0.00235	38.64	83.99	21.7	0.0802	0.0077	0.0483	0.68	0.41	3.342	-5.445	10.64	20.86	-1.1807	-0.3088	3980.75
11.89	102478.84	66.48	0.00235	39.01	85.57	21.7	0.0797	0.0077	0.0482	0.68	0.41	3.333	-5.456	10.64	20.85	-1.1807	-0.3088	3989.07
8.13	102760.31	66.54	0.00235	26.66	40.07	21.7	0.0919	0.0077	0.0481	0.54	0.28	3.857	-5.463	10.64	20.85	-1.1807	-0.3088	3992.63
15.74	102760.00	66.68	0.00235	51.63	150.27	21.7	0.0614	0.0072	0.0450	0.75	0.55	2.590	-5.129	10.64	20.85	-1.1807	-0.3088	4000.84
19.61	102571.04	66.71	0.00235	64.34	232.91	21.7	0.0353	0.0051	0.0321	0.75	0.68	1.485	-3.657	10.64	20.85	-1.1807	-0.3088	4002.52
22.99	102446.98	66.85	0.00235	75.44	319.78	21.7	0.0126	0.0028	0.0178	0.56	0.80	0.533	-2.037	6.23	20.85	-1.1807	-0.3088	4011.01
19.05	102502.47	66.86	0.00235	62.51	219.76	21.6	0.0394	0.0055	0.0343	0.76	0.66	1.667	-3.923	10.64	20.85	-1.1807	-0.3088	4011.45
23.05	102624.40	66.94	0.00235	75.63	322.01	21.7	0.0125	0.0029	0.0180	0.55	0.80	0.531	-2.066	6.19	20.85	-1.1807	-0.3088	4016.20
15.77	102468.04	66.95	0.00235	51.73	150.54	21.5	0.0614	0.0071	0.0444	0.75	0.55	2.603	-5.095	10.64	20.85	-1.1807	-0.3088	4016.81

APC Thin Electric 17x12 Propeller 4500 RPM																		
Velocity	Barometric Pressure	RPS	Density	Velocity	Dynamic Pressure	Test Section Temperature	Coefficient of Thrust	Coefficient of Torque	Coefficient of Power	Efficiency	Advance	Thrust	Torque	Current (I)	Voltage (V)	Thrust	Torque	RPM
(m/s)	(Pa)		(slugs/ft^3)	(ft/s)	(q)	(°C)	(C_t)		(C_p)		Ratio (J)	(lbf)	(in-lbf)			Tare	Tare	
8.98	102688.00	74.54	0.00235	29.48	48.96	21.6	0.0931	0.0077	0.0485	0.54	0.28	4.902	-6.904	10.64	20.86	-1.1807	-0.3088	4472.20
9.08	102412.78	74.56	0.00235	29.79	49.87	21.7	0.0925	0.0077	0.0482	0.54	0.28	4.862	-6.850	10.64	20.86	-1.1807	-0.3088	4473.38
21.60	102395.44	74.60	0.00235	70.85	281.90	21.8	0.0401	0.0056	0.0353	0.76	0.67	2.108	-5.018	10.64	20.85	-1.1807	-0.3088	4475.90
17.16	102536.04	74.60	0.00235	56.28	178.26	21.6	0.0649	0.0073	0.0460	0.75	0.53	3.419	-6.562	10.64	20.86	-1.1807	-0.3088	4476.13
13.16	102581.04	74.65	0.00235	43.16	104.87	21.6	0.0811	0.0078	0.0491	0.67	0.41	4.280	-7.008	10.64	20.86	-1.1807	-0.3088	4479.09
13.03	102457.33	74.65	0.00235	42.76	102.79	21.6	0.0815	0.0078	0.0488	0.68	0.40	4.296	-6.955	10.64	20.86	-1.1807	-0.3088	4479.28
17.47	102596.29	74.93	0.00235	57.32	184.88	21.8	0.0642	0.0074	0.0462	0.75	0.54	3.411	-6.643	10.64	20.86	-1.1807	-0.3088	4495.61
21.64	102679.73	74.99	0.00235	71.00	283.96	21.7	0.0409	0.0057	0.0359	0.76	0.67	2.181	-5.181	10.64	20.85	-1.1807	-0.3088	4499.68
26.11	102767.71	75.26	0.00235	85.67	413.48	21.9	0.0145	0.0031	0.0196	0.59	0.80	0.780	-2.851	9.23	20.85	-1.1807	-0.3088	4515.48
25.89	102438.78	75.28	0.00235	84.95	405.34	21.9	0.0150	0.0031	0.0197	0.60	0.80	0.802	-2.860	9.34	20.85	-1.1807	-0.3088	4516.60

APPENDIX B.3

RESULTS OF 16 IN STRAIGHT BLADE ALUMINIUM PROPELLER

Wind Tunnel Performance Results

16in Straight Blade Aluminum Propeller 3500 RPM																		
Velocity (m/s)	Barometric Pressure (Pa)	RPS	Density (slugs/ft^3)	Velocity (ft/s)	Dynamic Pressure (q)	Test Section Temperature (°C)	Coefficient of Thrust (C_t)	Coefficient of Torque	Coefficient of Power (C_p)	Efficiency	Advance Ratio (J)	Thrust (lbf)	Torque (in-lbf)	Current (I)	Voltage (V)	Thrust Tare	Torque Tare	RPM
9.13	101665.09	58.11	0.00233	29.96	50.16	21.1	0.0687	0.0065	0.0406	0.65	0.39	1.710	2.576	6.72	20.86	-0.8711	-0.1568	3486.53
11.04	101641.89	58.27	0.00233	36.22	73.28	21.1	0.0572	0.0060	0.0377	0.71	0.47	1.432	2.404	6.26	20.86	-0.8711	-0.1568	3495.95
13.18	101661.36	58.28	0.00233	43.25	104.53	21.1	0.0424	0.0051	0.0321	0.73	0.56	1.063	2.051	5.38	20.86	-0.8711	-0.1568	3496.93
6.78	101638.22	58.32	0.00233	22.26	27.66	21.2	0.0804	0.0067	0.0423	0.54	0.29	2.017	2.698	7.12	20.86	-0.8711	-0.1568	3499.23
6.91	101655.42	58.39	0.00234	22.67	28.73	20.8	0.0801	0.0068	0.0429	0.54	0.29	2.016	2.752	7.13	20.86	-0.8711	-0.2147	3503.51
15.54	101655.33	58.43	0.00234	50.99	145.40	20.8	0.0240	0.0035	0.0222	0.71	0.65	0.606	1.427	3.82	20.86	-0.9245	-0.2905	3505.84
15.61	101646.22	58.54	0.00233	51.20	146.45	21.2	0.0220	0.0035	0.0220	0.66	0.66	0.556	1.413	3.81	20.86	-0.8711	-0.1568	3512.34
13.44	101631.20	58.74	0.00233	44.09	108.61	21.1	0.0415	0.0051	0.0318	0.74	0.56	1.055	2.058	5.44	20.86	-0.8711	-0.1568	3524.20
9.19	101676.00	58.76	0.00234	30.16	50.90	20.8	0.0704	0.0066	0.0413	0.66	0.39	1.795	2.679	6.96	20.86	-0.9245	-0.2905	3525.38
11.21	101633.89	58.92	0.00233	36.78	75.58	21.1	0.0575	0.0061	0.0381	0.71	0.47	1.473	2.482	6.50	20.86	-0.8711	-0.1568	3535.31

16in Straight Blade Aluminum Propeller 5000 RPM																		
Velocity (m/s)	Barometric Pressure (Pa)	RPS	Density (slugs/ft^3)	Velocity (ft/s)	Dynamic Pressure (q)	Test Section Temperature (°C)	Coefficient of Thrust (C_t)	Coefficient of Torque	Coefficient of Power (C_p)	Efficiency	Advance Ratio (J)	Thrust (lbf)	Torque (in-lbf)	Current (I)	Voltage (V)	Thrust Tare	Torque Tare	RPM
9.88	101631.11	82.96	0.00233	32.40	58.65	21.0	0.0791	0.0065	0.0407	0.57	0.29	4.016	5.260	10.64	20.87	-0.8711	-0.1568	4977.65
12.76	101639.00	83.05	0.00233	41.88	97.97	21.1	0.0686	0.0062	0.0389	0.67	0.38	3.492	5.045	10.64	20.86	-0.8711	-0.1568	4983.19
19.19	101635.93	83.06	0.00233	62.97	221.48	21.2	0.0383	0.0045	0.0285	0.76	0.57	1.947	3.690	10.64	20.86	-0.8711	-0.1568	4983.65
15.73	101627.00	83.10	0.00233	51.61	148.83	21.0	0.0558	0.0056	0.0354	0.73	0.47	2.841	4.591	10.64	20.86	-0.8711	-0.1568	4985.80
16.12	101661.20	83.12	0.00234	52.90	156.51	20.8	0.0537	0.0056	0.0349	0.73	0.48	2.739	4.538	10.64	20.87	-0.8711	-0.2147	4987.48
9.83	101635.00	83.17	0.00233	32.26	58.19	20.9	0.0790	0.0066	0.0412	0.56	0.29	4.030	5.349	10.64	20.87	-0.8711	-0.2147	4989.96
18.83	101661.00	83.19	0.00233	61.78	213.20	21.3	0.0405	0.0047	0.0295	0.76	0.56	2.064	3.828	10.64	20.86	-0.8711	-0.1568	4991.23
12.59	101640.42	83.25	0.00234	41.32	95.47	20.8	0.0693	0.0063	0.0394	0.66	0.37	3.544	5.128	10.64	20.87	-0.8711	-0.2147	4995.23
22.11	101621.00	83.37	0.00233	72.55	293.74	21.4	0.0222	0.0032	0.0202	0.72	0.65	1.135	2.632	9.41	20.86	-0.8711	-0.1568	5002.31
22.09	101643.00	83.70	0.00233	72.48	293.59	21.0	0.0225	0.0033	0.0206	0.71	0.65	1.163	2.706	9.67	20.86	-0.8711	-0.1568	5022.30

APPENDIX B.4

RESULTS OF 16 IN SWEPT BLADE ALUMINIUM PROPELLER

Wind Tunnel Performance Results

16in Swept Blade Aluminum Propeller 3500 RPM																		
Velocity (m/s)	Barometric Pressure (Pa)	RPS	Density (slugs/ft^3)	Velocity (ft/s)	Dynamic Pressure (q)	Test Section Temperature (°C)	Coefficient of Thrust (C_t)	Coefficient of Torque (C_q)	Coefficient of Power (C_p)	Efficiency	Advance Ratio (J)	Thrust (lbf)	Torque (in-lbf)	Current (I)	Voltage (V)	Thrust Tare	Torque Tare	RPM
9.05	101292.31	58.18	0.00232	29.69	49.02	21.5	0.0711	0.0062	0.0393	0.69	0.38	1.765	2.483	6.77	20.86	-0.8297	-0.0712	3490.65
15.54	101289.42	58.34	0.00232	50.97	144.46	21.5	0.0229	0.0036	0.0223	0.67	0.66	0.573	1.420	4.07	20.86	-0.8297	-0.0712	3500.22
13.43	101317.49	58.42	0.00232	44.07	108.04	21.4	0.0403	0.0049	0.0309	0.74	0.57	1.009	1.974	5.42	20.86	-0.8297	-0.0712	3504.95
9.07	101311.38	58.48	0.00232	29.74	49.21	21.4	0.0681	0.0063	0.0396	0.66	0.38	1.709	2.531	6.87	20.86	-0.8297	-0.0712	3508.63
15.66	101269.44	58.51	0.00232	51.36	146.62	21.6	0.0252	0.0034	0.0216	0.77	0.66	0.633	1.381	4.07	20.86	-0.8297	-0.0712	3510.65
11.18	101395.91	58.52	0.00233	36.67	74.89	21.3	0.0569	0.0058	0.0366	0.73	0.47	1.432	2.346	6.39	20.86	-0.8711	-0.0211	3511.30
6.97	101327.76	58.54	0.00232	22.88	29.12	21.4	0.0802	0.0063	0.0398	0.59	0.29	2.019	2.554	7.08	20.86	-0.8711	-0.0211	3512.43
6.83	101303.00	58.61	0.00232	22.40	27.90	21.5	0.0784	0.0065	0.0410	0.55	0.29	1.976	2.635	7.10	20.86	-0.8297	-0.0712	3516.67
11.24	101282.38	58.75	0.00232	36.88	75.61	21.5	0.0569	0.0058	0.0365	0.73	0.47	1.441	2.356	6.46	20.86	-0.7722	-0.0712	3524.88
13.32	101319.13	58.78	0.00232	43.70	106.20	21.6	0.0423	0.0050	0.0315	0.75	0.56	1.072	2.036	5.63	20.85	-0.7722	-0.0712	3526.84

16in Swept Blade Aluminum Propeller 5000 RPM																		
Velocity (m/s)	Barometric Pressure (Pa)	RPS	Density (slugs/ft^3)	Velocity (ft/s)	Dynamic Pressure (q)	Test Section Temperature (°C)	Coefficient of Thrust (C_t)	Coefficient of Torque (C_q)	Coefficient of Power (C_p)	Efficiency	Advance Ratio (J)	Thrust (lbf)	Torque (in-lbf)	Current (I)	Voltage (V)	Thrust Tare	Torque Tare	RPM
9.63	101275.27	82.95	0.00232	31.60	55.49	21.6	0.0785	0.0062	0.0388	0.58	0.29	3.961	4.984	10.64	20.86	-0.7722	-0.0712	4977.03
21.81	101398.82	83.22	0.00233	71.56	285.23	21.3	0.0233	0.0034	0.0212	0.71	0.64	1.189	2.755	9.99	20.86	-0.8711	-0.0211	4993.37
9.65	101390.40	83.30	0.00233	31.67	55.85	21.3	0.0785	0.0062	0.0389	0.58	0.29	4.006	5.052	10.64	20.87	-0.8711	-0.0211	4998.03
12.96	101327.24	83.32	0.00232	42.51	100.49	21.6	0.0665	0.0059	0.0372	0.68	0.38	3.389	4.828	10.64	20.86	-0.7722	-0.0712	4999.19
12.63	101372.76	83.36	0.00233	41.45	95.68	21.3	0.0683	0.0060	0.0376	0.68	0.37	3.486	4.893	10.64	20.87	-0.8711	-0.0211	5001.72
15.61	101302.67	83.42	0.00232	51.22	145.92	21.4	0.0558	0.0055	0.0345	0.75	0.46	2.851	4.485	10.64	20.86	-0.8297	-0.0712	5004.92
18.86	101271.80	83.50	0.00232	61.88	212.74	21.6	0.0393	0.0045	0.0283	0.77	0.56	2.008	3.690	10.64	20.86	-0.7722	-0.0712	5010.07
15.81	101289.29	83.55	0.00232	51.88	149.58	21.6	0.0551	0.0055	0.0343	0.75	0.47	2.821	4.471	10.64	20.86	-0.8297	-0.0712	5013.30
21.80	101317.87	83.68	0.00232	71.53	284.45	21.6	0.0241	0.0034	0.0214	0.72	0.64	1.236	2.803	10.25	20.86	-0.7722	-0.0712	5020.63
18.77	101322.38	83.70	0.00232	61.58	210.95	21.4	0.0402	0.0046	0.0287	0.77	0.55	2.070	3.764	10.64	20.86	-0.8711	-0.0211	5021.95

APPENDIX C

TECHNICAL DRAWINGS FOR COPPER SPRINGS

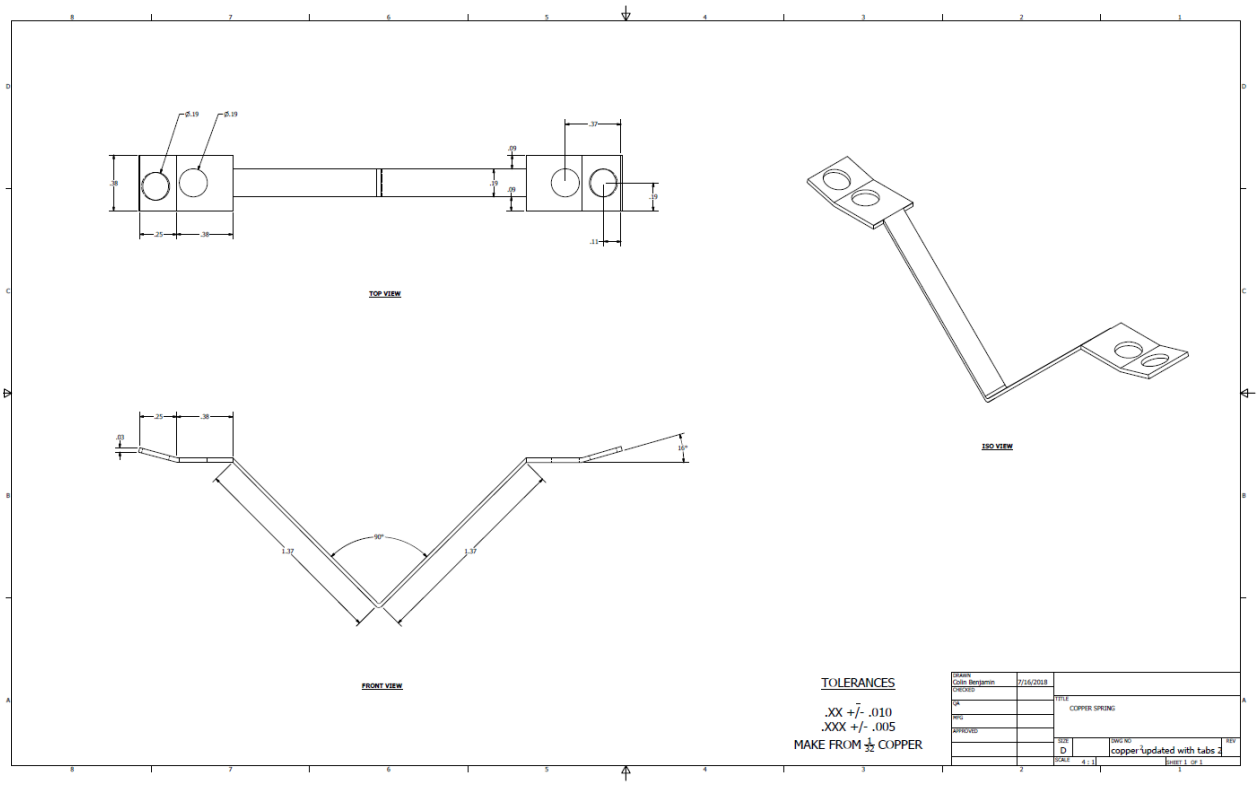

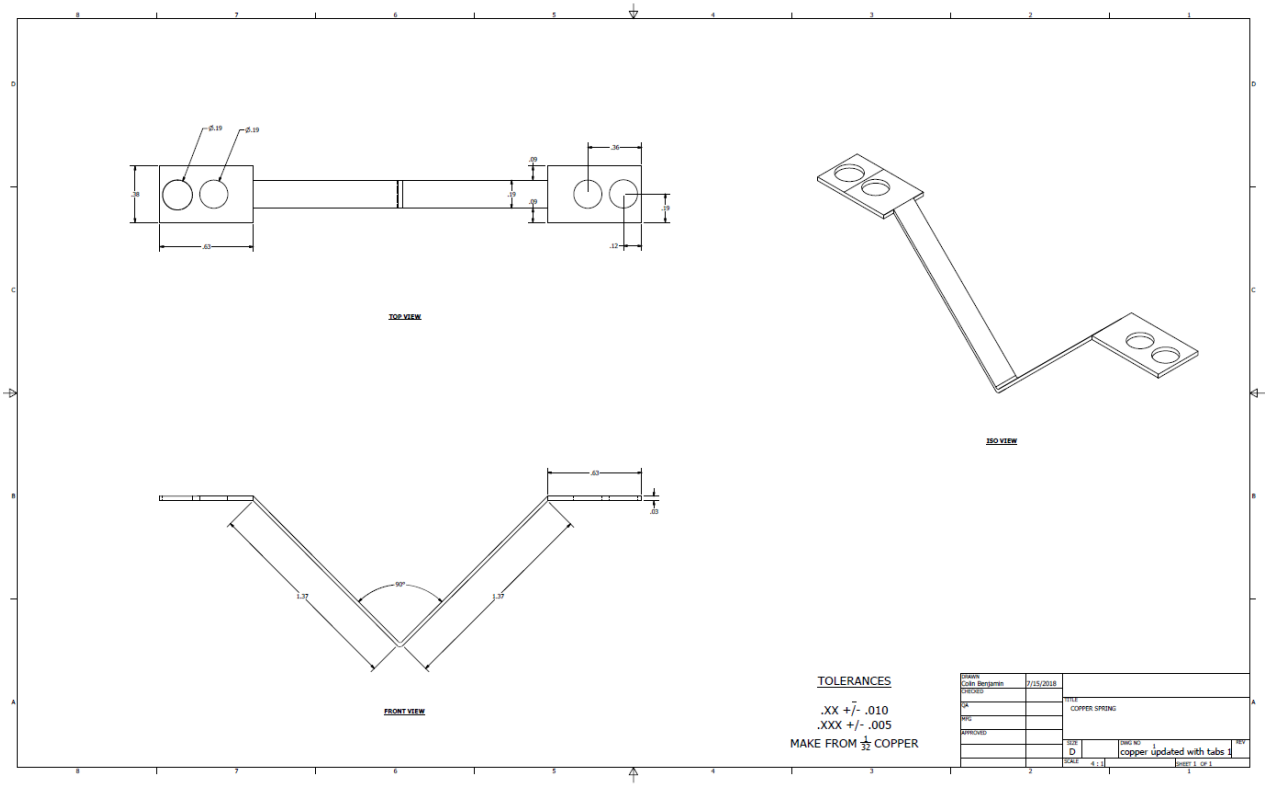

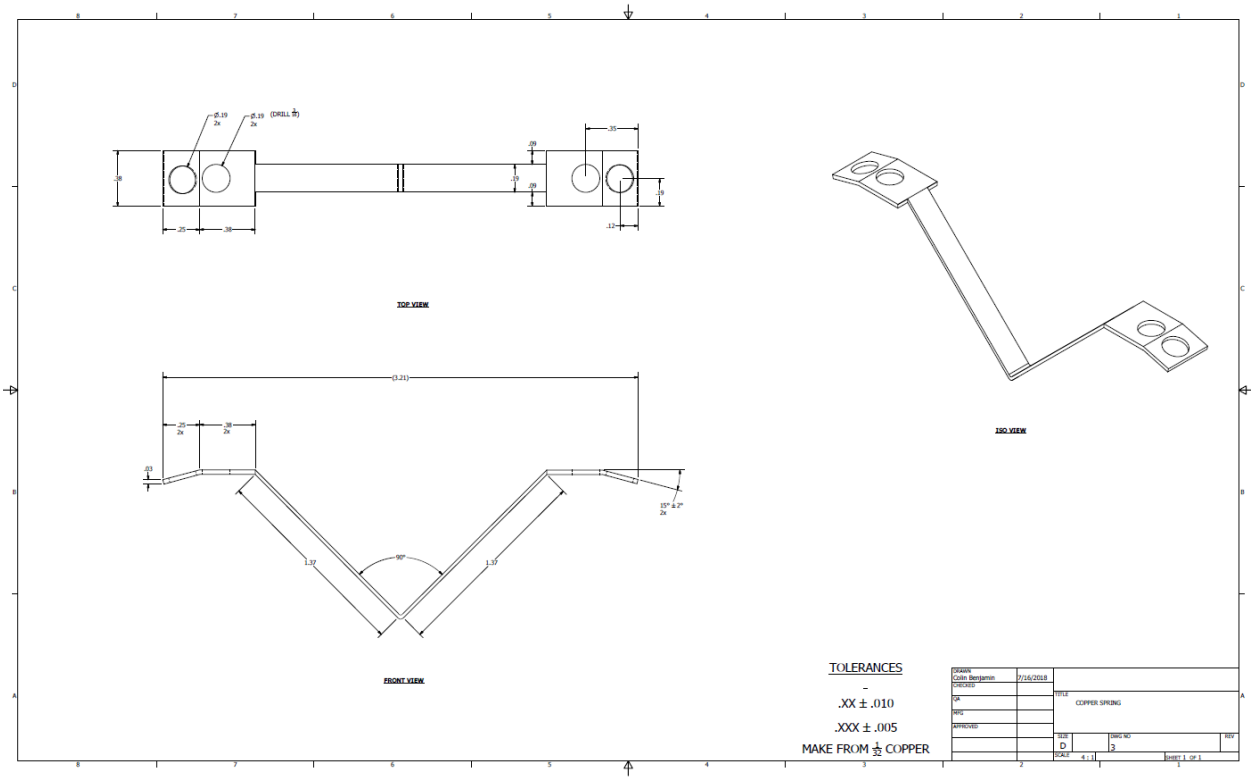
TOP VIEW
FRONT VIEW
ISO VIEW
TOLERANCES
.XX ± .010
.XXX ± .005
MAKE FROM 1/32 COPPER
Colin Benjamin
7/16/2018
COPPER SPRING
D
3
4 : 1
SHEET 1 OF 1

APPENDIX C.1

TECHNICAL DRAWING FOR AFT BULKHEADS NACELLE SUPPORT

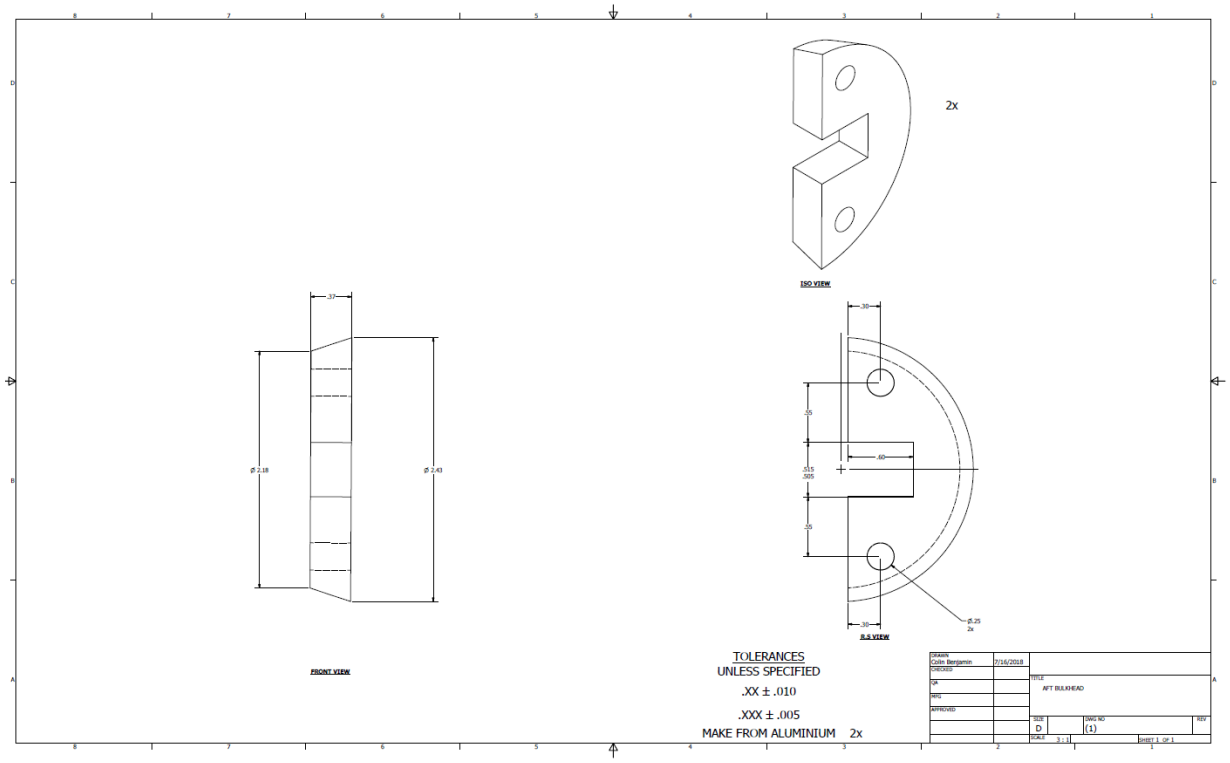

APPENDIX C.2

TECHNICAL DRAWINGS FOR FORWARD BULKHEADS NACELLE SUPPORT

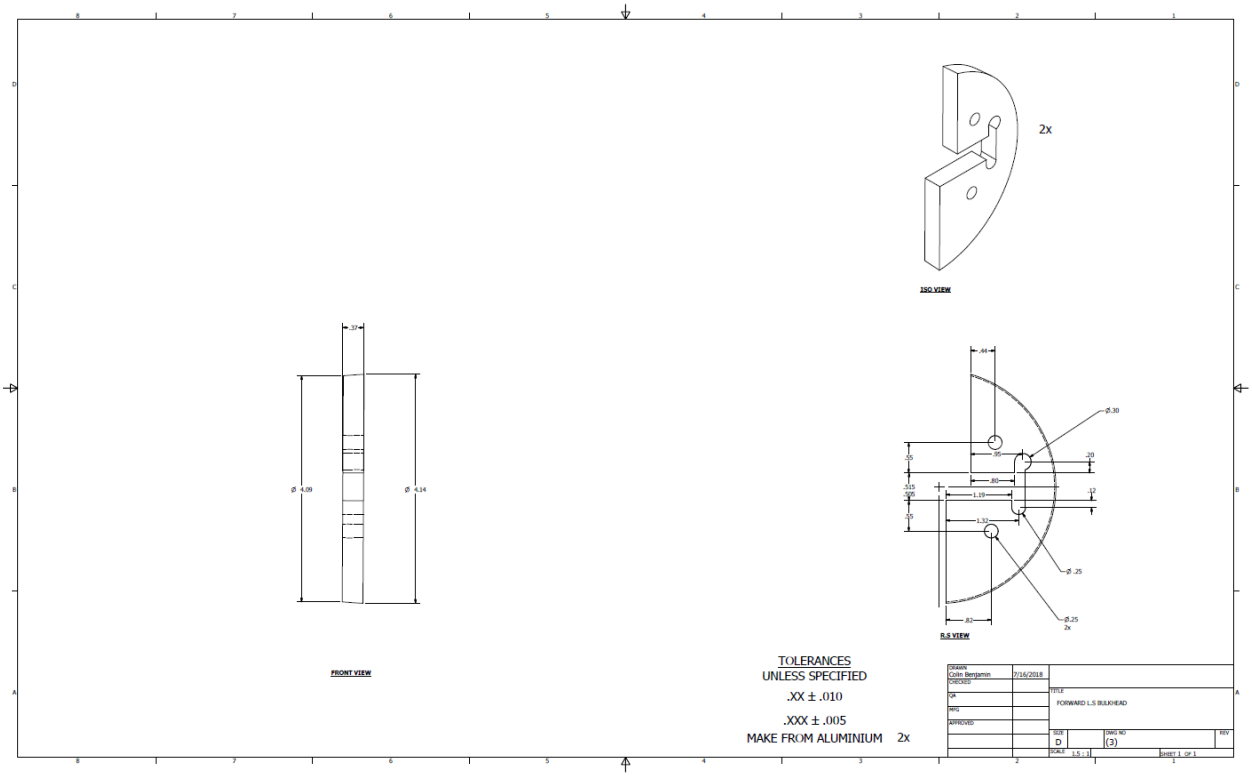

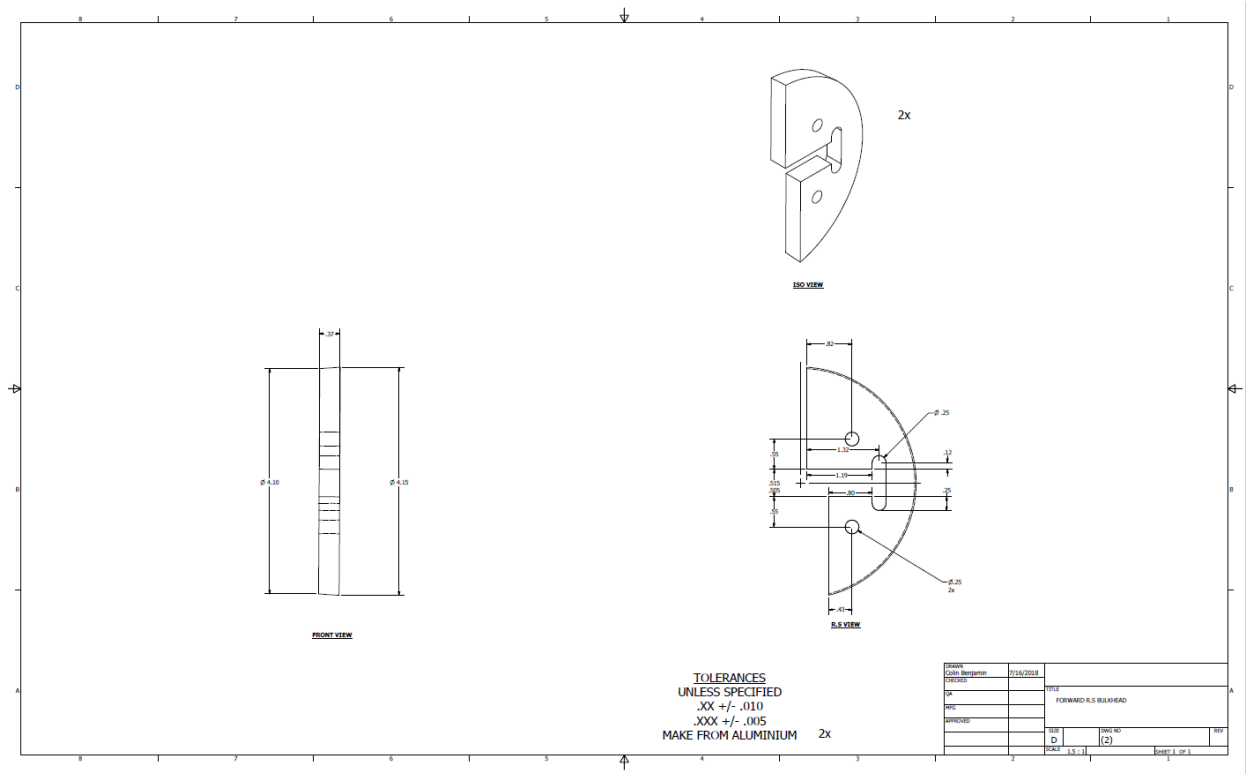

APPENDIX C.3

TECHNICAL DRAWING FOR RPM COUNTER

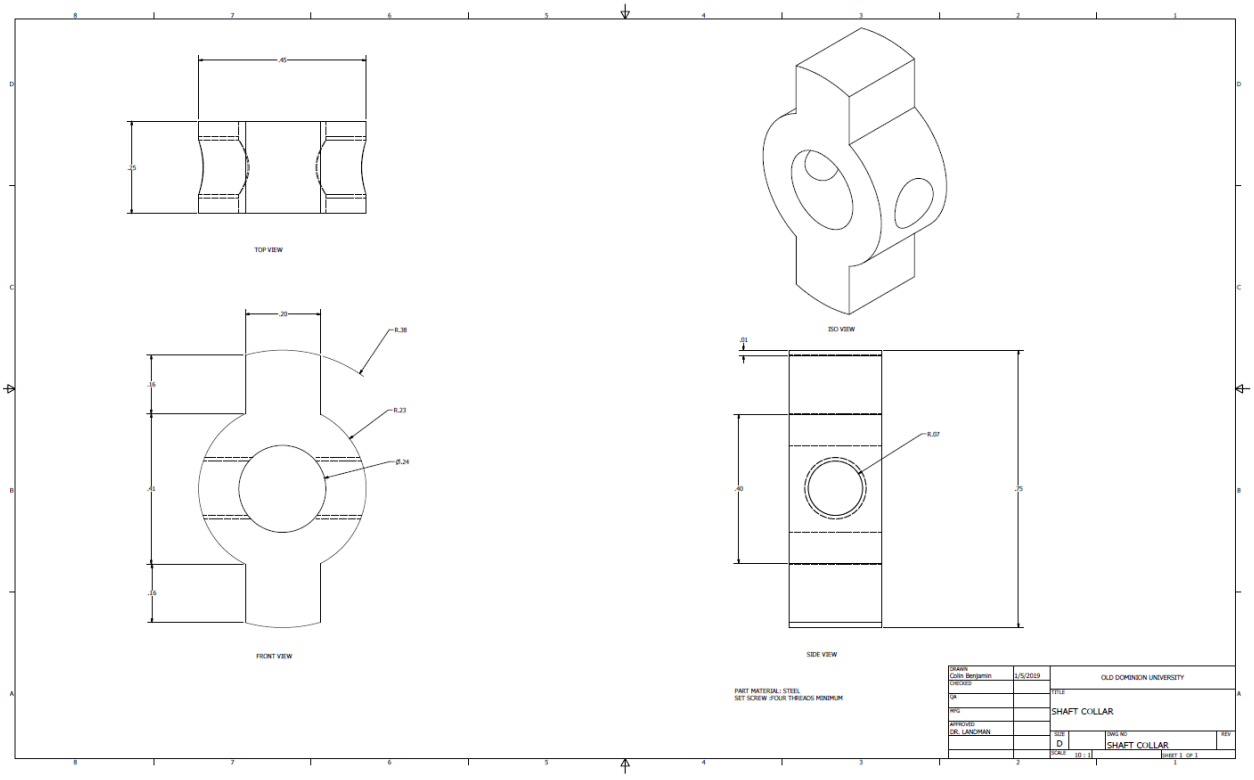

APPENDIX C.4

NACELLE PLUG X AND Y COORDINATES

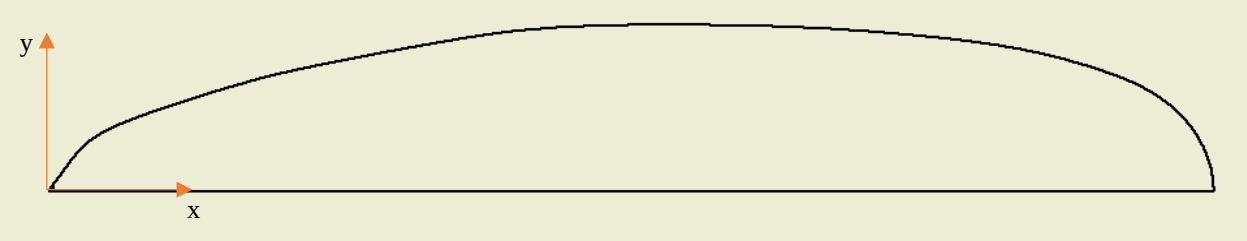

Nacelle Geometry	
X	**Y**
0	0
1	1.08
2	1.5
3	1.83
4	2.13
5	2.33
6	2.42
7	2.46
8	2.42
9	2.33
10	2.21
11	1.92
12	1.42
13	0.79
14	0.33
14.5	0

APPENDIX D

ACTUAL DESIGN FOR APC THIN ELECTRIC 12 x 8 PROPELLER

Std	Run	Factor 1 A:RPM	Factor 2 B:J	Response 1 Ct	Response 2 Cq	Response 3 Cp	Response 4 Eff
29	1	4988.96	0.655387	0.024627	0.004067	0.025554	0.631519
23	2	5010.64	0.381137	0.076823	0.007278	0.045731	0.640315
27	3	5991.98	0.508146	0.058148	0.006631	0.041666	0.709086
18	4	5981.60	0.103326	0.103207	0.007139	0.044853	0.237847
10	5	4007.87	0.507299	0.048038	0.005882	0.036955	0.659473
13	6	3989.87	0.642788	0.024379	0.004027	0.025301	0.619228
20	7	5007.04	0.244049	0.092615	0.007025	0.044138	0.514511
16	8	3991.65	0.103510	0.101078	0.006292	0.039535	0.264915
7	9	3939.20	0.380244	0.073547	0.006581	0.041346	0.676453
8	10	5010.48	0.384244	0.077100	0.007026	0.044148	0.671080
15	11	6027.25	0.643972	0.031085	0.004631	0.029096	0.688136
3	12	5981.00	0.097628	0.103650	0.006950	0.043671	0.231753
28	13	3996.49	0.646000	0.023605	0.003499	0.021988	0.692550
1	14	3991.97	0.100516	0.101226	0.006523	0.040982	0.248401
21	15	6006.19	0.233622	0.094503	0.007381	0.046378	0.476119
6	16	6005.22	0.233282	0.094715	0.007381	0.046379	0.476459
9	17	5996.50	0.387164	0.079041	0.007427	0.046668	0.655732
25	18	4002.75	0.504922	0.049010	0.005378	0.033791	0.740388
17	19	5014.34	0.105037	0.101480	0.006717	0.042201	0.252753
30	20	6020.03	0.653800	0.030507	0.004425	0.027805	0.717366
5	21	5011.60	0.238526	0.093692	0.007086	0.044526	0.501954
22	22	4019.91	0.385001	0.074723	0.006863	0.043121	0.667242
11	23	5020.75	0.515378	0.052604	0.005959	0.037442	0.724061
19	24	4034.95	0.228008	0.094934	0.007032	0.044185	0.489968
24	25	5996.02	0.377305	0.080969	0.007466	0.046911	0.651266
26	26	5028.58	0.500078	0.055728	0.006462	0.040603	0.686417
4	27	3988.62	0.248966	0.092572	0.007304	0.045894	0.502321
14	28	5014.47	0.644086	0.027750	0.004188	0.026314	0.679233
12	29	5999.38	0.514837	0.057593	0.006631	0.041664	0.711638
2	30	5011.51	0.105329	0.102222	0.006995	0.043953	0.245229
31	**31**	**4500**	**0.55**	**0.044929**	**0.005317**	**0.033410**	**0.732487**
32	**32**	**5500**	**0.30**	**0.087025**	**0.007516**	**0.047222**	**0.567525**
33	**33**	**4500**	**0.30**	**0.087966**	**0.007149**	**0.044921**	**0.568048**
34	**34**	**5500**	**0.55**	**0.046354**	**0.005696**	**0.035789**	**0.718694**

APPENDIX D.1

ACTUAL DESIGN FOR APC THIN ELECTRIC 14 X 12 PROPELLER

Std	Block	Run	Factor 1 A:RPM	Factor 2 B:J	Response 1 Ct	Response 2 Cq	Response 3 Cp	Response 4 Eff
7	Block 1	1	2509.8463	0.5047067	0.08101337	0.00868038	0.05454041	0.74975032
8	Block 1	2	3005.5691	0.09692624	0.10345993	0.00873677	0.05489476	0.18269966
16	Block 1	3	2473.3993	0.90462172	0.01119581	0.00188076	0.01181715	0.8458769
28	Block 1	4	2533.9551	0.09463927	0.10346276	0.00858576	0.05394592	0.1815475
15	Block 1	5	3537.5384	0.90335997	0.01106668	0.00240848	0.01513293	0.6603985
24	Block 1	6	3507.1582	0.29365119	0.09937402	0.00847613	0.05325711	0.54794286
13	Block 1	7	2535.0546	0.70883704	0.04147237	0.0053277	0.03347493	0.87851014
25	Block 1	8	2531.0136	0.09524143	0.10313814	0.00880076	0.05529682	0.17765059
29	Block 1	9	3029.605	0.90125403	0.01002132	0.00205996	0.0129431	0.69668849
2	Block 1	10	2970.5973	0.70326459	0.04230485	0.00560501	0.03521734	0.84486457
1	Block 1	11	2475.2442	0.90451106	0.01165795	0.00202775	0.0127407	0.81234026
27	Block 1	12	3522.9532	0.10108445	0.10844968	0.00817803	0.05138405	0.21335061
12	Block 1	13	3525.3216	0.10029147	0.10762725	0.00818243	0.0514117	0.2099643
20	Block 1	14	2980.0177	0.50604863	0.0823801	0.00877067	0.05510774	0.75663081
5	Block 1	15	2994.9356	0.50411191	0.08418897	0.00872184	0.05480094	0.77459597
3	Block 1	16	3474.407	0.89252206	0.01253477	0.00256445	0.01611294	0.69322035
4	Block 1	17	2504.2097	0.29759539	0.10230539	0.0083578	0.05251359	0.58002852
19	Block 1	18	2505.1284	0.30739441	0.10217016	0.00840266	0.05279547	0.59499115
18	Block 1	19	3476.8823	0.49747455	0.08358555	0.00882022	0.0554191	0.75033793
6	Block 1	20	3477.608	0.69408578	0.0460434	0.00625766	0.03931802	0.8127705
30	Block 1	21	3548.0699	0.29078772	0.10015299	0.00851474	0.05349968	0.54437873
22	Block 1	22	2510.546	0.50801219	0.08042854	0.00840077	0.05278361	0.77408031
17	Block 1	23	2979.5325	0.09619139	0.10153818	0.00854224	0.05367247	0.18197956
14	Block 1	24	3031.8558	0.70942204	0.04281362	0.00577654	0.0362951	0.83670406
9	Block 1	25	3508.257	0.69223843	0.04656562	0.00636353	0.03998324	0.80625133
23	Block 1	26	3011.2877	0.3114328	0.10059499	0.00861817	0.05414953	0.57854463
26	Block 1	27	3016.757	0.28638709	0.10272464	0.00853072	0.05360013	0.54895822
21	Block 1	28	3490.8764	0.5007537	0.08289039	0.0087914	0.05523798	0.7514497
11	Block 1	29	3023.1804	0.91131774	0.00841813	0.00184801	0.01161139	0.65557139
10	Block 1	30	2533.9048	0.70747392	0.0411133	0.00536892	0.03373394	0.86238562
31	**Block 1**	**31**	**2759.275**	**0.7917677**	**0.0266475**	**0.0038556**	**0.02422554**	**0.87003581**
32	**Block 1**	**32**	**3276.926**	**0.2014591**	**0.1041686**	**0.0082836**	**0.05204758**	**0.40323886**
33	**Block 1**	**33**	**2747.818**	**0.1902425**	**0.1071764**	**0.0083946**	**0.05274502**	**0.38658067**
34	**Block 1**	**34**	**3283.059**	**0.7895225**	**0.028014**	**0.0043399**	**0.02726827**	**0.81022974**
35	Block 2	35	4975.6076	0.1	0.1059879	0.00868276	0.05455539	0.20650916
36	Block 2	36	4985.2477	0.1	0.10553205	0.00868385	0.05456226	0.20574712

37	Block 2	37	4984.1294	0.3	0.09695239	0.00903327	0.0567577	0.5136069
38	Block 2	38	4981.1752	0.3	0.09731156	0.00904541	0.05683401	0.51555474
39	Block 2	39	4984.6678	0.5	0.08117643	0.00937943	0.05893272	0.6959574
40	Block 2	40	4968.7108	0.5	0.08092973	0.00932356	0.05858165	0.70166513
41	Block 2	41	5032.186	0.7	0.05290298	0.00778445	0.04891116	0.75490317
42	Block 2	42	4991.1858	0.7	0.05142171	0.00769861	0.04837181	0.74579051
43	Block 2	43	5033.0828	0.9	0.01490666	0.00376581	0.02366129	0.56221063
44	Block 2	44	5037.0091	0.9	0.01459345	0.00367193	0.02307141	0.56631223
45	**Block 1**	**45**	**4470.538**	**0.2**	**0.1019109**	**0.008702**	**0.05467608**	**0.37978187**
46	**Block 1**	**46**	**4472.509**	**0.6**	**0.0692874**	**0.0089249**	**0.05607707**	**0.75026753**

APPENDIX D.2

ACTUAL DESIGN FOR APC THIN ELECTRIC 17 x 12 PROPELLER

Std	Block	Run	Factor 1 A:RPM	Factor 2 B:J	Response 1 Ct	Response 2 Cq	Response 3 Cp	Response 4 Eff
15	Block 1	1	4472.201	0.27916404	0.09307529	0.00771125	0.04845123	0.53627673
4	Block 1	2	3395.056	0.4095587	0.0790461	0.0075958	0.04772584	0.67833968
2	Block 1	3	3976.546	0.2782514	0.0923224	0.00758397	0.04765148	0.53909389
8	Block 1	4	3980.754	0.4110752	0.0802145	0.00768843	0.04830783	0.6825863
3	Block 1	5	4473.382	0.2820886	0.0925485	0.00767114	0.04819917	0.54164417
12	Block 1	6	4475.905	0.6704577	0.0400987	0.00561537	0.03528238	0.76198006
7	Block 1	7	3396.831	0.5417123	0.0593817	0.00689417	0.04331735	0.74260572
14	Block 1	8	3989.0738	0.41422124	0.07974207	0.00767862	0.0482462	0.68462997
13	Block 1	9	3400.6429	0.53350764	0.06071982	0.00703879	0.04422604	0.73246958
9	Block 1	10	4476.1335	0.53256017	0.06489483	0.00732691	0.04603635	0.75070816
10	Block 1	11	3403.2798	0.40949809	0.07954122	0.00769475	0.04834751	0.6737122
6	Block 1	12	4479.0893	0.40813008	0.08110541	0.00781161	0.04908179	0.6744208
11	Block 1	13	3992.6292	0.28282034	0.09186545	0.00765403	0.04809167	0.54024901
5	Block 1	14	4000.8386	0.54657801	0.0614376	0.00715602	0.04496259	0.74684003
1	Block 1	15	3406.3264	0.26949637	0.09238724	0.00752972	0.04731063	0.52626708
24	Block 2	16	4479.2753	0.40429898	0.08149653	0.00776203	0.04877025	0.67581451
25	Block 2	17	3407.478	0.27871174	0.09127678	0.00751685	0.04722979	0.53864182
26	Block 2	18	4002.5184	0.68078041	0.03526176	0.00510674	0.03208657	0.74814683
28	Block 2	19	3408.5198	0.67113214	0.03298704	0.0048911	0.03073169	0.72038319
20	Block 2	20	4011.0141	0.79655874	0.01262581	0.00283721	0.01782673	0.5641639
19	Block 2	21	3416.1233	0.79452594	0.01069118	0.00256498	0.01611626	0.52712018
23	Block 2	22	4011.4467	0.65995382	0.03942001	0.00545712	0.03428809	0.75873192
21	Block 2	23	4495.6128	0.54002436	0.06419416	0.00735431	0.04620852	0.75020958
29	Block 2	24	4016.1958	0.79754628	0.01251923	0.00286388	0.01799428	0.55487132
30	Block 2	25	4499.6828	0.66832161	0.04092792	0.00571918	0.03593467	0.76117945
22	Block 2	26	3420.89	0.808225	0.00784632	0.0023184	0.0145669	0.460417
18	Block 2	27	4515.4768	0.80354797	0.01452513	0.00312451	0.01963186	0.59452241
27	Block 2	28	4516.5991	0.79662076	0.01497818	0.00314215	0.01974273	0.6043584
16	Block 2	29	3421.3007	0.67959309	0.03166679	0.00467546	0.0293768	0.73259161
17	Block 2	30	4016.8076	0.54548622	0.06138534	0.00706801	0.04440963	0.75399553
31	**Block 1**	**31**	**3646.217**	**0.7403373**	**0.0206243**	**0.0036758**	**0.02309542**	**0.661126**
32	**Block 1**	**32**	**4244.536**	**0.3579762**	**0.0854475**	**0.0077113**	**0.04845171**	**0.63130973**
33	**Block 1**	**33**	**3649.546**	**0.3390207**	**0.0863962**	**0.0076141**	**0.04784088**	**0.61223309**
34	**Block 1**	**34**	**4241.403**	**0.7317606**	**0.0270095**	**0.0043682**	**0.02744645**	**0.72010039**

APPENDIX D.3

ACTUAL DESIGN FOR 16 IN SWEPT BLADE ALUMINIUM PROPELLER

Std	Block	Run	Factor 1 A:RPM	Factor 2 B:J	Response 1 Ct	Response 2 Cq	Response 3 Cp	Response 4 Eff
10	Block 1	1	4993.3721	0.64488799	0.02334795	0.003381	0.02124347	0.7087558
5	Block 1	2	3511.2965	0.46994861	0.05687926	0.00582504	0.03659978	0.73038314
2	Block 1	3	4998.0324	0.2851182	0.07853618	0.0061894	0.03888916	0.57579385
4	Block 1	4	5001.7197	0.37293077	0.06825218	0.00598734	0.03761956	0.67662341
8	Block 1	5	5021.955	0.55175438	0.04023203	0.00457285	0.02873206	0.7726117
1	Block 1	6	3512.4273	0.29309095	0.08021191	0.00634145	0.03984452	0.59002859
7	Block 1	7	3504.9483	0.56576646	0.04025088	0.00492387	0.0309376	0.73611971
3	Block 1	8	3508.628	0.38144344	0.06805665	0.00629903	0.03957799	0.6559155
6	Block 1	9	5004.9226	0.46049992	0.05580079	0.00548673	0.03447417	0.74537681
9	Block 1	10	3500.2212	0.65531453	0.02292541	0.00355439	0.02233291	0.6729353
16	Block 2	11	5013.2957	0.46565111	0.05507014	0.00545555	0.03427825	0.74811865
11	Block 2	12	3516.6676	0.28662452	0.078382	0.00653109	0.04103604	0.54747805
~~19~~	~~Block 2~~	~~13~~	~~3510.6527~~	~~0.65835496~~	~~0.02522135~~	~~0.00343702~~	~~0.02159545~~	~~0.76908582~~
13	Block 2	14	3490.6461	0.382767	0.07105396	0.00624736	0.03925329	0.69287838
20	Block 2	15	5020.63	0.64115407	0.02406336	0.00341028	0.02142739	0.72002539
14	Block 2	16	4999.1858	0.38268459	0.06652171	0.0059229	0.03721465	0.68406851
17	Block 2	17	3526.8391	0.55763978	0.0422932	0.00501889	0.0315346	0.74796993
15	Block 2	18	3524.8793	0.47081558	0.05690098	0.00581502	0.03653685	0.73321753
18	Block 2	19	5010.0717	0.55575761	0.03925639	0.00450958	0.02833452	0.77000601
12	Block 2	20	4977.0313	0.28568972	0.07848571	0.00617121	0.03877486	0.5782777
21	**Block 1**	**21**	**3751.889**	**0.3260129**	**0.0777148**	**0.006395**	**0.04018084**	**0.63057042**
22	**Block 1**	**22**	**4732.415**	**0.6023739**	**0.0311723**	**0.0039785**	**0.02499793**	**0.75130161**
23	**Block 1**	**23**	**3724.354**	**0.6099048**	**0.0350078**	**0.0042891**	**0.02694915**	**0.79277458**
24	**Block 1**	**24**	**4743.878**	**0.339312**	**0.0726606**	**0.0060828**	**0.03821926**	**0.64508678**

APPENDIX E

ANOVA FOR APC 12 x 8 PROPELLER (C_T, C_Q, C_P, AND EFFICIENCY RESPECTIVELY)

Source	Sum of Squares	df	Mean Square	F-value	p-value	
Model	0.0227	4	0.0057	1383.57	< 0.0001	
A-RPM	0.0001	1	0.0001	34.79	< 0.0001	significant
B-J	0.0219	1	0.0219	5326.59	< 0.0001	
AB	0	1	0	11.29	0.0025	
B^2	0.0009	1	0.0009	207.22	< 0.0001	
Residual	0.0001	25	4.10E-06			
Cor Total	0.0228	29				

Source	Sum of Squares	df	Mean Square	F-value	p-value	
Model	0	4	0	212.06	< 0.0001	
A-RPM	2.44E-06	1	2.44E-06	51.24	< 0.0001	significant
B-J	0	1	0	508.35	< 0.0001	
AB	1.52E-07	1	1.52E-07	3.19	0.0861	
B^2	0	1	0	305.39	< 0.0001	
Residual	1.19E-06	25	4.75E-08			
Cor Total	0	29				

Source	Sum of Squares	df	Mean Square	F-value	p-value	
Model	0.0016	4	0.0004	212.06	< 0.0001	
A-RPM	0.0001	1	0.0001	51.24	< 0.0001	significant
B-J	0.001	1	0.001	508.35	< 0.0001	
AB	5.99E-06	1	5.99E-06	3.19	0.0861	
B^2	0.0006	1	0.0006	305.38	< 0.0001	
Residual	0	25	1.88E-06			
Cor Total	0.0016	29				

Source	Sum of Squares	df	Mean Square	F-value	p-value	
Model	0.8773	4	0.2193	441.57	< 0.0001	
A-RPM	0	1	0	0.0515	0.8223	significant
B-J	0.6721	1	0.6721	1353.11	< 0.0001	
AB	0.0026	1	0.0026	5.14	0.0322	
B^2	0.1945	1	0.1945	391.53	< 0.0001	
Residual	0.0124	25	5.00E-04			
Cor Total	0.8897	29				

APPENDIX E.1

ANOVA FOR APC 14 x 12 PROPELLER (C_T, C_Q, C_P, AND EFFICIENCY RESPECTIVELY)

Source	Sum of Squares	df	Mean Square	F-value	p-value	
Model	0.0498	2	0.0249	1820.4	< 0.0001	significant
B-J	0.0464	1	0.0464	3391.99	< 0.0001	
B^2	0.0034	1	0.0034	250.58	< 0.0001	
Residual	0.0005	37	0.00E+00			
Cor Total	0.0503	39				

Source	Sum of Squares	df	Mean Square	F-value	p-value	
Model	0.0002	4	0.0001	363.77	< 0.0001	significant
A-RPM	6.43E-06	1	6.43E-06	39.17	< 0.0001	
B-J	0.0001	1	0.0001	873.84	< 0.0001	
AB	3.01E-06	1	3.01E-06	18.35	0.0001	
B^2	0.0001	1	0.0001	385.89	< 0.0001	
Residual	5.75E-06	35	1.64E-07			
Cor Total	0.0002	39				

Source	Sum of Squares	df	Mean Square	F-value	p-value	
Model	0.0094	4	0.0024	363.77	< 0.0001	significant
A-RPM	0.0003	1	0.0003	39.17	< 0.0001	
B-J	0.0057	1	0.0057	873.84	< 0.0001	
AB	0.0001	1	0.0001	18.35	0.0001	
B^2	0.0025	1	0.0025	385.89	< 0.0001	
Residual	0.0002	35	6.48E-06			
Cor Total	0.0097	39				

Source	Sum of Squares	df	Mean Square	F-value	p-value	
Model	2.034710594	13	0.1565162	886.761681	5.802E-31	significant
A-RPM	3.33527E-05	1	3.33527E-05	0.188964013	0.667367	
B-J	0.072913629	1	0.072913629	413.1010899	1.753E-17	
AB	0.000295551	1	0.000295551	1.674481647	0.2070363	
A^2	0.000922048	1	0.000922048	5.223975941	0.0306746	
B^2	0.009169924	1	0.009169924	51.95332572	1.18E-07	
A^2B	0.00055725	1	0.00055725	3.157166314	0.0872975	
AB^2	0.001101864	1	0.001101864	6.242747291	0.0191201	
A^3	0.0010038	1	0.0010038	5.687154019	0.0246704	
B^3	0.002260214	1	0.002260214	12.80551815	0.0013889	
A^2B^2	0.00196082	1	0.00196082	11.10926744	0.0025854	
A^3B	0.000696508	1	0.000696508	3.946149094	0.0576137	
AB^3	0.002239104	1	0.002239104	12.68591682	0.0014495	
B^4	0.003426471	1	0.003426471	19.41308874	0.0001612	
Residual	0.004589081	26	0.000176503			
Cor Total	2.039299675	39				

APPENDIX E.2

ANOVA FOR 16 IN SWEPT BLADE ALUMINIUM PROPELLER (C_T, C_Q, C_P, AND EFFICIENCY RESPECTIVELY)

Source	Sum of Squares	df	Mean Square	F-value	p-value	
Block	0.0001	1	5.61E-05			
Model	0.0068	3	0.002265872	2873.3276	< 0.0001	significant
A-RPM	0.0000	1	2.43397E-05	30.864937	< 0.0001	
B-J	0.0067	1	0.006668971	8456.8495	< 0.0001	
B^2	0.0001	1	6.92956E-05	87.872947	< 0.0001	
Residual	0.0000	14	7.89E-07			
Cor Total	0.0069	18				

Source	Sum of Squares	df	Mean Square	F-value	p-value	
Block	1.85E-07	1	1.85E-07			
Model	0.0000	3	6.296E-06	1421.71	< 0.0001	significant
A-RPM	6.682E-07	1	6.682E-07	150.88	< 0.0001	
B-J	0.0000	1	0.0000	3866.32	< 0.0001	
B^2	1.646E-06	1	1.646E-06	371.62	< 0.0001	
Residual	6.200E-08	14	4.428E-09			
Cor Total	0.0000	18				

Source	Sum of Squares	df	Mean Square	F-value	p-value	
Block	7.29E-06	1	7.29E-06			
Model	0.000746394	3	0.0002	1421.70	< 0.0001	significant
A-RPM	0.0000	1	0.0000	150.88	< 0.0001	
B-J	0.0007	1	0.0007	3866.30	< 0.0001	
B^2	0.0001	1	0.0001	371.61	< 0.0001	
Residual	2.448E-06	14	1.748E-07			
Cor Total	0.0008	18				

Source	Sum of Squares	df	Mean Square	F-value	p-value	
Block	0.0001	1	0.0001			
Model	0.0857	4	0.0214	181.65	< 0.0001	significant
A-RPM	0.0016	1	0.0016	13.98	0.0025	
B-J	0.0079	1	0.0079	66.74	< 0.0001	
B^2	0.0362	1	0.0362	307.02	< 0.0001	
B^3	0.0005	1	0.0005	4.52	0.0533	
Residual	0.0015	13	0.0001			
Cor Total	0.0874	18				

APPENDIX F

MODELS TERM COEFFICIENT FOR APC 12 x 8 PROPELLER

	C_T	C_Q	C_P	η
Factor	**Coefficient Estimate**			
Intercept	0.1067629	0.0047833	0.0300541	0.1001125
RPM	-2.25E-07	1.84E-07	1.16E-06	-2.101E-05
J	-0.0499906	0.0099475	0.062502	2.4262723
RPM*J	7.651E-06	4.36E-07	2.74E-06	5.866E-05
J^2	-0.1712688	-0.0223709	-0.1405608	-2.589145

APPENDIX F.1

MODELS TERM COEFFICIENT FOR APC 14 x 12 PROPELLER

	C_T	C_Q	C_P	η
Factor	**Coefficient Estimate**			
Intercept	0.10604196	0.008827499	0.05546481	0.453257229
RPM	-	-3.62E-07	-2.28E-06	-0.000438771
J	0.01716667	0.007806712	0.049051049	2.971018863
RPM*J	-	1.04397E-06	6.55947E-06	-0.000117215
RPM^2	-	-	-	-1.12075E-07
J^2	-0.1368315	0.018612448	-0.1169455	-7.656844268
$RPM^2 * J$	-	-	-	6.84796E-07
$RPM * J^2$	-	-	-	-0.00044837
RPM^3	-	-	-	1.10367E-11
J^3	-	-	-	10.34236266
$RPM^2 * J^2$	-	-	-	1.65511E-07
$RPM^3 * J$	-	-	-	-7.29678E-11
$RPM * J^3$	-	-	-	-0.000586971
J^4	-	-	-	-4.354588528

APPENDIX F.2

MODELS TERM COEFFICIENTS FOR APC 17 x 12 PROPELLER

	C_T	C_Q	C_P	η
Factor	**Coefficient Estimate**			
Intercept	0.109594	0.0051138	0.0321307	-0.388644064
RPM	-1.18E-06	-2.60E-07	-1.63E-06	-0.000137678
J	-0.0420619	0.0153013	0.096141	7.449337917
RPM*J	8.92E-06	1.19E-06	7.49E-06	0.0009423
J^2	0.1372186	0.0270266	0.1698135	-22.64474062
RPM * J^2	-	-	-	-0.002122081
J^3	-	-	-	34.97964739
RPM * J^3	-	-	-	0.001628671
J^4	-	-	-	-21.49563376

APPENDIX F.3

MODEL TERM COEFFICIENTS FOR 16 IN SWEPT BLADE ALUMINIUM PROPELLER

	C_T	C_Q	C_P	η
Factor	**Coefficient Estimate**			
Intercept	0.1030028	0.0054754	0.03440297	+0.174909
RPM	-1.53E-06	-2.53E-07	-1.59E-06	+0.000013
J	-0.019591	0.012982709	0.08157262	+0.785682
J^2	-0.1437355	-0.022150314	-0.13917438	+2.64797
J^3	-	-	-	-4.23500

APPENDIX G

NORMAL PROBABILITY PLOTS FOR APC 12 x 8 PROPELLER (C_T, C_Q, C_P, AND EFFICIENCY RESPECTIVELY)

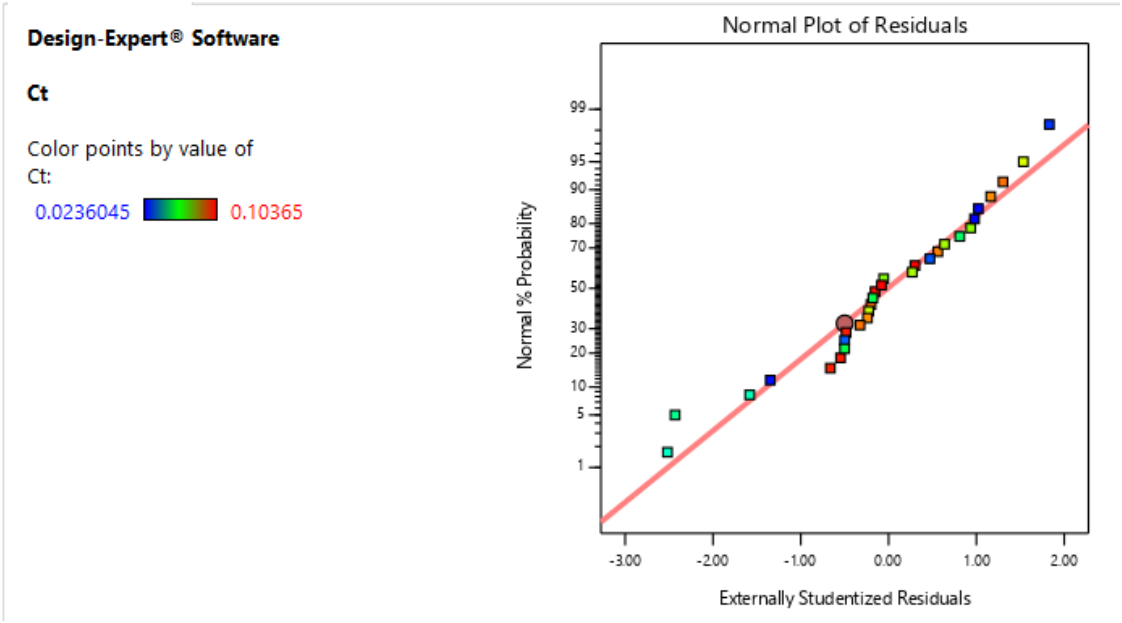

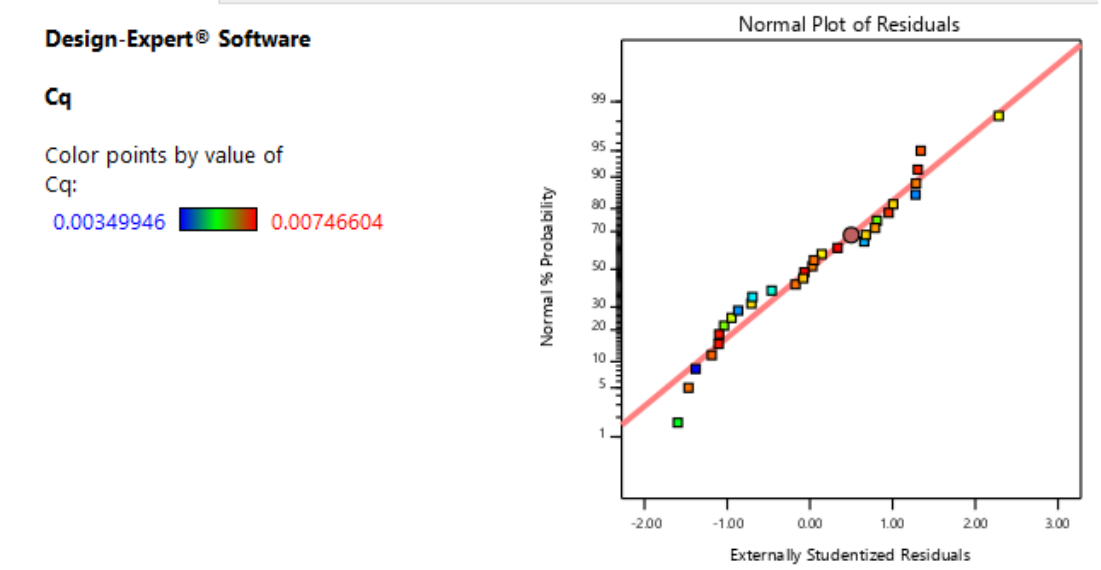

Design-Expert® Software

Cp

Color points by value of
Cp:

0.0219878 0.0469105

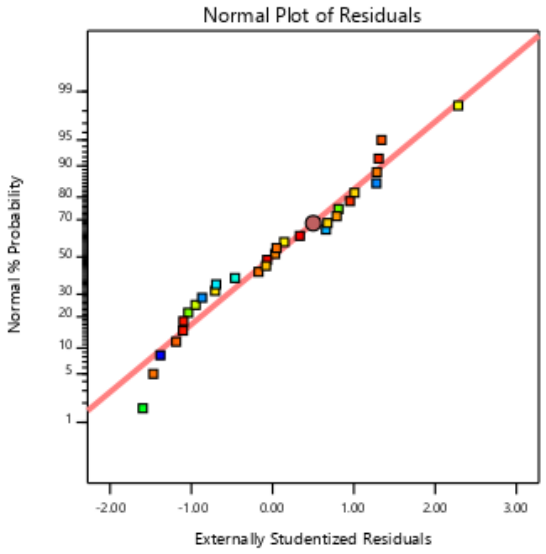

Design-Expert® Software

Eff

Color points by value of
Eff:

0.231753 0.740388

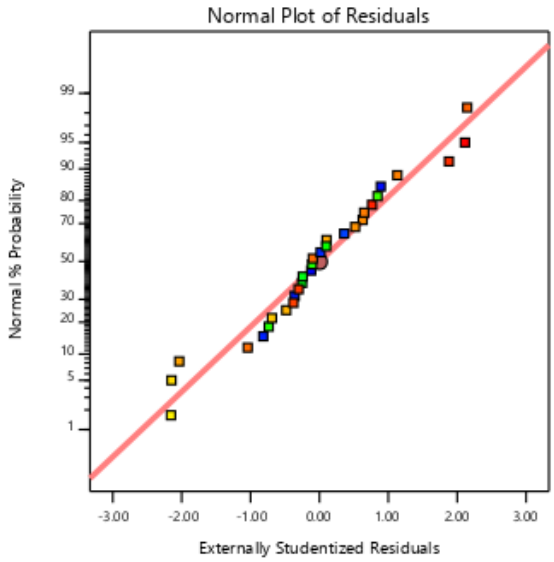

APPENDIX G.1

NORMAL PROBABILTY PLOTS FOR APC 14 x 12 PROPELLER (C_T, C_Q, C_P, AND EFFICIENCY RESPECTIVELY)

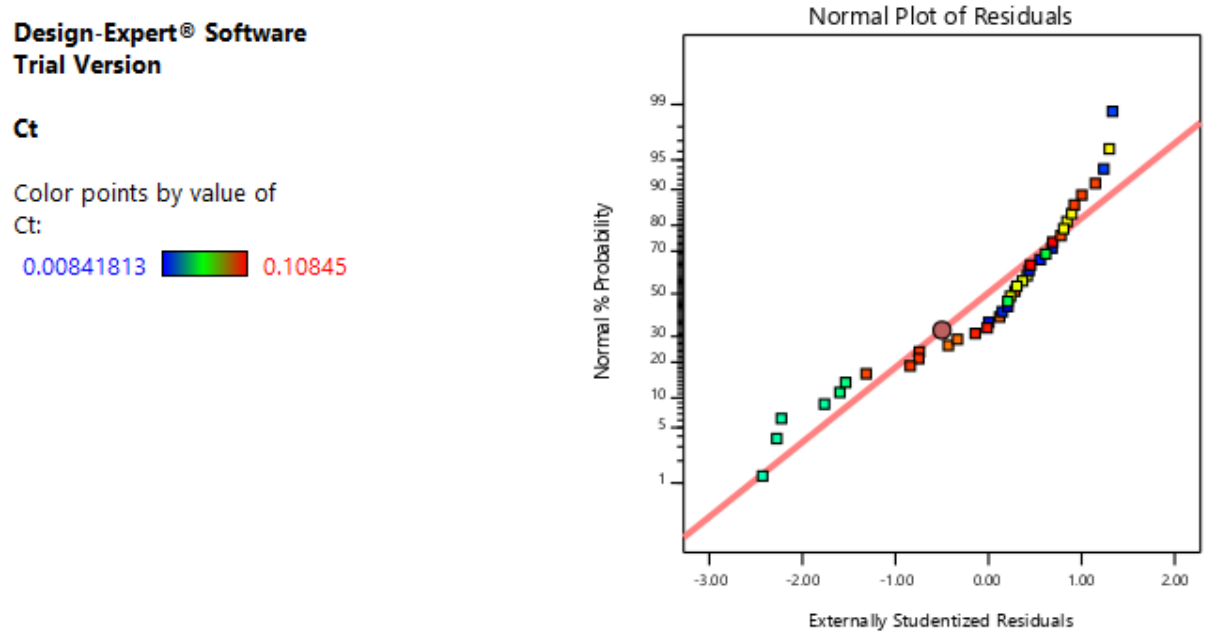

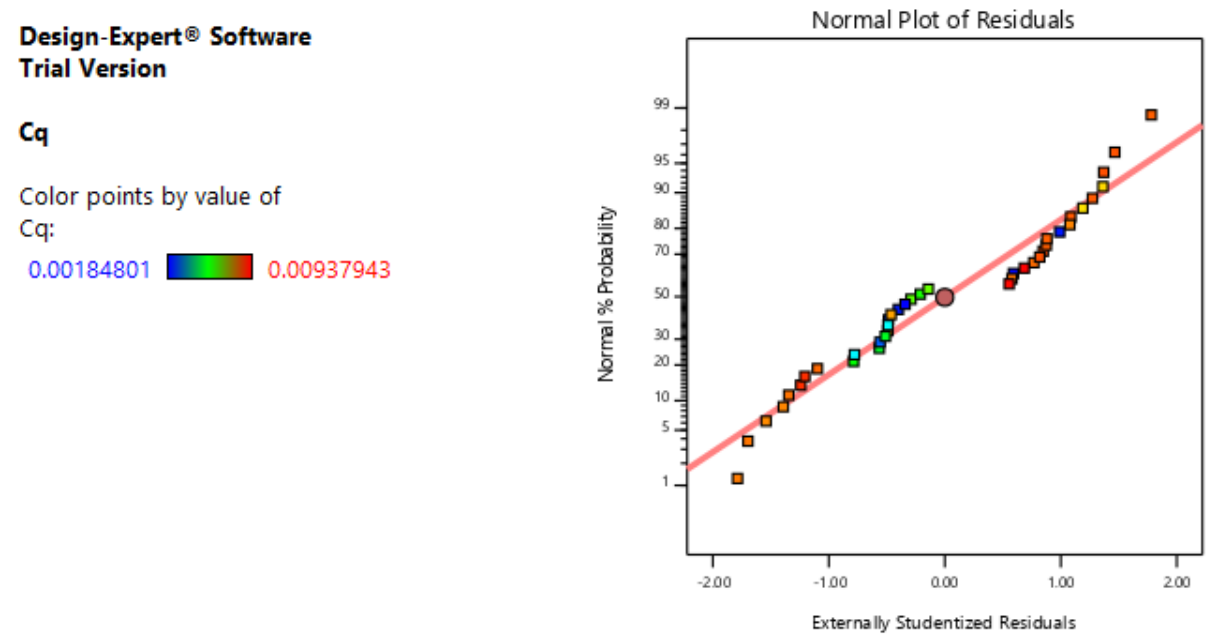

Design-Expert® Software
Trial Version

Cp

Color points by value of
Cp:
0.0116114 0.0589327

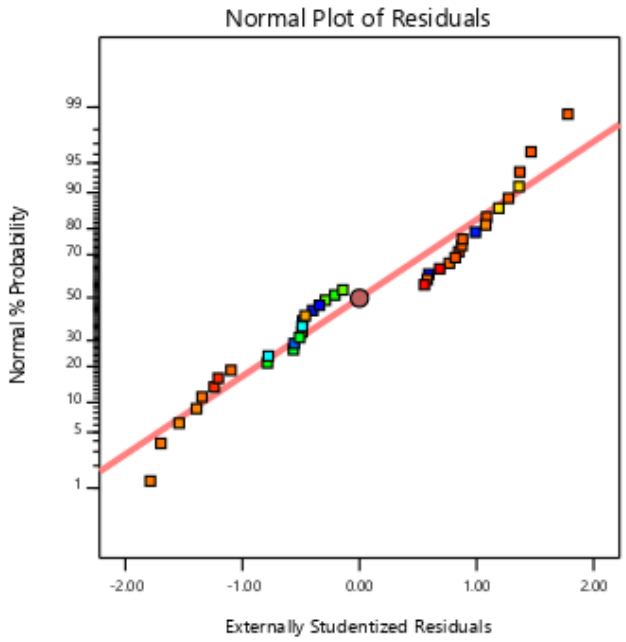

Design-Expert® Software
Trial Version

Eff

Color points by value of
Eff:
0.177651 0.87851

Std # 3 Run # 3
X: 3.760
Y: 98.8

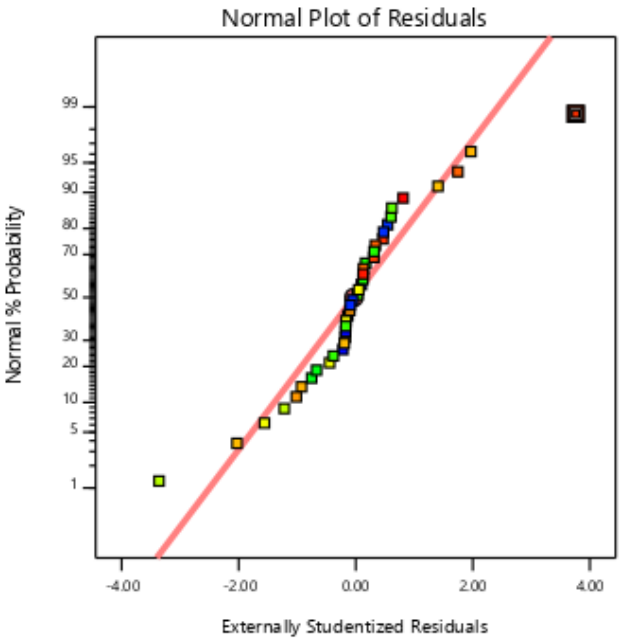

APPENDIX G.2

NORMAL PROBABILITY PLOTS FOR APC 17 x 12 PROPELLER (C_T, C_Q, C_P, AND EFFICIENCY RESPECTIVELY)

Design-Expert® Software
Trial Version

Ct

Color points by value of
Ct:
0.00784632 0.0930753

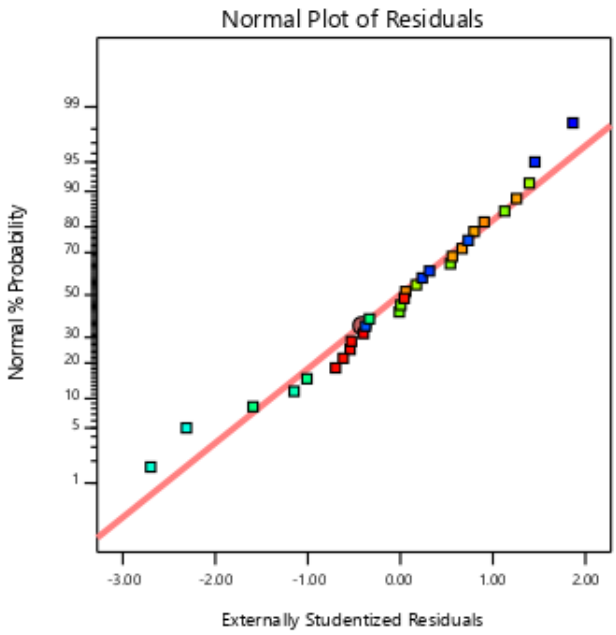

Design-Expert® Software
Trial Version

Cq

Color points by value of
Cq:
0.0023184 0.00781161

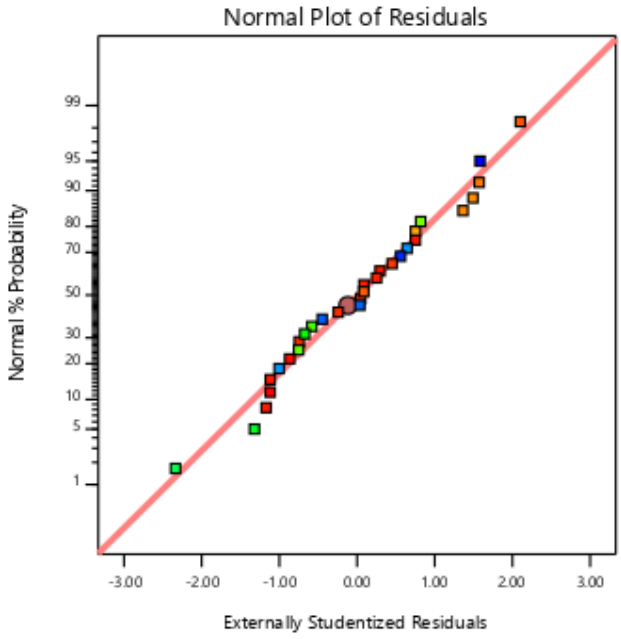

Design-Expert® Software
Trial Version

Cp

Color points by value of
Cp:
0.0145669 0.0490818

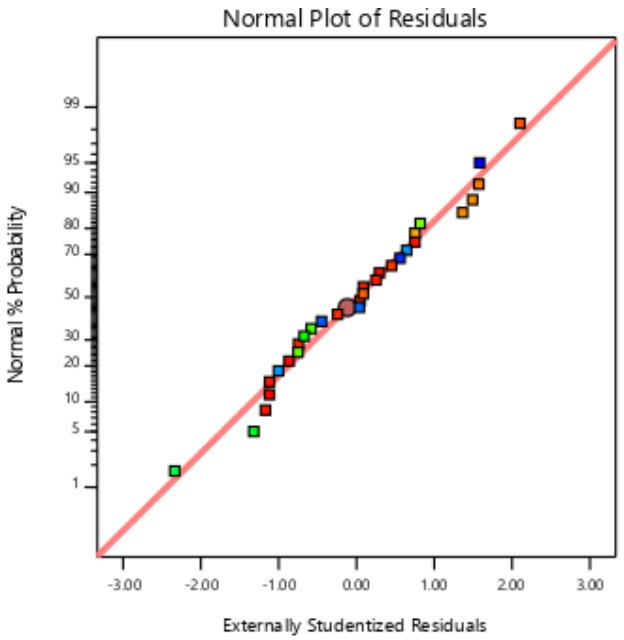

Design-Expert® Software
Trial Version

Eff

Color points by value of
Eff:
0.460417 0.76198

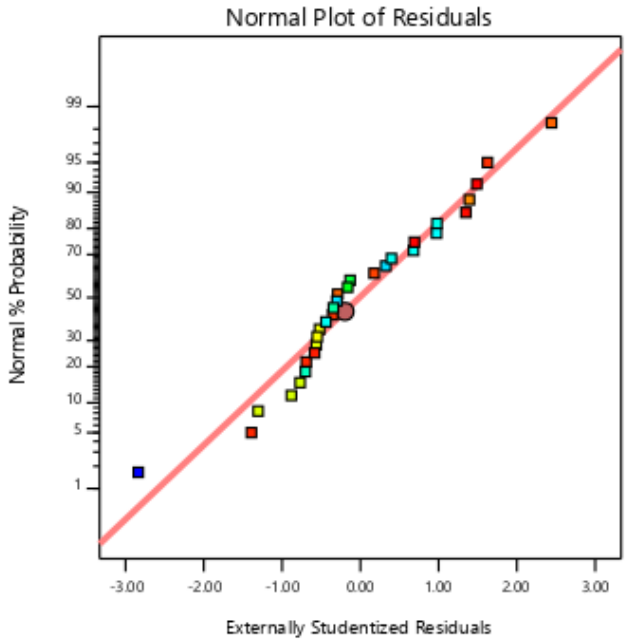

APPENDIX G.3

NORMAL PROBABILITY PLOTS OF EFFICIENCY FOR 16 IN SWEPT BLADE ALUMINIUM PROPELLER (C_T, C_Q, C_P, AND EFFICIENCY RESPECTIVELY)

Design-Expert® Software
Trial Version

Ct

Color points by value of
Ct:
0.0229254 0.0802119

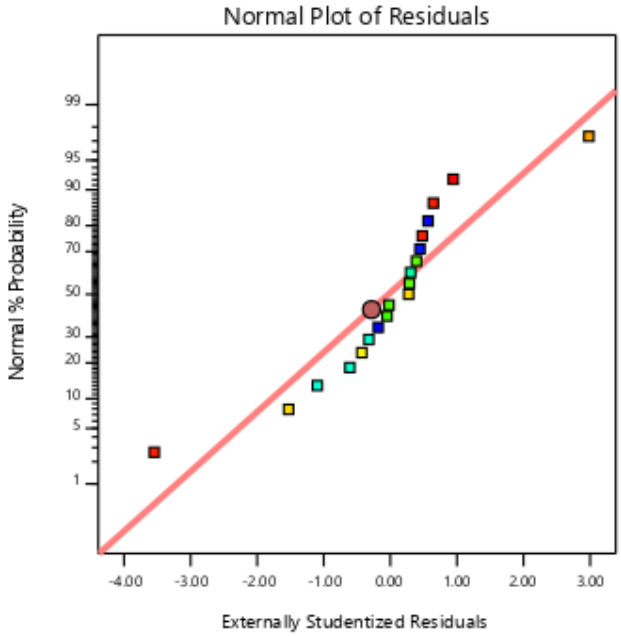

Design-Expert® Software
Trial Version

Cq

Color points by value of
Cq:
0.003381 0.00653109

Std # 1 Run # 6
X: -3.969
Y: 2.6

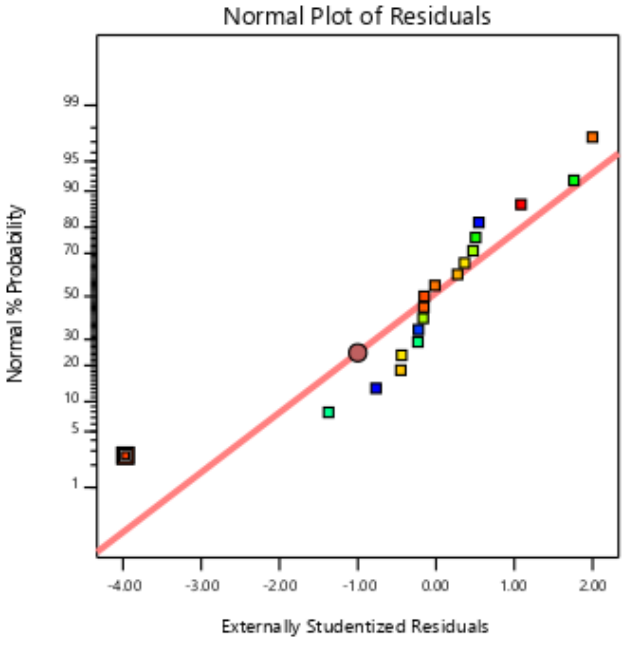

Design-Expert® Software
Trial Version

Cp

Color points by value of
Cp:
0.0212435 0.041036

Std # 1 Run # 6
X: -3.969
Y: 2.6

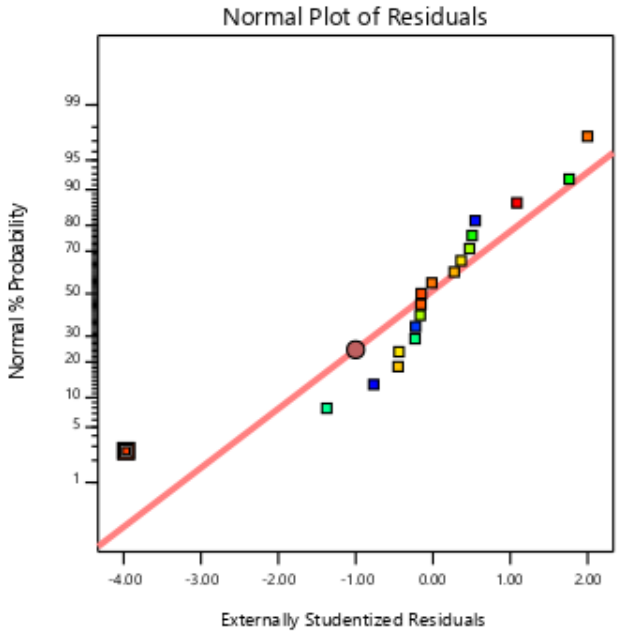

Design-Expert® Software
Trial Version

Eff

Color points by value of
Eff:
0.547478 0.772612

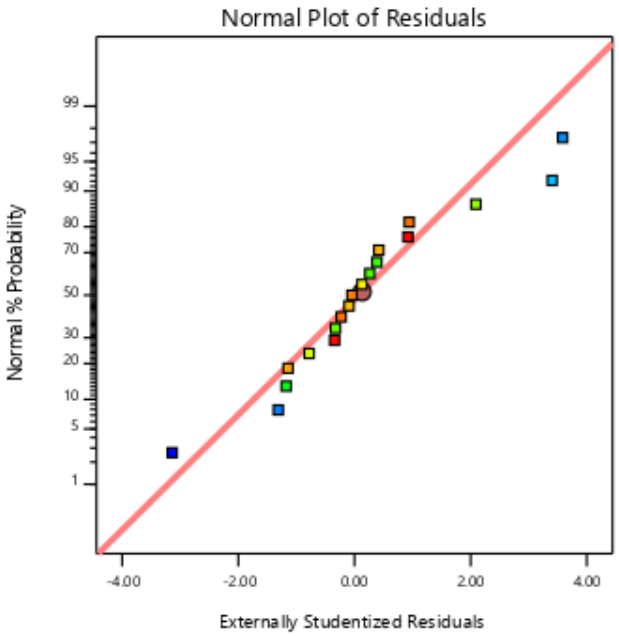

APPENDIX H

RESIDUALS VS. PREDICTED PLOTS FOR APC THIN ELECTRIC 12 x 8 PROPELLER (C_T, C_Q, C_P, AND EFFICIENCY RESPECTIVELY)

Design-Expert® Software

Ct

Color points by value of
Ct:
0.0236045 0.10365

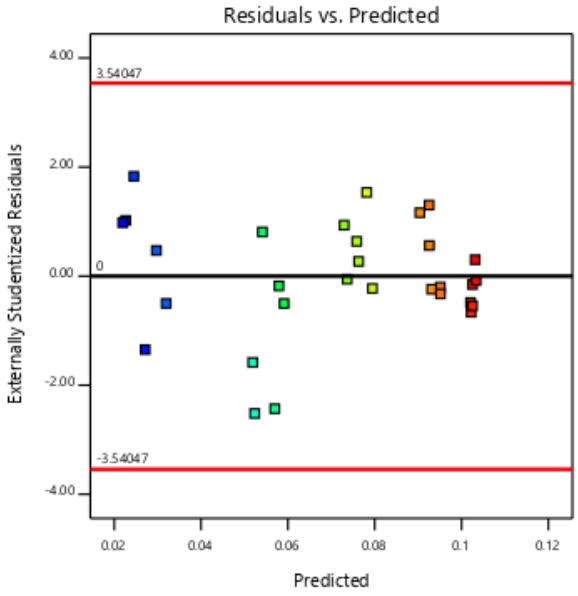

Design-Expert® Software

Cq

Color points by value of
Cq:
0.00349946 0.00746604

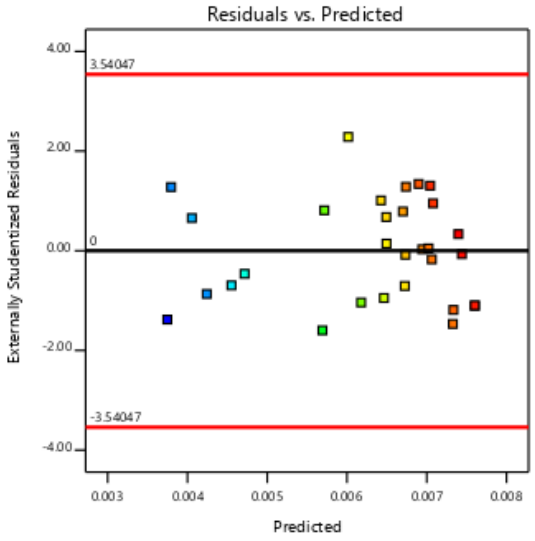

Design-Expert® Software

Cp

Color points by value of
Cp:

0.0219878 0.0469105

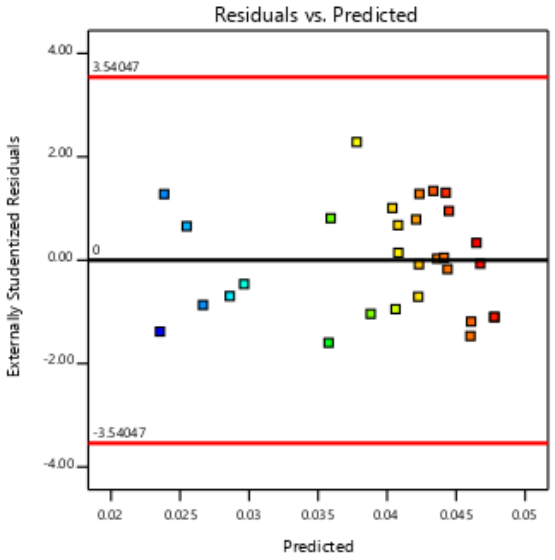

Design-Expert® Software

Eff

Color points by value of
Eff:

0.231753 0.740388

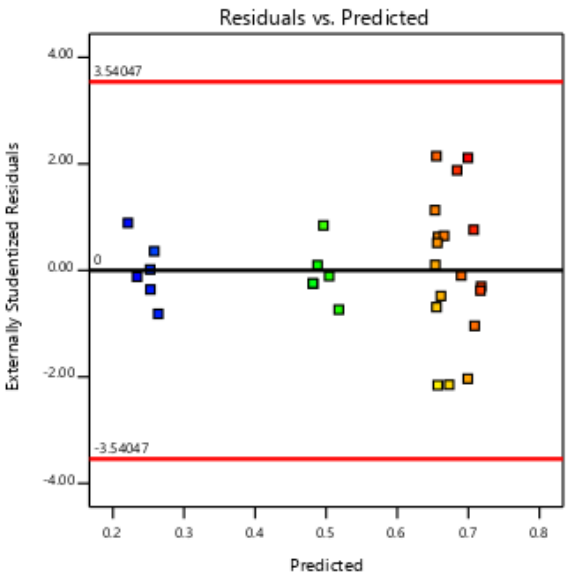

APPENDIX H.1

RESIDUALS VS. PREDICTED PLOTS FOR APC THIN ELECTRIC 14 x 12 PROPELLER (C_T, C_Q, C_P, AND EFFICIENCY RESPECTIVELY)

Design-Expert® Software
Trial Version

Ct

Color points by value of
Ct:
0.00841813 0.10845

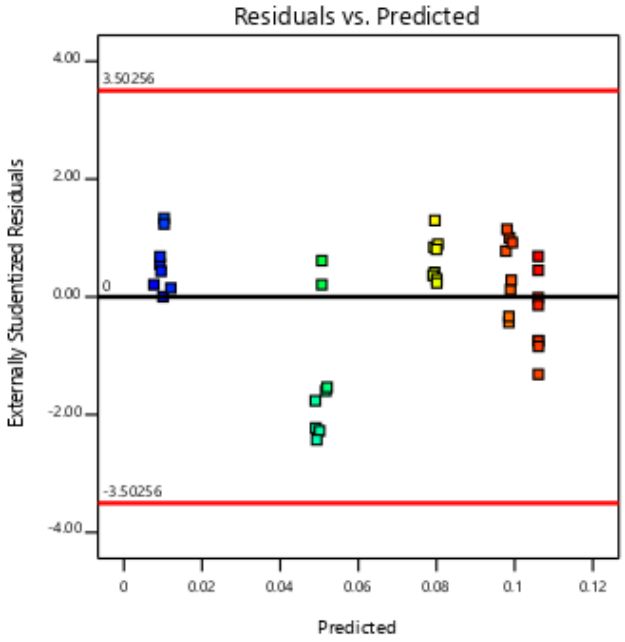

Design-Expert® Software
Trial Version

Cq

Color points by value of
Cq:
0.00184801 0.00937943

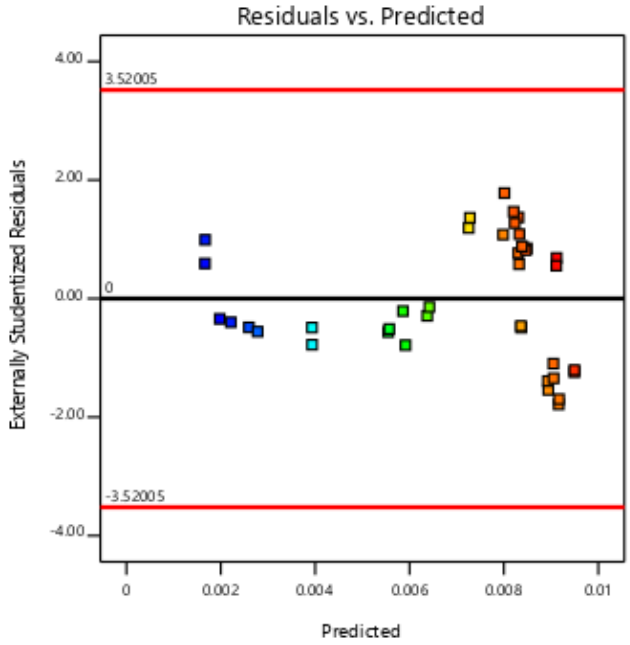

Design-Expert® Software
Trial Version

Cp

Color points by value of
Cp:
0.0116114 0.0589327

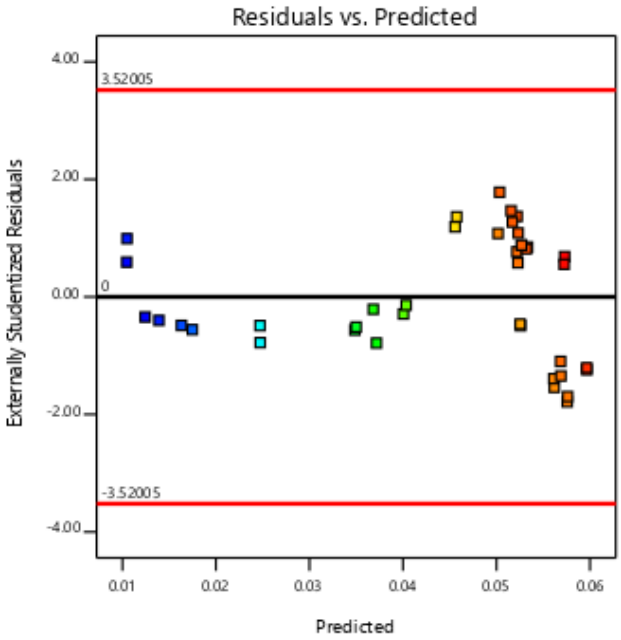

Design-Expert® Software
Trial Version

Eff

Color points by value of
Eff:
0.177651 0.87851

Std # 3 Run # 3
X: 0.774712
Y: 3.760

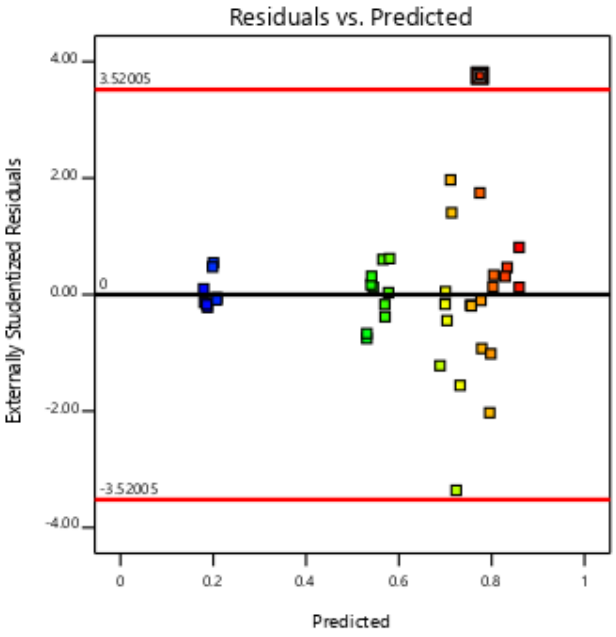

APPENDIX H.2

RESIDUALS VS. PREDICTED PLOTS FOR APC THIN ELECTRIC 17 x 12 PROPELLER (C_T, C_Q, C_P, AND EFFICIENCY RESPECTIVELY)

Design-Expert® Software
Trial Version

Ct

Color points by value of
Ct:
0.00784632 0.0930753

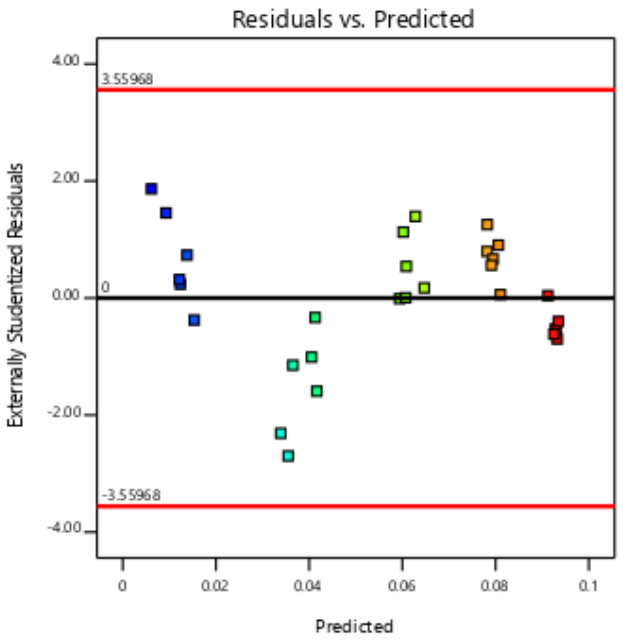

Design-Expert® Software
Trial Version

Cq

Color points by value of
Cq:
0.0023184 0.00781161

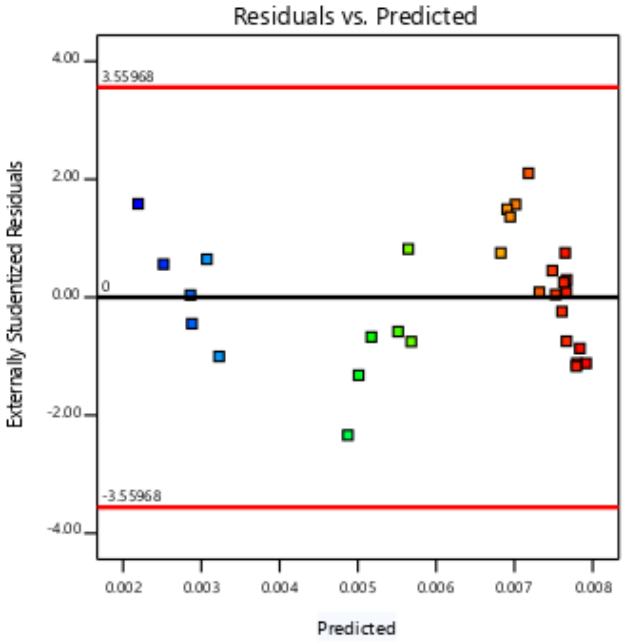

Design-Expert® Software
Trial Version

Cp

Color points by value of
Cp:
0.0145669 0.0490818

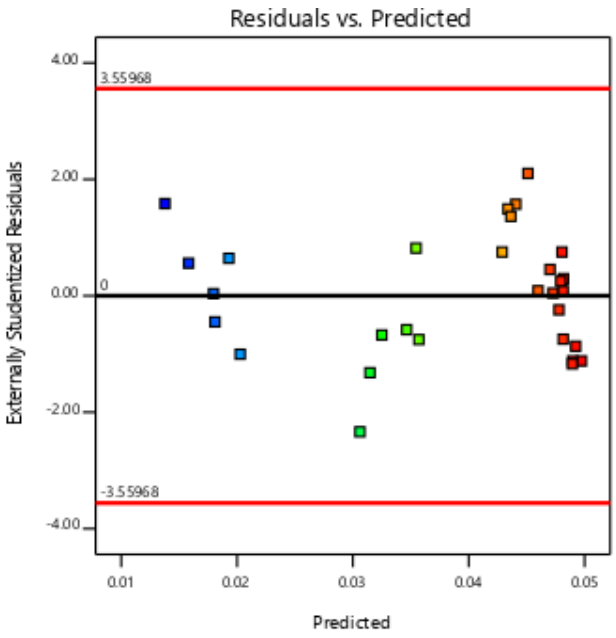

Design-Expert® Software
Trial Version

Eff

Color points by value of
Eff:
0.460417 0.76198

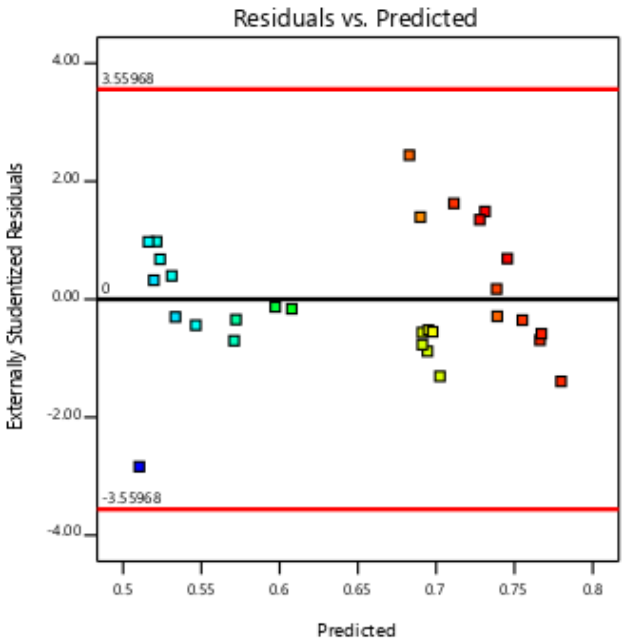

APPENDIX H.3

RESIDUALS VS. PREDICTED PLOTS FOR 16 IN SWEPT BLADE ALUMINUM PROPELLER (C_T, C_Q, C_P, AND EFFICIENCY RESPECTIVELY)

Design-Expert® Software
Trial Version

Ct

Color points by value of
Ct:
0.0229254 0.0802119

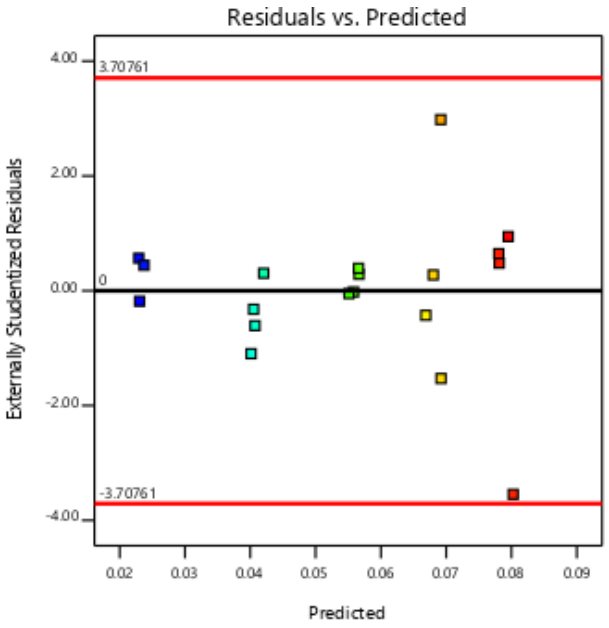

Design-Expert® Software
Trial Version

Cq

Color points by value of
Cq:
0.003381 0.00653109

Std # 1 Run # 6
X: 0.00647155
Y: -3.969

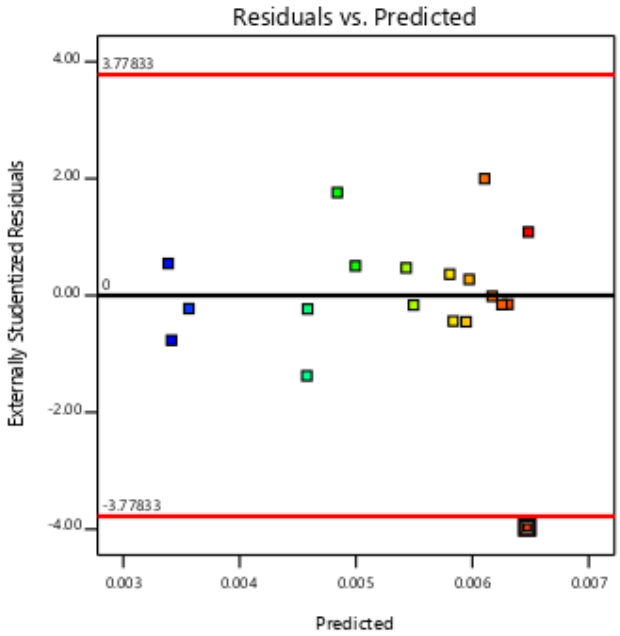

Design-Expert® Software
Trial Version

Cp

Color points by value of
Cp:
0.0212435 0.041036

Std # 1 Run # 6
X: 0.040662
Y: -3.969

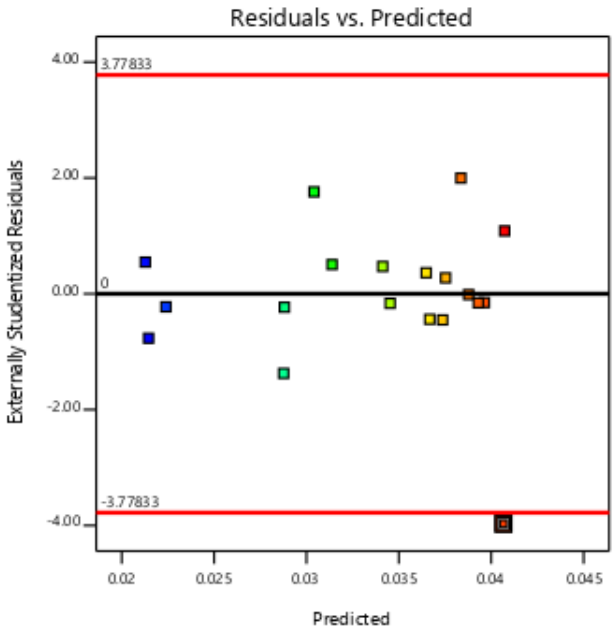

Design-Expert® Software
Trial Version

Eff

Color points by value of
Eff:
0.547478 0.772612

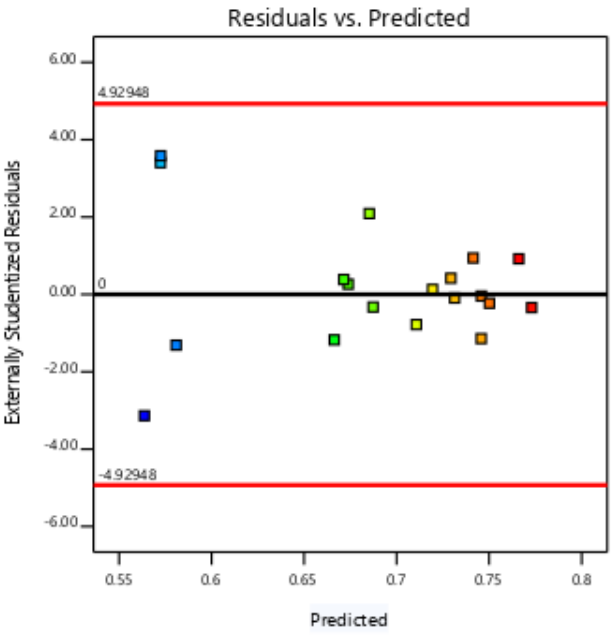

APPENDIX I

RESIDUALS VS. RUN PLOTS FOR APC 12 x 8 PROPELLERS (C_T, C_Q, C_P, AND EFFICIENCY RESPECTIVELY)

Design-Expert® Software

Ct

Color points by value of
Ct:
0.0236045 0.10365

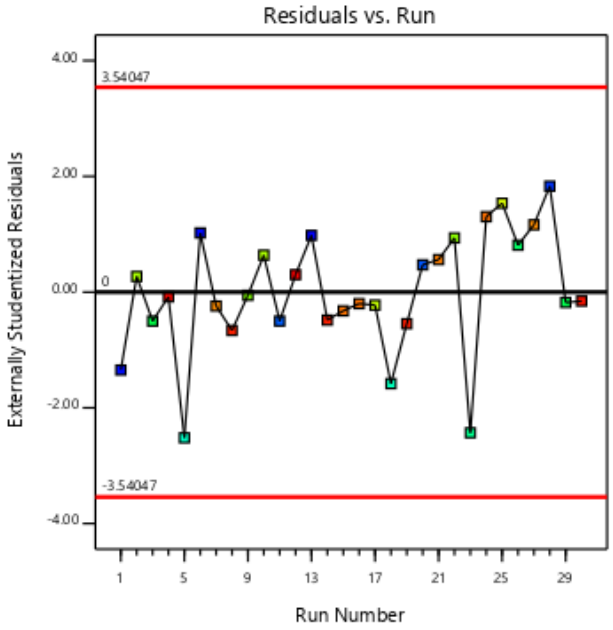

Design-Expert® Software

Cq

Color points by value of
Cq:
0.00349946 0.00746604

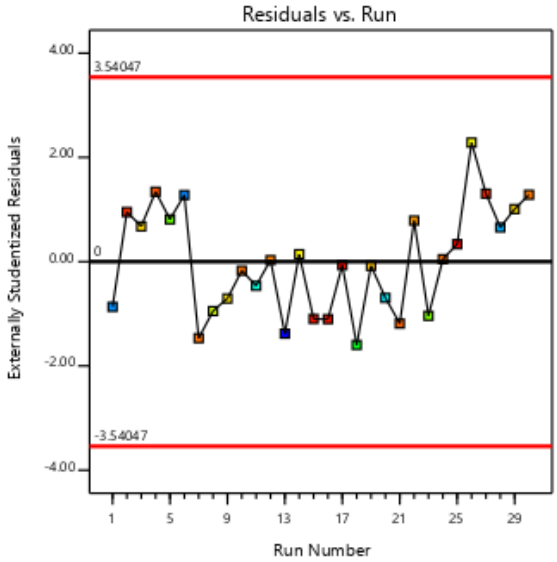

Design-Expert® Software

Cp

Color points by value of
Cp:

0.0219878 0.0469105

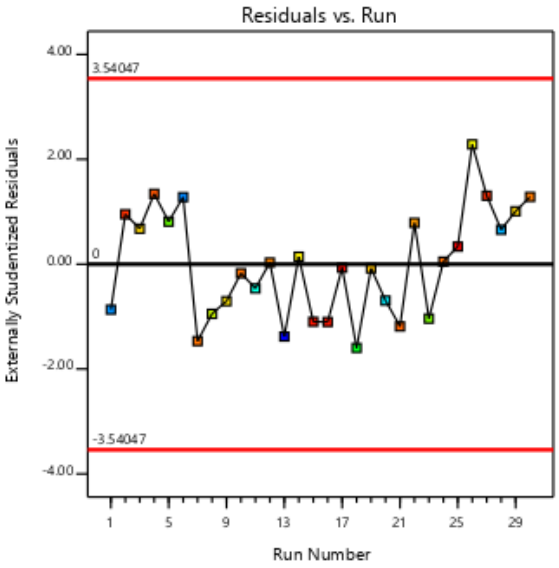

Design-Expert® Software

Eff

Color points by value of
Eff:

0.231753 0.740388

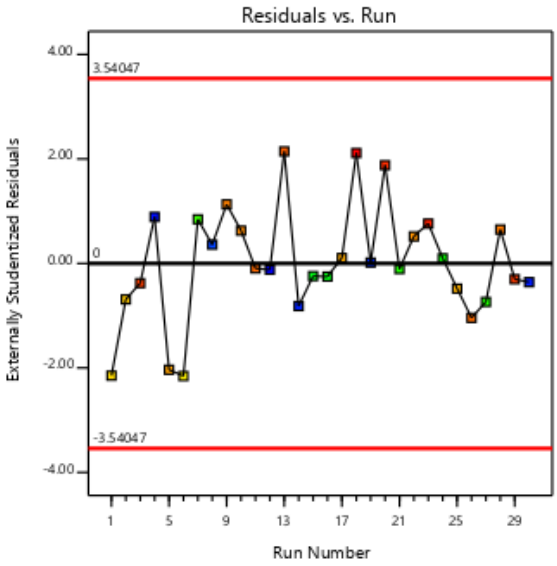

APPENDIX I.1

RESIDUALS VS. RUN PLOTS FOR APC 1 4 x 12 PROPELLER (C_T, C_Q, C_P, AND EFFICIENCY RESPECTIVELY)

Design-Expert® Software
Trial Version

Ct

Color points by value of
Ct:
0.00841813 0.10845

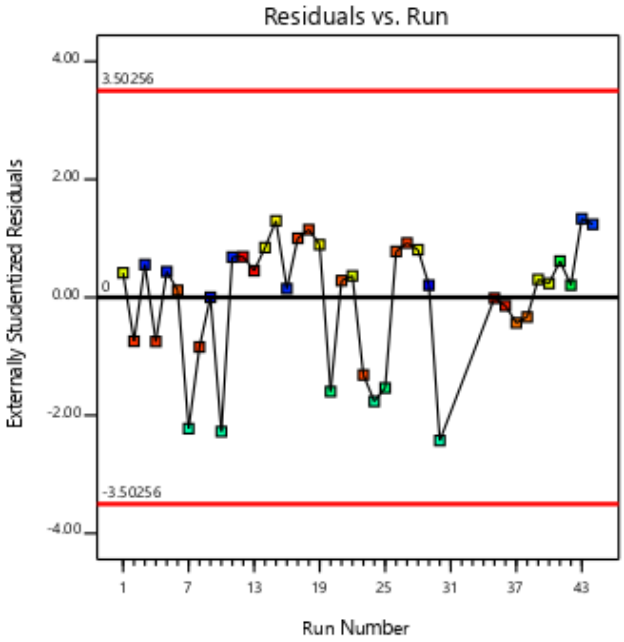

Design-Expert® Software
Trial Version

Cq

Color points by value of
Cq:
0.00184801 0.00937943

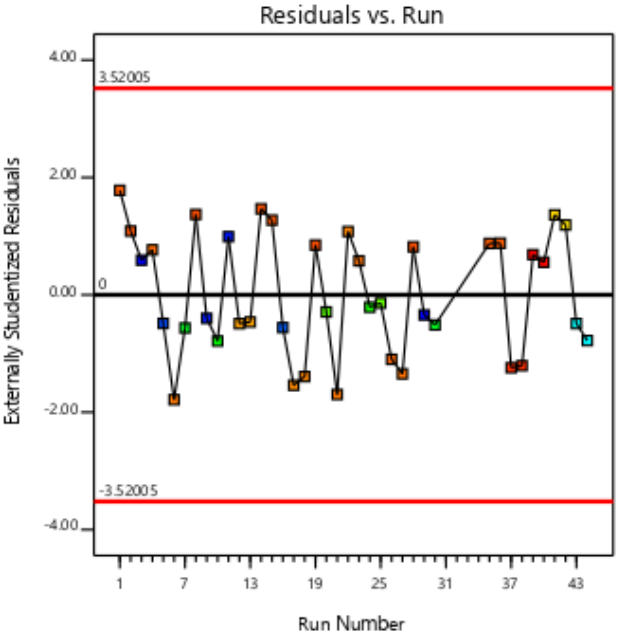

Design-Expert® Software
Trial Version

Cp

Color points by value of
Cp:
0.0116114 0.0589327

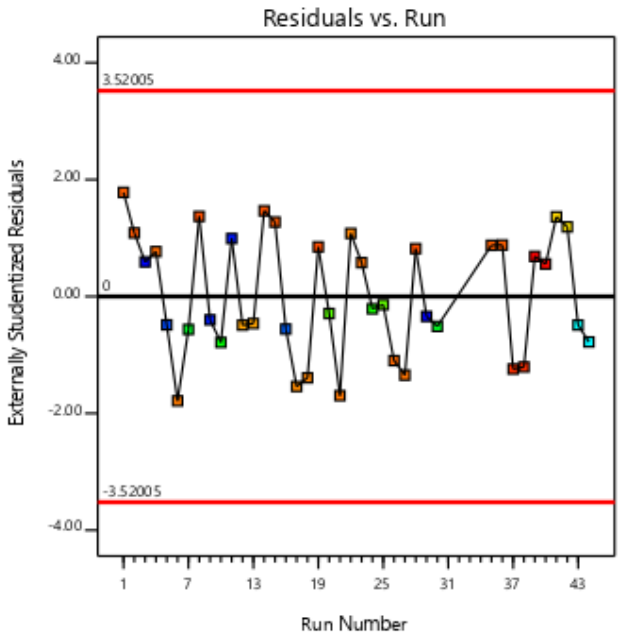

Design-Expert® Software
Trial Version

Eff

Color points by value of
Eff:
0.177651 0.87851

Std # 3 Run # 3
X: 3
Y: 3.760

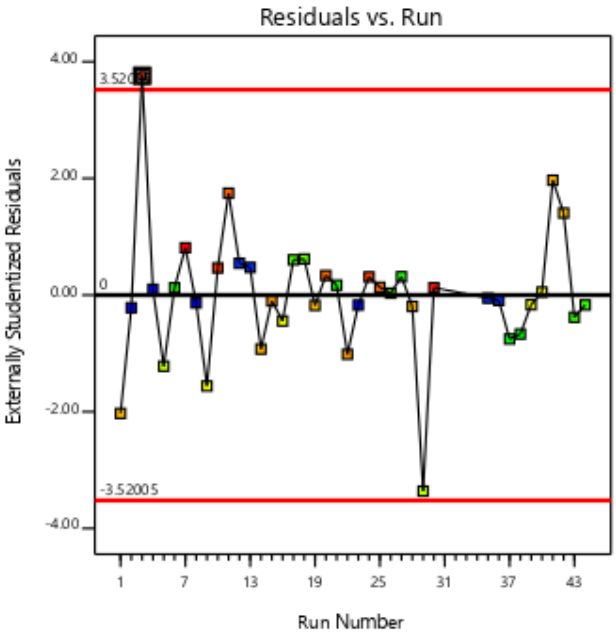

APPENDIX I.2

RESIDUALS VS. RUN PLOTS FOR APC 17 x 12 PROPELLER (C_T, C_Q, C_P, AND EFFICIENCY RESPECTIVELY)

Design-Expert® Software
Trial Version

Ct

Color points by value of
Ct:
0.00784632 0.0930753

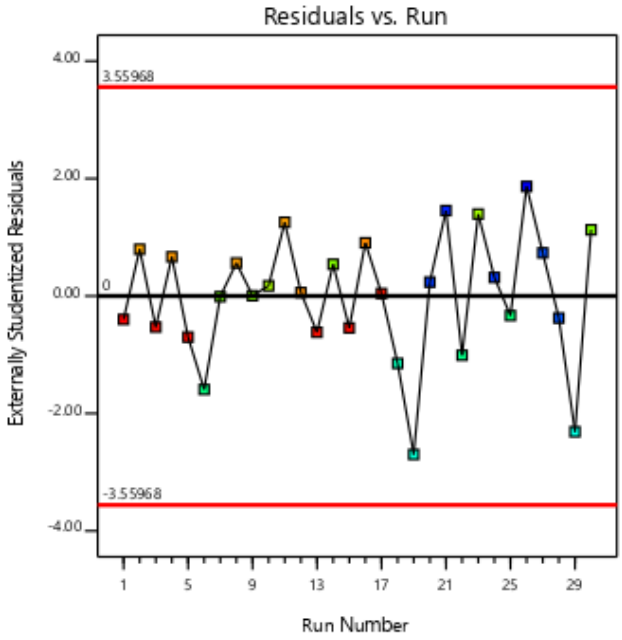

Design-Expert® Software
Trial Version

Cq

Color points by value of
Cq:
0.0023184 0.00781161

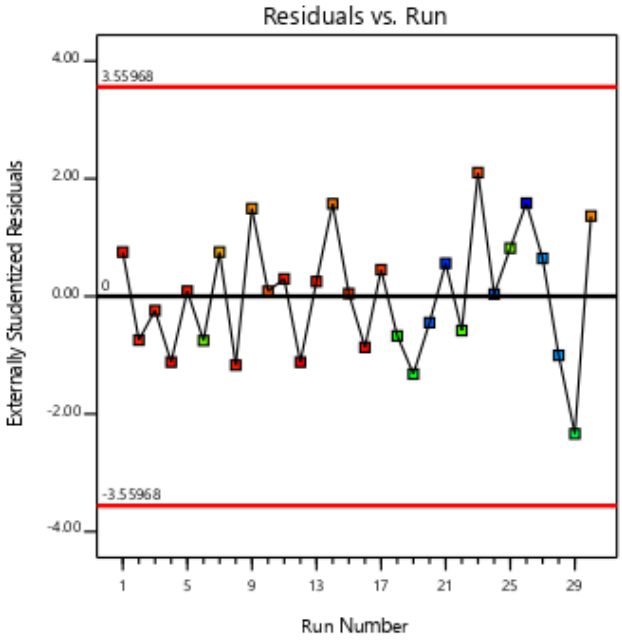

Design-Expert® Software
Trial Version

Cp

Color points by value of
Cp:
0.0145669 0.0490818

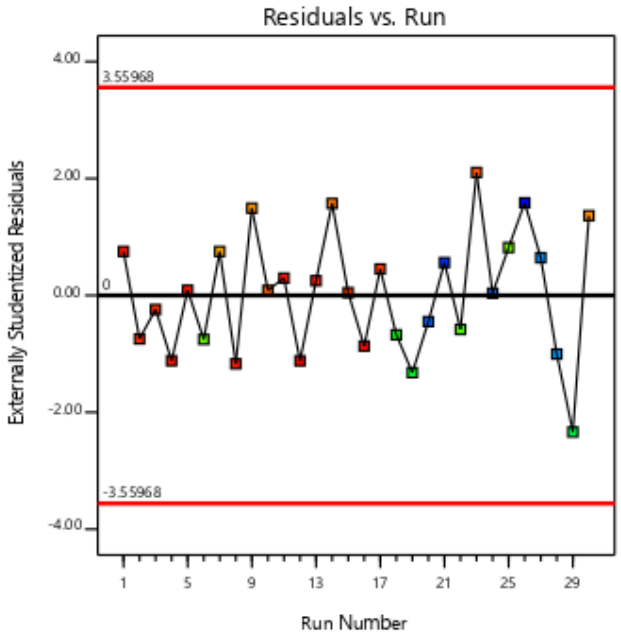

Design-Expert® Software
Trial Version

Eff

Color points by value of
Eff:
0.460417 0.76198

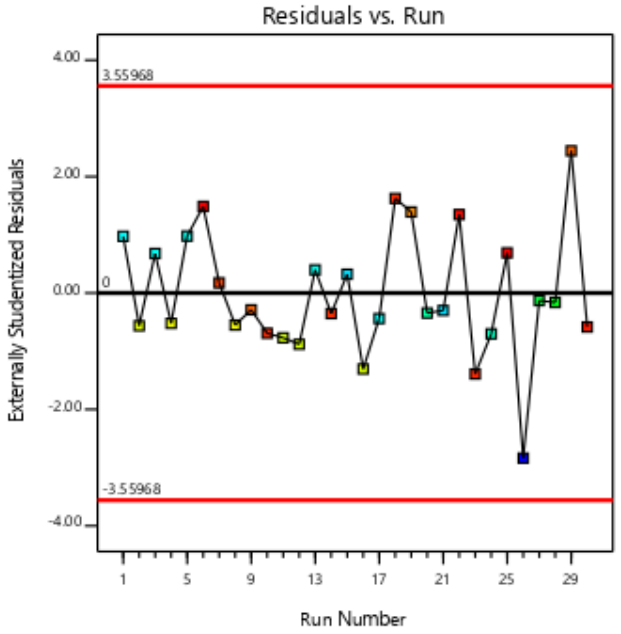

APPENDIX I.3

RESIDUALS VS. RUN PLOTS FOR 16 IN SWEPT BLADE ALUMINUM PROPELLER (C_T, C_Q, C_P, AND EFFICIENCY RESPECTIVELY)

Design-Expert® Software
Trial Version

Ct

Color points by value of
Ct:
0.0229254 0.0802119

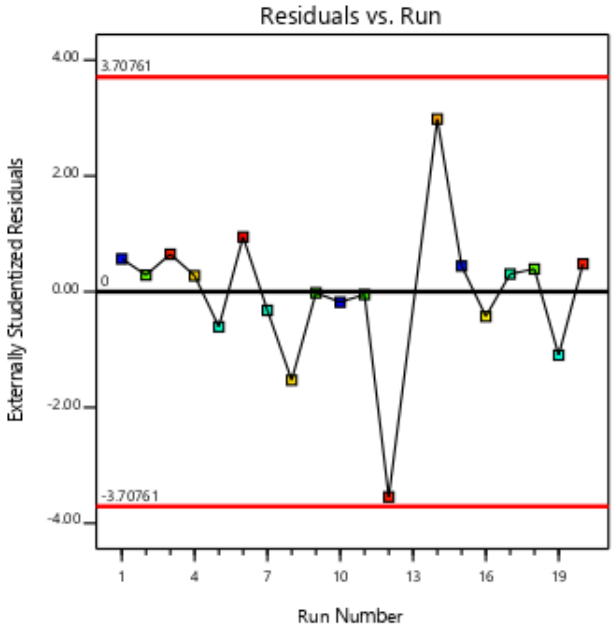

Design-Expert® Software
Trial Version

Cq

Color points by value of
Cq:
0.003381 0.00653109

Std # 1 Run # 6
X: 6
Y: -3.969

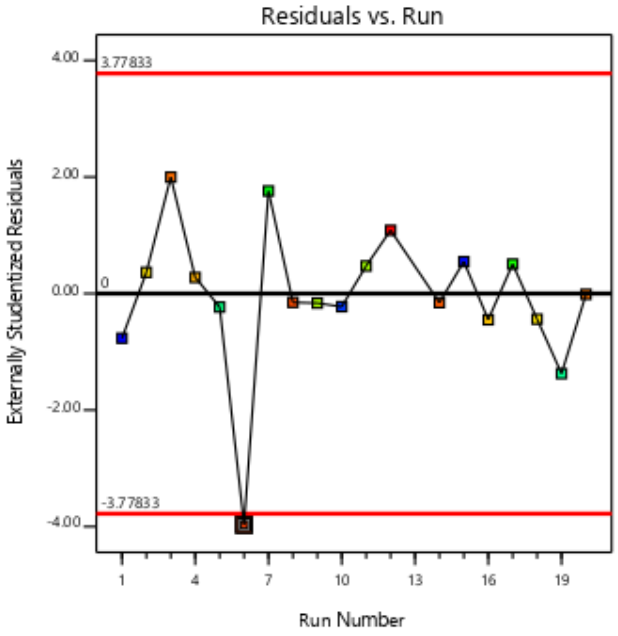

Design-Expert® Software
Trial Version

Cp

Color points by value of
Cp:
0.0212435 0.041036

Std # 1 Run # 6
X: 6
Y: -3.969

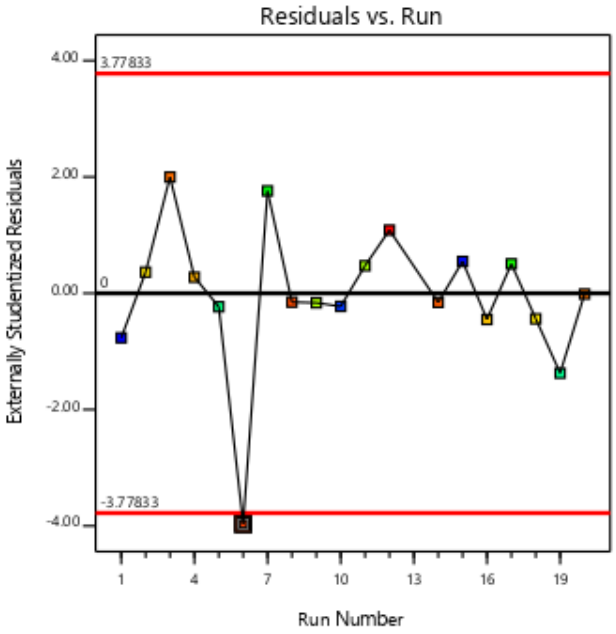

Design-Expert® Software
Trial Version

Eff

Color points by value of
Eff:
0.547478 0.772612

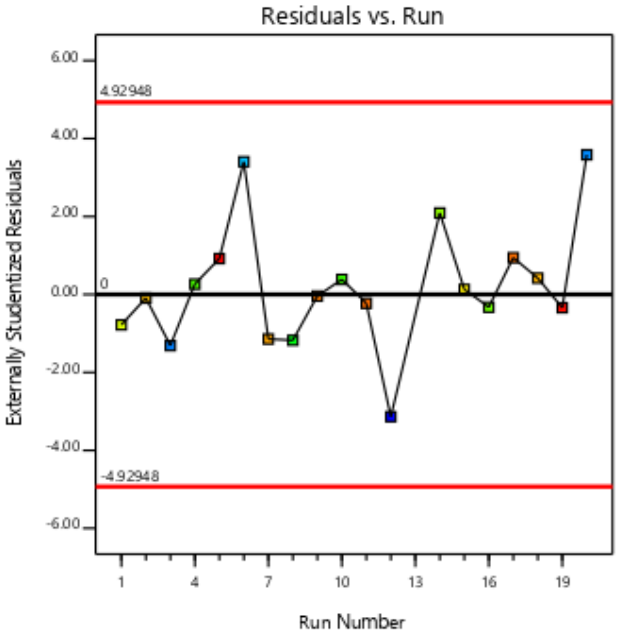

APPENDIX J

CONFIRMATION FOR APC THIN- ELECTRIC 12 x 8 PROPELLER

Verification Run 31 Response	Predicted Mean	Observed	95% PI low	95% PI high
C_T	0.0453838	**0.0449292**	0.0419987	0.0487688
C_Q	0.0053958	**0.0053174**	0.0049698	0.0058217
C_P	0.0339025	**0.0334102**	0.0312264	0.0365786
η	0.7019747	**0.7324869**	0.6569792	0.7469701

Verification Run 32 Response	Predicted Mean	Observed	95% PI low	95% PI high
C_T	0.0877389	**0.0870246**	0.0843502	0.0911275
C_Q	0.0074873	**0.0075156**	0.0070609	0.0079136
C_P	0.0470440	**0.0472216**	0.0443650	0.0497229
η	0.5761956	**0.5675251**	0.5311522	0.6212389

Verification Run 33 Response	Predicted Mean	Observed	95% PI low	95% PI high
C_T	0.0856685	**0.0879659**	0.0822808	0.0890561
C_Q	0.0071722	**0.0071494**	0.0067459	0.0075984
C_P	0.0450640	**0.0449211**	0.0423859	0.0477422
η	0.5796093	**0.5680483**	0.5345792	0.6246394

Verification Run 34 Response	Predicted Mean	Observed	95% PI low	95% PI high
C_T	0.0493670	**0.0463544**	0.0459845	0.0527495
C_Q	0.0058199	**0.0056959**	0.0053943	0.0062455
C_P	0.0365674	**0.0357887**	0.0338933	0.0392415
η	0.7132255	**0.7186944**	0.6682636	0.7581874

APPENDIX J.1

CONFIRMATION FOR APC THIN- ELECTRIC 14 x 12 PROPELLER

Verification Run 31 Response	Predicted Mean	Observed	95% PI low	95% PI high
C_T	0.0338549	**0.0266475**	0.0261429	0.0415668
C_Q	0.0338549	**0.0038556**	0.0036763	0.0055661
C_P	0.0290358	**0.0242255**	0.0230989	0.0349727
η	0.834135	**0.870036**	0.802505	0.865765

Verification Run 32 Response	Predicted Mean	Observed	95% PI low	95% PI high
C_T	0.1039469	**0.1041686**	0.0962289	0.1116650
C_Q	0.0091463	**0.0082836**	0.0082767	0.0100159
C_P	0.0574679	**0.0520476**	0.0520040	0.0629318
η	0.41978	**0.403239**	0.388879	0.450681

Verification Run 33 Response	Predicted Mean	Observed	95% PI low	95% PI high
C_T	0.1043556	**0.1071764**	0.0966266	0.1120845
C_Q	0.0091888	**0.0083946**	0.0082355	0.0101421
C_P	0.0577351	**0.0527450**	0.0517453	0.0637249
η	0.399996	**0.386581**	0.368324	0.431667

Verification Run 34 Response	Predicted Mean	Observed	95% PI low	95% PI high
C_T	0.0343021	**0.0280140**	0.0265918	0.0420124
C_Q	0.0049052	**0.0043399**	0.0040380	0.0057723
C_P	0.0308200	**0.0272683**	0.0253717	0.0362683
η	0.79243	**0.81023**	0.761684	0.823176

Verification Run 45 Response	Predicted Mean	Observed	95% PI low	95% PI high
C_T	0.1040020	**0.1019109**	0.0962827	0.1117214
C_Q	0.0089574	**0.0087020**	0.0080997	0.0098151
C_P	0.0562811	**0.0546761**	0.0508919	0.0616702
η	0.403361	**0.379782**	0.357886	0.448836

Verification Run 46 Response	Predicted Mean	Observed	95% PI low	95% PI high
C_T	0.0670826	**0.0692874**	0.0593560	0.0748093
C_Q	0.0079915	**0.0089249**	0.0071442	0.0088388
C_P	0.0502119	**0.0560771**	0.0448882	0.0555357
η	0.797473	**0.750268**	0.75815	0.836796

APPENDIX J.2

CONFIRMATION FOR APC THIN- ELECTRIC 17 X 12 PROPELLER

Verification Run 31 Response	Predicted Mean	Observed	95% PI low	95% PI high
C_T	0.0230323	**0.0206243**	0.0204777	0.0255870
C_Q	0.0039003	**0.0036758**	0.0036789	0.0041216
C_P	0.0245061	**0.0230954**	0.0231153	0.0258970
η	0.661655	**0.661126**	0.647061	0.67625

Verification Run 32 Response	Predicted Mean	Observed	95% PI low	95% PI high
C_T	0.0855134	**0.0854475**	0.0829891	0.0880377
C_Q	0.0078366	**0.0077113**	0.0076179	0.0080553
C_P	0.0492388	**0.0484517**	0.0478645	0.0506132
η	0.638096	**0.63131**	0.62419	0.652003

Verification Run 33 Response	Predicted Mean	Observed	95% PI low	95% PI high
C_T	0.0863067	**0.0863962**	0.0837629	0.0888504
C_Q	0.0077218	**0.0076141**	0.0075014	0.0079422
C_P	0.0485174	**0.0478409**	0.0471324	0.0499023
η	0.6243573	**0.6122331**	0.5705153	0.6781993

Verification Run 34 Response	Predicted Mean	Observed	95% PI low	95% PI high
C_T	0.0280312	**0.0270095**	0.0255002	0.0305622
C_Q	0.0044377	**0.0043682**	0.0042184	0.0046570
C_P	0.0278829	**0.0274465**	0.0265048	0.0292609
η	0.618093	**0.612233**	0.603886	0.6323

APPENDIX J.3

CONFIRMATION FOR 16 IN STRAIGHT BLADE ALUMINUM PROPELLER

Verification Run 21 Response	Predicted Mean	Observed	95% PI low	95% PI high
C_T	0.0760492	**0.0775221**	0.0749697	0.0771287
C_Q	0.0066559	**0.0064142**	0.0065851	0.0067267
C_P	0.0418204	**0.0403017**	0.0413756	0.0422651
η	0.601562	**0.631766**	0.59213	0.610993

Verification Run 22 Response	Predicted Mean	Observed	95% PI low	95% PI high
C_T	0.0371865	**0.0328134**	0.0339111	0.040462
C_Q	0.004167	**0.00404157**	0.004096	0.00423801
C_P	0.026182	**0.0253939**	0.0257359	0.0266282
η	0.789972	**0.774782**	0.770483	0.809461

Verification Run 23 Response	Predicted Mean	Observed	95% PI low	95% PI high
C_T	0.0369483	**0.03285**	0.0333387	0.0405579
C_Q	0.00427384	**0.00409662**	0.00420061	0.00434707
C_P	0.0268533	**0.0257398**	0.0263932	0.0273134
η	0.775608	**0.77776**	0.754545	0.796672

APPENDIX K

16 IN STRAIGHT BLADE PROPELLER PERFORMANCE PLOTS OF C_T, C_P, C_Q, AND η RESPECTIVELY

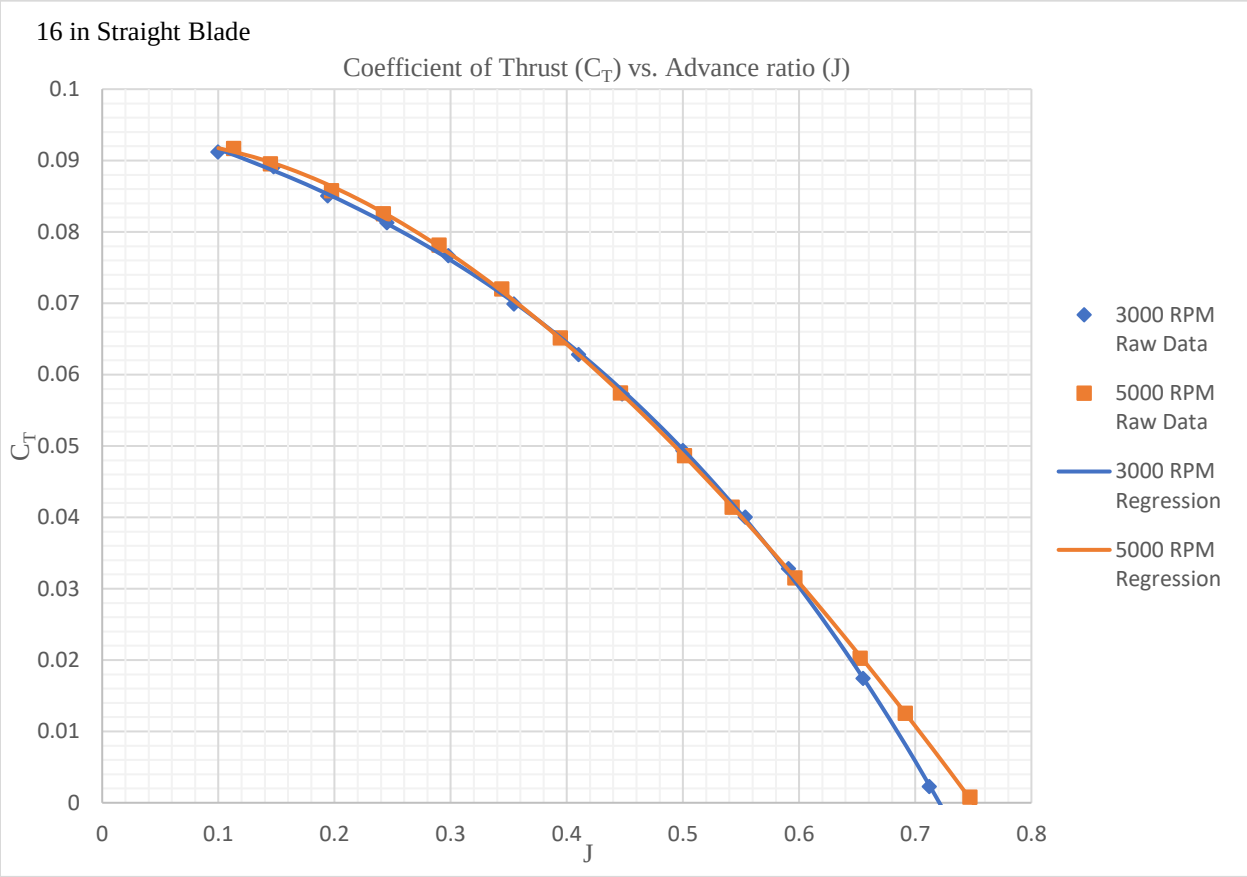

16 in Straight Blade

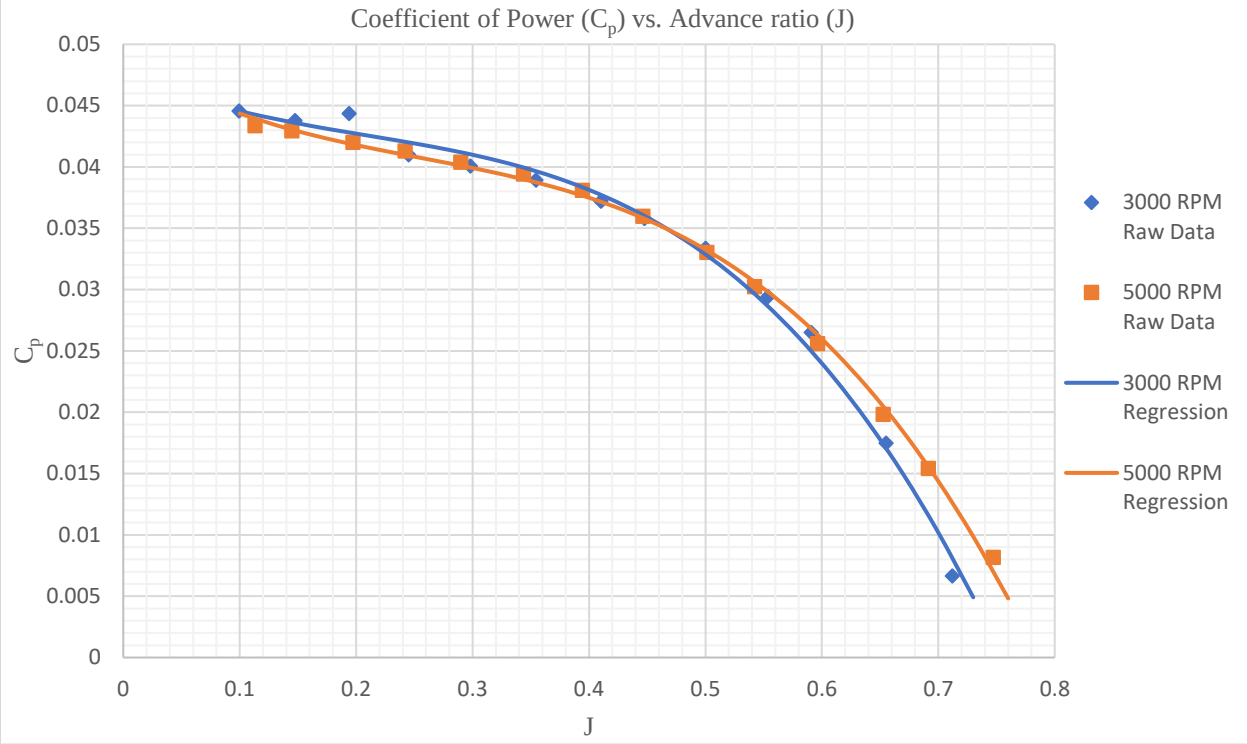

16 in Straight Blade

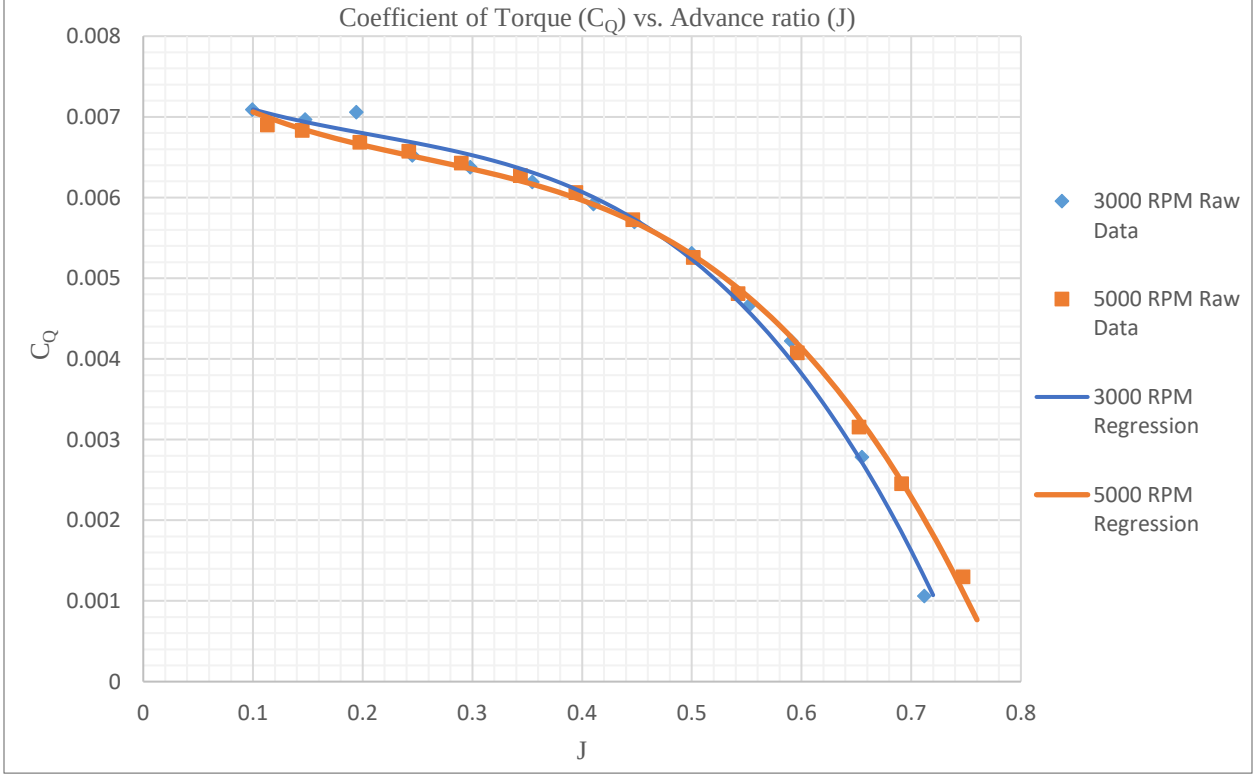

16 in Staright Blade

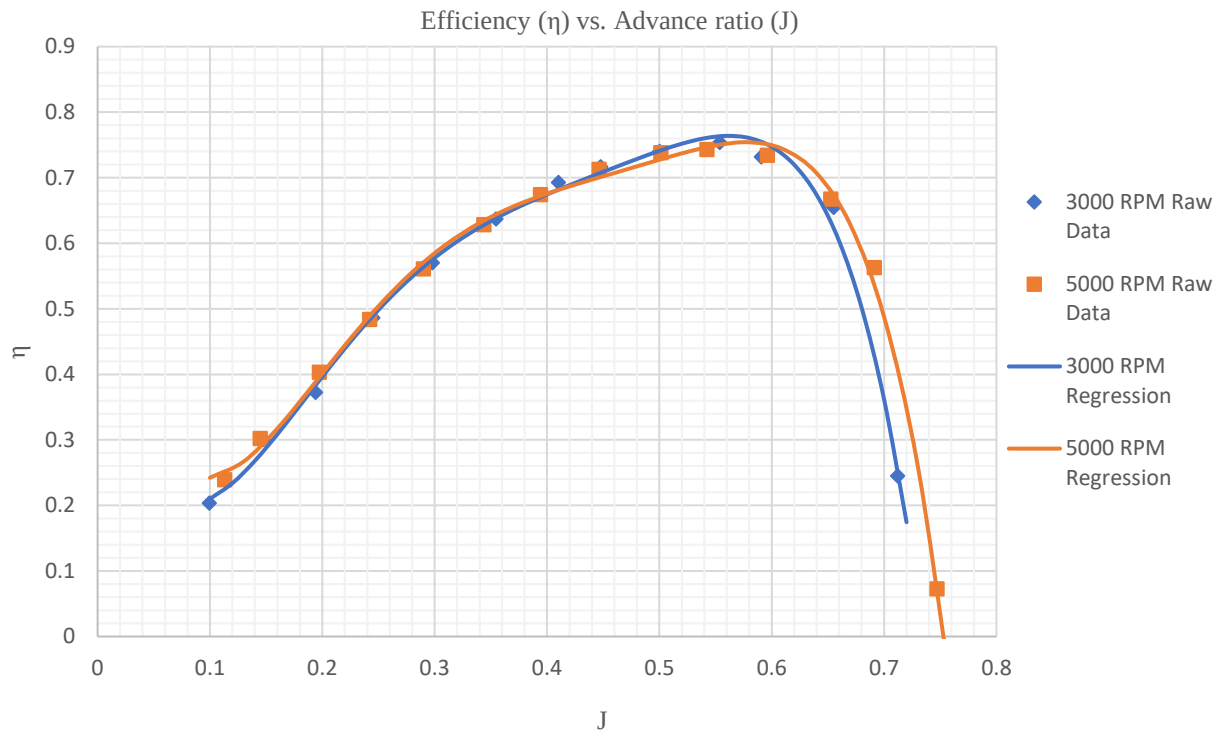

APPENDIX L

MODEL TERM COEFFICIENTS OF C_T, C_Q, C_P, AND η FOR 16 IN STRAIGHT BLADE ALUMINIUM PROPELLER (WIDE J RANGE)

	C_T	C_Q	C_P	η
Factor	**Coefficient Estimate**			
Intercept	+0.102803	+0.007338	+0.046105	+0.200929
RPM	-1.98112E-06	+8.90180E-08	+5.59330E-07	+0.000083
J	-0.136514	-0.003045	-0.019134	-3.94667
RPM*J	+0.000030	-1.28097E-06	-8.04860E-06	-0.001113
J^2	+0.258268	+0.013960	+0.087713	+51.66365
RPM * J^2	-0.000102	+2.32746E-06	+0.000015	+0.005474
J^3	-0.373043	-0.033302	-0.209241	-189.65859
RPM * J^3	+0.000098	-	-	-0.011235
J^4	-0.030692	-	-	+303.96744
RPM * J^4	-	-	-	+0.008039
J^5	-	-	-	-181.53206

VITA

Born and raised in Jamaica W.I., Colin Bruce Leighton Benjamin always had an interest in engineering and technology. After moving to the United States, he lived in the Bronx, NY for approximately one and a half years where he then enlisted in the US Navy. While serving eight years in the US Navy as a gas turbine systems technician, he served five years onboard a US Navy cruiser, completing two and a half deployments in the Mediterranean where he then served his final three years at the Gas Turbine Shop at Norfolk Naval Base. He received two Navy and Marine Corps Achievement Medals for his outstanding military duty while he served. He always desired a degree in mechanical and aerospace engineering, so while serving as an enlisted member, he attended college at any giving opportunity he got. While on active duty he obtained his Associate of Science degree in Engineering from Tidewater Community College in May 2017. He also started attending Old Dominion University (ODU) while on active duty. Later, he then decided to separate from the Navy in May 2017 to complete his degrees at ODU. He obtained his Bachelor of Science degree from ODU in August 2018. While Colin was obtaining his bachelor's degree, he also knew he wanted to pursue his Master of Science degree in aerospace engineering. He applied and got accepted to the BS/MS program and will obtain his M.S. degree in Spring of 2019.